University of Cape Town
Department of Physics
RONDEBOSCH 7700
Cape Town, RSA

Hadronic Gas Description of Relativistic Heavy Ion Collisions incorporating Exact Conservation of Quantum Numbers.

Azwinndini Muronga

Submitted in partial fulfillment
of the requirements for the degree of
Master of Science
at the
University of Cape Town

October 1996

The University of Cape Town has been given the right to reproduce this thesis in whole or in part. Copyright is held by the author.

The copyright of this thesis vests in the author. No quotation from it or information derived from it is to be published without full acknowledgement of the source. The thesis is to be used for private study or non-commercial research purposes only.

Published by the University of Cape Town (UCT) in terms of the non-exclusive license granted to UCT by the author.

University of Cape Town

DST 530 MURO
97/10639
/ 1997

62

Hadronic Gas Description of Relativistic Heavy Ion Collisions incorporating Exact Conservation of Quantum Numbers.

Azwinndini Muronga

October, 1996

Hadronic Gas Description of Relativistic Heavy Ion Collisions incorporating Exact Conservation of Quantum Numbers.

Azwinndini Muronga

University of Cape Town, Rondebosch 7700, RSA

Research supported by Foundation for Research Development (FRD).

Submitted in partial fulfillment of the requirements for the degree of Master of Science at the University of Cape Town.

Abstract

The hadron production (especially kaon production) and the hadronic ratios (especially K/π) in heavy ion collisions are studied assuming that particles are produced in a hadron gas at both thermal and chemical equilibrium. The final state in relativistic ion collision is described by a hadronic gas model which is governed by two freeze out parameters, namely, temperature T and baryon density B/V. It is found that for large interaction volumes and/or large net baryon number, a description using the grand canonical ensemble could be justified. For a small system however, corrections arising solely from exact strangeness and baryon number conservation cannot be neglected. Analytic results for the partition function and the particle numbers are presented. A detailed numerical evaluation is made. A comparison of the behaviour of the results with the experimental information is made. A review of kaon production and K/π ratio and the comparisons of the hadron gas model with recent experimental results is made.

Contents

List of Figures

List of Tables

Acknowledgments

I am grateful to my supervisor, Prof. Jean Cleymans, for letting me join the Institute of Theoretical Physics. His advice throughout the year during my work has been essential for me to carry out my studies towards this thesis. Discussing Physics with him has been one of the most delightful experiences of my studies.

I want to thank Duncan Elliott for many valuable discussions.

Several visitors to Prof. Cleymans motivated me to appreciate this field of Physics. They include, amongst them, M. Gorenstein, M. Chaichan, B. Müller, L. McLerran, K. Redlich, D. Srivastava and H. Miller.

Special thanks go to Berndt Müller and Larry McLerran for setting up my visit to Brookhaven National Laboratory for RHIC Summer Study '96 which motivated me to continue with research in Physics.

I want to thank Tshiwela Maiwashe for her encouraging support during the times of writing my thesis. She read my thesis from the first to the last word, correcting many misprints. I want to thank Alice McLerran for her appreciation of my studies and the shared love of theater.

I am grateful to the Foundation for Research Development (FRD) for the financial contribution to my studies.

A special thanks goes to Joan Parsons, for all the support she gave me. Her generous encouraging support makes me comfortable in the Department. The typing of this thesis relied much upon her enthusiastic help with her experience. She kept on helping me to fight the bugs of LaTeX.

My strength to go all the way through from elementary school comes from my beloved parents and my uncle. Without their constant support, hope and sacrifice, I would not be able to get to where I am now.

Chapter 1

Relativistic Heavy Ion Collisions

1.1 In search of Quark Gluon Plasma

Heavy ion collisions at ultra-relativistic energies offer the opportunity to study strongly interacting matter under the extreme conditions of high temperature and density. The study of ultra-relativistic heavy ion collisions is an emerging field which brings together aspects of both nuclear and high energy physics. One of the basic aims of heavy ion collisions is to study the hadronic matter under extreme densities and temperatures. It is believed that heavy ion collisions such as those done at CERN and BNL experiments can create the conditions similar to those in the early Universe and might have produced a state of matter known as the Quark Gluon Plasma (QGP) in the laboratory for the first time. The early Universe, at $\sim 1\mu sec$ [1] after the *Big Bang* is believed to have been a plasma of weakly interacting quarks, gluons and leptons. This plasma might even still exist in the deep interiors of neutron stars [2]. Observing the plasma is one of the world's most important scientific goals. Detection of the QGP would not only serve as the direct evidence of quarks and gluons, but would also open a new era of physics. Measurements and studies of its properties would hopefully allow us to answer some of the fundamental questions about the origin of the universe, such as how matter was formed, how the cosmic asymmetry between matter and anti-matter came about, etc. At almost the same time that the QGP was theoretically recognized to be possible, heavy ion collisions were realized to be the most efficient way to

create extended regions of hot and dense matter in the laboratory [3]. Experimental effort started almost simultaneously at the AGS of BNL and at the SPS of CERN ten years ago, with relatively light ions, O and Si of 14 GeV/u at BNL and O and S ions of up to 200 GeV/u at CERN. This light ion phase is now completed and has provided very interesting results. A new round of experiments, with really heavy ions, was started in 1992 with Au ions of 11 GeV/u at the AGS and two years ago with Pb ions of 160 GeV/u at CERN. Here there is a considerable increase in the volume of the system together with a slightly larger energy density.

To the best of our knowledge everything in the universe is made up of hadrons and leptons. The hadrons are made up of quarks which often come in twos and threes. Baryons, such as protons and neutrons consist of three quarks. Mesons such as pions consist of a quark and an antiquark. These quarks are bound together by a strong force. Thus quarks are confined in the hadrons. In the so-called quark gluon plasma, quarks are no longer confined in hadrons (the collective name for mesons and baryons). In this new state of matter quarks and gluons will be free particles on their own. In addition to electric charge, the strongly interacting particle - quarks and gluons that bind them together - also have a color charge that is described by using the fundamental colors red, blue and green. Baryons are considered to be white because they contain one quark of each color; and mesons are considered to be white because antiquarks have anticolor. Since the time when the concept of quarks was introduced by Gell-Mann [4] and Zweig [5] in 1964 free quarks have been continuously searched for, and none yet has been found.

It is believed that in high energy heavy ion collisions a large fraction of energy is deposited into a small region of space in a short duration of time. The energy density can be high [1]. As an example the Relativistic Heavy-Ion Collider (RHIC) at Brookhaven National Laboratory (BNL) is designed to accelerate nuclei to energies of about 100 GeV per nucleon. For $Au-Au$ collision where $\sqrt{s}$ is about 200 GeV/A, one would expect an enormous amount of energy deposited in the collision region, and to attain even higher centre of mass energies there is the Large Hadron Collider (LHC) at CERN which will follow RHIC in its program. LHC will have $\sqrt{s}$ of about 6300 GeV/A for $Pb-Pb$ [6]. Quantum Chromodynamics (QCD) predicted a phase transition from hot hadronic matter to a quark-gluon plasma state, where

quarks and gluons are free to move over a large volume compared to the normal size of a hadron ($\sim 1\ fm$). There is little doubt that such a state of matter exists and this is still under debate. However an interesting question is whether this state can be created and detected in the laboratory. Quantum Chromodynamics is, to date, a precise microscopic theory that describes successfully strong interactions of quarks and gluons. Nucleons which consist of uud (protons) and udd (neutrons) are known to compose all currently known existing matter. These nucleons are massive compared to u, d current masses and so chiral symmetry is spontaneously broken, resulting in the light quark constituent mass of 310 MeV, in order to make nucleon mass of about 940 MeV. It is expected that under extreme conditions (high temperature and nuclear density), there exists a new state of matter in which chiral symmetry is restored [3, 7] where the masses drop to zero. Lattice QCD predicts that the phase transition should occur at around $T_c = 140\ MeV$ [8].

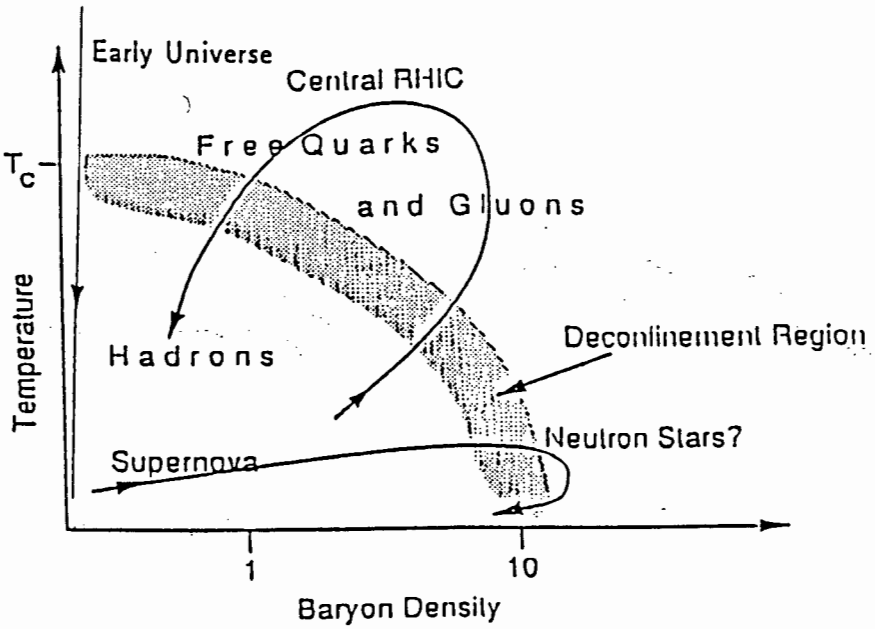

Figure 1.1: Expected phase diagram for nuclear matter [9].

Figure 1.1 shows a schematic phase diagram of the transition from hadronic to quark matter. The ordinate is the temperature, and the abscissa is the baryon density. At high temperature and low density, the conditions are those which presumably prevailed in the universe a few microseconds after the big bang, whereas the other extreme of low temperature and high density the conditions may be close to those inside neutron stars. The early Universe is believed to have had high temperature and low baryon density, whilst the neutron star is

cool but has a high density. The heavy ion collision scenario occurs between these two limits. Three situations where quark-gluon plasma should be possible are discussed below:
At times of $t \sim 10^{-5}$ sec the early universe was extremely hot and hence was in a deconfined state. As it cooled hadronization occurred. An alternative possibility is that the cores of massive neutron stars are sufficiently dense that hadronic matter becomes deconfined. A further alternative, is the possibility of the collision of high energy heavy ions, to create a region of sufficiently high energy density that the deconfinement transition is undergone. These conditions are illustrated in Fig. 1.1 The present ultra-relativistic heavy ion collision programs at CERN-SPS (at 160 GeV/A $Pb+Pb$) and at BNL-AGS (at 11.6GeV/A $Au+Au$) are examples of such an attempt to produce a quark-gluon plasma experimentally. For these fixed-target experiments the center-of mass energy may not be high enough to create the quark-gloun plasma. However we do hope that at RHIC and LHC we might see this QGP.

1.2 Global and Hadronic observables

Global observables, like transverse energy E_T and charged particle distributions; and hadronic observables, like p_T distributions, particle production cross sections and two particle correlations provide crucial information about the reaction dynamics and in particular about the energy density achieved, and the size of the hadronic system at freeze-out (i.e when the system ceases to interact). Figure 1.2 shows the transverse energy distribution as measured by the NA49 experiment in $Pb - Pb$ collisions. An increase by a factor of three in the maximum transverse energy is observed. In both cases the shape is entirely governed by the geometry of the collision; a plateau corresponding to large range of impact parameters where the two nuclei overlap, rapidly falling when reaching central collisions at $b = 0$. The question whether these collisions produce a system of high enough density has already been positively answered by the results obtained with O and Si ions at the SPS [15] and the recent Pb results confirm it. The energy density is inferred from the energy deposited in the system - reflected in the measured transverse energy or alternatively in the number of produced particles - together with a model for the initial interaction volume. The most widely used model is the one proposed by Bjorken [1]. In his scenario of boost invariant expansion, the

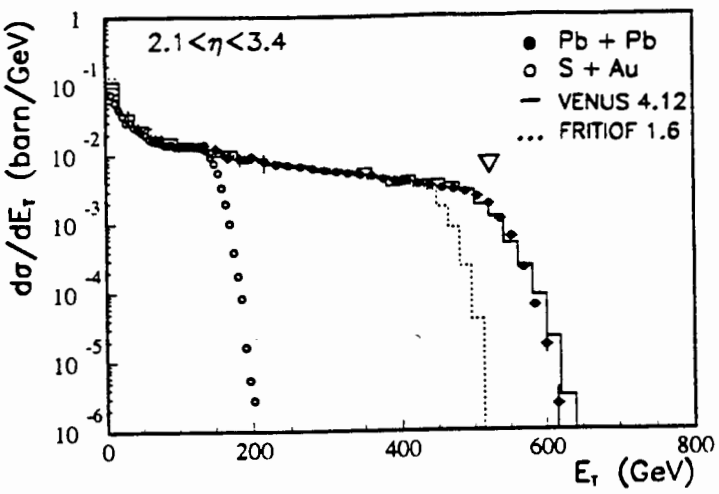

Figure 1.2: Transverse energy distribution of $Pb - Pb$ at 160 GeV/A and $S - Au$ at 200 GeV/A compared to calculations using the FRITIOF and VENUS event generators [11].

energy density ε is proportional to the transverse energy density in rapidity space dE_T/dy

$$\varepsilon = \frac{1}{\pi R^2 \tau} \frac{dE_T}{dy} \quad ,$$

where R is the projectile radius ($R = 1.12A^{1/3}$), and τ is the formation time which is usually assumed to be 1 fm/c. The energy densities achieved at SPS are 2.6 GeV/fm^3 ($S - Au$ at 158 GeV/A) and 3.2 GeV/fm^3 ($Pb - Pb$ at 160 GeV/A) [11]. These values are about 20 times larger than the one for the normal nuclear matter (~ 0.16 GeV/fm^3), and about 7 times larger than that inside the nucleon. More importantly these values are within the range of values predicted for the deconfinement transition phase to occur.

1.3 The Bag and String Models

Since quarks are confined inside a hadron, a useful phenomenological description of quarks in hadrons is provided by the *bag model*. Of the many versions of the model, the MIT bag model [12] has the necessary characteristics of the phenomenology of quark confinement. For a review of the Bag Model see [13, 14]. In this section we shall use the MIT Bag Model to understand how quarks can become deconfined in new phases of matter. The MIT Bag Model

treats hadrons as individual bags containing only quarks. It is a semi-phenomenological model in the sense that physics inside the bag is treated differently from that outside. Quarks are massless inside the bag and infinitely massive outside, phenomenologically explaining their confinement. Confinement in the model is the result of the balance of the *bag pressure*, B, which is directed inward, and the stress arising from the kinetic energy of the quarks. The bag pressure, B, is a phenomenological quantity and is introduced to take into account the non-pertubative effects of QCD. According to QCD, quarks carry a new intrinsic quantum number, color. As mentioned earlier there are three colors, namely: red, blue and green. If quarks are confined in the bag, gluons should also be confined in the bag. And according to "Gauss's law" the net color charge of the matter inside the bag must be colorless. As there are three different types of color, the bag model would imply that the allowable hadronic bags should include colorless qqq and $q\bar{q}$ states. Consider a system of N quarks confined in a spherical bag of radius R. The total energy of this system is given [16] by

$$E = \frac{2.04N}{R} + \frac{4}{3}\pi R^3 B \, . \tag{1.1}$$

where the first term arises from kinetic energy and the second term from the potential energy of the confined quarks. Here and throughout this work the conventional units $\hbar = c = k = 1$ are used. The number 2.04 comes from the spherical Bessel functions. The tendency to increase radius due to kinetic energy of the quarks is counterbalanced by this inward pressure, B, directed from the region outside the bag towards the region inside the bag. The equilibrium of the system is located at the radius R determined by $\frac{dE}{dR} = 0$, which leads to a bag pressure constant B related to the radius by

$$B^{1/4} = \left(\frac{2.04N}{4\pi}\right)^{1/4} \frac{1}{R} \, . \tag{1.2}$$

If we take the confinement radius to be 0.8 fm for a three quark system in a baryon, we obtain an estimate of the bag pressure constant

$$B^{1/4} = 206 \; MeV \, . \tag{1.3}$$

If the pressure of the bag is greater than B, then the bag will break up, leading to the deconfinement of the quarks, or the formation of the quark matter. In other words, if the pressure of the quark matter inside the bag is increased, there will be a point when the pressure directing outward is greater than the inward bag pressure. And when that happens,

the bag pressure cannot balance the outward quark matter pressure and the bag cannot confine the quark matter contained inside. A new phase of matter containing the quarks and gluons in an unconfined state is then possible. A large pressure of quark matter arises 1) when the temperature of the matter is high, and or 2) when the baryon number density is large. In the bag model, hadron bags are often nearly spherical in shape, corresponding to the ground state or low energy state of hadrons. As a hadron is excited to a higher energy state, the quarks inside the bag have more energy so that the bag might become distorted. One extreme case is that the bag becomes long and thin like a string. Hence the string model which can be thought of as an extension of the bag model. The energy of the quark system in the string model is given [17] by

$$E = -\frac{4\alpha_s}{3R} + \sigma R \ , \tag{1.4}$$

where R is the length of the string and α_s is the strong coupling constant. The second term arises, of course, from the string picture, where the string tension, σ is roughly 1 GeV/fm. When the quark and anti-quark in a $q\bar{q}$ pair are far apart, the flux tube of color-electric field between them would have so much energy that the string breaks producing another $q\bar{q}$ pair in between. In this picture, it seems that quarks are never able to reach de-confinement. However, in a dense state, strings should not be long and quarks ought to overlap.

1.4 Thermodynamics

If QGP is formed, we have a situation which is much like a chemical mixture in which chemical compounds interact to change to other momentum states and to transform to other chemicals. In this mixture, there will be a stage when the momentum distributions of the particles do not change, even though momentum exchanges continue through the interaction between particles. When this stage is reached we say the system has reached *thermal equilibrium*. Equilibration results from the balance in the gain and loss of the momentum distribution of forward and reverse or other reactions, respectively. In a similar way, *chemical equilibrium* is reached when the densities of different particles reach a steady state even though the particles continue to interact and transform from one kind to another. Equilibration results from the balance in the gain and the loss in density of forward and

reverse reaction or other reactions, respectively. Thus, the state of quark gluon plasma is said to be in thermal and chemical equilibrium when the interactions of the constituents do not change the momentum distributions and the densities of different types of particles in the plasma. The state of the plasma is then governed by the temperature T and various chemical potentials μ_i for the different particles i.

We do not know whether the system created in heavy ion collisions does reach thermal and chemical equilibrium so that one can use statistical QCD to describe these collisions. There should be sufficient scattering and re-scattering of incident and produced particles so that thermalisation occurs (i.e all particles in the fireball can be described by one temperature). When the measured transverse energy, E_T, is compared with event generators (with and without scattering) it seems that a large degree of scattering and re-scattering does indeed take place [18]. Thus, although we do not know for sure if we have achieved thermal equilibrium in current heavy ion collision experiments, local thermalisation might have been reached. So, it is worthwhile to review some thermodynamical properties of a system at equilibrium.

In an infinitely large system with temperature T, the particle density is proportional to

$$d^3n \propto \frac{1}{e^{(E-\mu)/T} \pm 1} d^3p \ , \tag{1.5}$$

according to Bose-Einstein statistics for bosons (minus sign) and Fermi statistics for fermions (plus sign). Here μ is the chemical potential, the energy needed to add one more particle in the system, $\mu = dE/dN$. For $e^{(E-\mu)/T} \gg 1$, which generally holds for heavy particles or in classical system in which the particle population per state is low, Eq. 1.5 reduces to the Boltzmann approximation

$$d^3n \propto e^{-E/T} d^3p \ . \tag{1.6}$$

Let's first consider a high temperature system with a vanishing net baryon number. Assume that QGP is formed in such a system, so that we can treat quarks and gluons thermodynamically as non interacting point particles. Equal numbers of quarks and anti-quarks require them to have a vanishing chemical potentials. Therefore the number density of quarks is given by integrating the fermion statistical distribution

$$n_q = n_{\bar{q}} = \frac{g_q}{2\pi^2} \int_0^\infty \frac{p^2 dp}{e^{p/T} + 1} \simeq \frac{0.9}{\pi^2} g_q T^3 \ , \tag{1.7}$$

where g_q is the quark degeneracy number. Gluons with vanishing chemical potential as well, can be treated in the same manner as photons in an open system such as blackbody radiation. The number density of gluons is given by integrating the boson distribution,

$$n_g = \frac{g_g}{2\pi^2}\int_0^\infty \frac{p^2 dp}{e^{p/T}-1} \simeq \frac{1.2}{\pi^2} g_g T^3 \ , \tag{1.8}$$

where g_g is the gluon degeneracy number. Both the above integrations involve a Riemann Zeta function. The mathematical detail is found in Appendix B. Quarks have three colors and are spin 1/2 particles. If we consider only the two light quarks (u,d), assumed massless in the above calculation, we get $g_q = g_{\bar{q}} = 12$. There are a total of 8 types of gluons and since gluons are spin-1 massless particles, then $g_g = 16$. For QGP with $T \approx 200\ MeV$ we solve Eqs. 1.7 and 1.8 to get number densities of quarks, anti-quarks and gluons, $n_q = n_{\bar{q}} \approx 1.7/fm^3$ and $n_g \approx 2.0/fm^3$ respectively. This is of course a very simplistic calculation. A more sophisticated analysis [19] has shown that the strong coupling constant α_s (α_s =0.6 at 1 GeV energy scale) should be considered, resulting in

$$n_g = \frac{g_g}{2\pi^2}\int_0^\infty \frac{p^2 dp}{e^{p/T}-1}(1-\frac{15\alpha_s}{4\pi}) \ . \tag{1.9}$$

We will neglect the α_s term (not necessarily small but constant) in subsequent discussions. The energy density of the quarks or anti-quarks is given by

$$\varepsilon_q = \frac{g_q}{2\pi^2}\int_0^\infty \frac{p^3 dp}{e^{p/T}+1} = \frac{7}{8}\frac{\pi^2}{30} g_q T^4 \ , \tag{1.10}$$

and that of gluons is given by

$$\varepsilon_g = \frac{g_g}{2\pi^2}\int_0^\infty \frac{p^3 dp}{e^{p/T}-1} = \frac{\pi^2}{30} g_g T^4 \ . \tag{1.11}$$

For a QGP containing quarks and gluons, the energy density is then

$$\varepsilon_{QGP} = g\frac{\pi^2}{30}T^4, \tag{1.12}$$

with the degeneracy number

$$g = g_g + \frac{7}{8}(g_q + g_{\bar{q}}) = 37 \ . \tag{1.13}$$

At $T \approx 200\ MeV$, this gives an energy density of 2.54 GeV/fm^3. For a system of massless particles, the pressure is simply

$$P = \frac{1}{3}\varepsilon = g\frac{\pi^2}{90}T^4. \tag{1.14}$$

Recalling the phenomenological bag vacuum energy, B, in Eq. 1.3 we can obtain from Eq. 1.14 the critical temperature at which such a system breaks up,

$$T_c = \left(\frac{90}{37\pi^2}\right)^{1/4} B^{1/4} \sim 144\ MeV \ .$$

Now let's briefly consider a relativistic pion gas. Since pions are bosons, we can just use the same formalism that was used for the gluons, namely Eqs. 1.8 and 1.11, to calculate the number and energy density of the pions. However we use a different degeneracy number. The degeneracy number for pions is 3, accounting for the three types of pions (π^+, π^-, π^0). At $T \approx 200\ MeV$, this leads to $n_\pi \sim 0.38/fm^3$ and $\varepsilon_\pi \sim 0.21\ GeV/fm^3$.

From $dE = -PdV + TdS + \mu dN$, with vanishing μ in our case, we have an entropy density of

$$\frac{dS}{dV} = \frac{\varepsilon + P}{T} \ , \tag{1.15}$$

or an entropy per particle of

$$\frac{dS}{dN} = \frac{\varepsilon + P}{nT} \ . \tag{1.16}$$

Using Eqs. 1.7, 1.8, 1.10, 1.11 and 1.14 we get

$$\left(\frac{dS}{dN}\right)_{boson} \approx 0.037\pi^4 \ , \tag{1.17}$$

$$\left(\frac{dS}{dN}\right)_{fermion} \sim 0.043\pi^4 \ , \tag{1.18}$$

for bosons and fermions respectively. The entropy needed to create a pion is (≈ 3.6) in a pion gas. The entropy needed to create a quark or an anti-quark is ($\approx 1.4\ units$) and that for a gluon is ($\approx 1.2\ units$) in a quark gluon plasma. The difference in the entropy values between the QGP and the pion gas lies in the huge difference in their degeneracy numbers. The QGP has 37 degrees of freedom, while the pion has only 3. The entropy needed to produce all types of particles in the QGP is therefore much greater than that required to produce all types of particles in a hadronic pion gas.

Now let's consider a quark matter with a high baryon density. Because of the asymmetry in the numbers of quarks and antiquarks, $n_q << n_{\bar{q}}$, the chemical potentials for quarks, μ_q,

and for the antiquarks, $\mu_{\bar{q}} = -\mu_q$, are not zero any longer. For simplicity we shall constrain ourselves to the extreme case, T =0, only.

The quark density is given by

$$n_q = \frac{g_q}{(2\pi)^3} \int_0^{\mu_q} 4\pi p^2 dp = \frac{g_q}{6\pi^2} \mu_q^3 \,, \tag{1.19}$$

Similarly, the energy density is

$$\varepsilon_q = \frac{g_q}{8\pi^2} \mu_q^4 \,,$$

and the degeneracy pressure is $P_q = \frac{1}{3}\varepsilon$. Considering the bag model, deconfinement requires

$$\mu_q = \left(\frac{24\pi^2}{g_q} B \right)^{1/4} \,. \tag{1.20}$$

To compress ordinary nuclear matter to produce the QGP, we need $\mu_{u,d} = 430$ MeV and $n_B = \frac{1}{3} n_q = 0.7/fm^3$, compared to $\mu_{u,d} \approx 260 MeV$ and $n_B \approx 0.17/fm^3$ in an ordinary nuclear matter.

1.5 Signatures of QGP

Many signatures of QGP have been proposed several years ago and the most prominent ones are :

1. *Dilepton Production*,
2. *J/ψ Suppression*,
3. *Photon Production*,
4. *Strangeness Production*.

The J/ψ suppression and strangeness enhancement (e.g the K^+/π^+ ratio) have been seen in experiments. (For strangeness production and the K/π ratio, see Chapter 4). Unfortunately, no signature for QGP formation seems unique. It is unlikely that QGP will be created at current available energies in heavy ion collisions. However, heavy ion experiments at the *Relativistic Heavy Ion Collider* (RHIC) at BNL, scheduled to start in the year 2000, will

open a new chapter on heavy ion physics research. There, thermal and chemical equilibrium, necessary steps towards QGP formation, will be expected. If a transition from hadronic matter to QGP takes place, dramatic differences in dynamical observables from a hadronic gas fireball and a QGP would allow us to ask if deconfinement of quarks is experimentally achieved, and if so, what the properties of the QGP are.

1.5.1 Motivations for these QGP Signatures

- Dilepton and Photon production

The measurement of dileptons has always been emphasized as one of the most relevant probes to study the dynamics of relativistic heavy ion collisions. The argument is simple and was first proposed by Shuryak more than fifteen years ago [21]. Since the dileptons interact with the particles in the collision region only through the electromagnetic interaction, the interaction is not strong. Consequently the mean free path of the produced dileptons is quite large compared to the size of the system formed in these collisions; therefore once produced they can leave the interaction region and reach the detectors without any further interaction, carrying with them information about the conditions and properties of the matter at the time of their production. Dileptons can be emitted throughout the entire lifetime of the collision, from the hot early stages up to long after freeze-out time when hadrons cease to interact. However, since the emission rate is a strongly increasing function of the temperature, they are produced most abundantly at the early stages when the temperature and the energy density have their largest values, thus making them a potential signature of QGP formation. Of more interest is the identification of the thermal radiation emitted once the system reaches thermal equilibrium, during the expansion and cooling phases up to freeze-out. The thermal radiation could tell us about the nature of the matter formed, the conjectured quark-gluon plasma (QGP) or a high-density hadron gas (HG). The motivation to search for direct photons is the same as for the measurement of the dileptons since real and virtual photons carry the same physics information. Single direct photons are therefore expected to be emitted as thermal radiation by the hot and dense matter formed at the early stages of the collision in analogy to the thermal dileptons.

- J/ψ Suppression

The suppression of J/ψ was one of the first predicted signatures of deconfinement [22]. The suppression results from the Debye color screening effect of the plasma. The Debye screening length is inversely proportional to the temperature. At high temperatures, the range of the attractive interaction becomes so small, and this makes it impossible for a $c\bar{c}$ pair, formed

in the initial hard collisions mainly via gluon fusion $gg \longrightarrow c\bar{c}$, to form a J/ψ bound state because the color screening radius will be smaller than the size of the J/ψ. The $c\bar{c}$ pair separates into a c quark and a $\bar{c}$ antiquark in the plasma. The c quark and $\bar{c}$ antiquark subsequently hadronize by combining with light quarks or light anti quarks appearing later as two open charm mesons such as $D(c\bar{u},$ and $c\bar{d})$ and $\overline{D}(\bar{c}u,$ and $\bar{c}d)$. If a quark-gluon plasma is formed in the region of J/ψ production, then the effect of the plasma will be to make the J/ψ particle unbound, and the final yield of J/ψ particles will be suppressed, as compared with the case when there is no quark-gluon plasma. Using the same picture, a stronger suppression is predicted for the ψ' which is less bound and has a radius almost twice as large as that of the J/ψ. The suppression was also predicted to decrease with p_T since a fast $c\bar{c}$ may escape the medium before forming the J/ψ.

1.6 Thesis Goals

In this thesis, we study the particle production and the hadronic ratios. We investigate the dependence of the particle production and hadronic ratios on the size of the system. Of more interest will be the kaon production and the K/π ratio. Mostly we compare the behaviour of the experimental information to the model expectations. However, in some cases we directly compare the experimental data to the model.

The thesis is organized in the following way: In Chapter 2, the statistical formalisms to describe a hadronic gas with more emphasis on the canonical formalism is presented. In Chapter 3, the results of a hadronic gas model are discussed. In Chapter 4, the experimental information in comparison to the hadronic gas model expectations is reviewed. The application of the hadronic gas model to the experimental data is made for comparison.

Chapter 2

Canonical Description of a Hadronic Gas

2.1 Relativistic Statistical Thermodynamics of a Hadron Gas

The subject of statistical thermodynamics in strongly interacting matter has been studied since more than twenty years ago [23, 24, 25]. For a review see also [26]. In high-energy hadron-hadron and heavy ion collisions, a hadronic matter which is hot and not in peaceful equilibrium is formed. This highly excited matter is called a fireball and is in a state of collective motion. Because this fireball is hot, one can use thermodynamics to describe its conditions and because it is not in total thermodynamic equilibrium, one should also consider relativistic kinematics. Thus, in order to describe what happens in high-energy ion collision one combines thermodynamics and relativistic kinematics. In order to apply equilibrium thermodynamics to this highly excited hadronic matter, an assumption is made that collective motions appear only in the direction of the collision axis and do not give rise to turbulence. Also one assume that heat motion is small and nearly independent of the collision energy. In this work, the hadron gas consists of infinitely many components. Hence one talks of strong interactions. The resonant states of strong interactions will also be treated

as particles in their own right. Because particles can be created and absorbed one will have many degrees of freedom, even if the average number of created real particles is relatively small. Our system decays in about $10^{-23}s$ and somehow equilibrium must be achieved in an even shorter span of time. This cannot go via many collisions among each other of already created secondaries. This equilibrium, if it exists, must therefore be something instantaneous and at least taking much less than $10^{-23}s$ to establish it. It turns out that particles seem to be created into pre-established equilibrium [25]. Relativistic statistical thermodynamics is applied in some parts of high-energy physics ranging from cosmology to particle collisions in the laboratory. Let us assume that our system has the requirements which lead one to use a thermodynamic description.

2.2 Canonical versus Grand Canonical

In the nonrelativistic limit particle numbers are conserved since the energies are small compared to the masses of the particles. However, in relativistic heavy ion collision, where the space-time regions and number of particles involved are larger than in collisions of elementary particles and where it is hoped that the phase transition to quark gluon plasma might be observed experimentally, and where particles can be created from kinetic energy, it seems reasonable to further develop equilibrium thermodynamics. In this section we shall address ourselves to one particular question as done by Hagedorn and Redlich [27]. In particular we want to see when can one use canonical or/and grand canonical treatment of conservation laws. In non-relativistic thermodynamics particle numbers are, in the absence of chemical reactions, conserved. Therefore the canonical N-particle partition function is essential. For an ideal gas it reads

$$Z_N(T,V) = \frac{1}{N!} Z_1(T,V)^N \ , \tag{2.1}$$

where $Z_1(T,V)$ is the one particle partition function. To go to the grand canonical partition function one introduces the fugacity $\lambda \equiv \exp(\mu/T)$. The grand canonical partition function Z(T,V,λ) is then given by

$$Z(T,V,\lambda) = \sum_{N=0}^{\infty} \frac{\lambda^N}{N!} Z_1(T,V)^N = \exp[\lambda Z_1(T,V)] \ .$$

Now only the average particle number $< N >$ is determined :

$$\begin{aligned} < N > &= \frac{\sum \frac{\lambda^N}{N!} Z_1^N}{\sum N \frac{\lambda^N}{N!} Z_1^N} \\ &= \lambda \frac{\partial}{\partial \lambda} \ln Z(T, V, \lambda) \\ &= \lambda Z_1(T, V) \ . \end{aligned} \tag{2.2}$$

One only has to choose

$$\lambda = \frac{< N >}{Z_1} \ .$$

to obtain a prescribed particle number.

In the case of relativistic thermodynamics, particles can be created from kinetic energy and thus the particle number N is not conserved. One cannot, therefore, use the canonical partition function for N particles. One uses the grand canonical partition function with $\lambda = 1$ (after differentiations) or equivalently with the chemical potential $\mu = 0$ after differentiations.

If there are K kinds of particles then one introduces an extra λ_i for each kind i (Z $= Z_1 ... Z_K$):

$$\ln Z(T, V, \lambda_1 ... \lambda_K) = \sum_{i=1}^{K} \lambda_i Z_1^{(i)}(T, V)$$

$$< N_i >= \lambda_i \frac{\partial}{\partial \lambda_i} \ln Z \Big|_{\lambda_1 = \lambda_2 = ... = \lambda_K = 1} \ . \tag{2.3}$$

In view of the above, we see that with respect to particle numbers we are forced, in relativistic statistical thermodynamics, to use only the grand canonical formalism with all $\lambda_i = 1$ (after differentiations). It is also clear that all conservation laws can be treated grand canonically by introducing a chemical potential for each conserved quantity. However, since conservation laws do impose constraints on particle production, with respect to conservation laws we have, in relativistic statistical thermodynamics, the choice between the canonical and grand canonical formalisms [24]. That is, in a relativistic system, where particle production and annihilation are possible, the concept of particle number conservation has to be replaced by conservation of quantum numbers. As pair production (at quark level language) is a generating process for strangeness, the following internal conservation law of hadronic matter has to be taken into account : conservation of electric charge, baryon number, and strangeness. In

view of the fluctuations inherent in statistical thermodynamics it seems necessary, however, to use the canonical formalism and compare the results. In our calculations, the canonical case is extensively discussed and the results are compared to the grand canonical case. The use of canonical formalisms has been considered by many people [28, 29, 30, 31, 32]. We neglect quantum statistics. Thus we assume temperature and density regimes such that all particles can be treated as Boltzmann particles. The generalization to quantum statistics is straight-forward but the formulae are much more complicated. For the inclusion of quantum statistics see for example [33, 34, 35]. For the temperatures to be considered later the distinction doesn't play any role. We also neglect interactions, thus dealing with ideal Boltzmann gases. In our calculations we presently do not include electric charge since the computation becomes complicated (but for a system which is symmetric in the number of neutrons and protons, it is a simple case). It was shown [34] that isospin conservation in $p\overline{p}$ annihilations leads to certain changes in the statistical distributions, which can be accounted for by changing the volume, and/or temperature of the fireball. It is also easy to incorporate charge conservation in the grand canonical formalism than in canonical formalism in terms of computation. Our considerations are for the gas which is composed of all resonances found in the Particle Physics Data Book [36]. We shall consider the gas which contains particles with strangeness quantum number up to $S_{\pm 3}$.

2.3 Exact baryon number (B) conservation

It was shown by Hagedorn [23] many years ago that the production of heavy particles in high-energy proton-proton collisions calls for the use of the canonical ensemble. In particular he showed that the production of $\overline{^3He}$ is wrong by seven orders of magnitude when the grand canonical ensemble in its standard form is used. It is known that the number of kaons as well as the number of heavy antibaryons being produced in nucleon-nucleon collisions is too small. In view of this, Hagedorn argued that in order to produce a heavy particle like $\overline{^3He}$, it is necessary to produce an extra three nucleons in order to have baryon number conservation. Thus

$$p + p \longrightarrow \overline{^3He}\ (m_{He} \approx 3m_p) + X\ ,$$

where X could be anything.
The number of produced anti-helium-3 is $\propto e^{\frac{-E_{\overline{^3He}}}{T}}$ where T is $\sim$ 150-160 MeV, and this is $\approx e^{-18}$ which is very small. So the Boltzmann factor which determine the number becomes effectively :

$$\exp(-6m_N/T) \ ,$$

instead of

$$\exp(-3m_N/T) \ ,$$

as would be appropriate for $\overline{^3He}$. Thus one should have at least 3 more protons in addition to the original two. Hagedorn showed that one would then have the number of $\overline{^3He} \sim e^{\frac{-6m_p}{T}}$ which gives the correct answer.

Thus there should be net baryon number conservation:

$$p + p \longrightarrow \overline{^3He} + p + p + p + p + p \ .$$

On the right hand $B = 2$ and on the left $B = 2$.

We start with the simple case of the $p+\overline{p}$ and $p+p$ collisions. For $p+\overline{p}$ collision one considers a gas of one sort of baryons and antibaryons with baryonic charges ± 1 respectively. The net baryon number $B = N(\text{baryons}) - \overline{N}(\text{antibaryons})$ is conserved, while N and $\overline{N}$ individually are not. In order to control B we introduce a baryon fugacity λ_B (or correspondingly the baryon chemical potential μ_B) exclusively related to conservation law. Since the one particle partition function depends only on the temperature, T, volume, V, and the mass, m, of the particle, it is the same for particles and antiparticles.

From the statistical trace

$$Z = \mathrm{Tr}\left[e^{-\frac{(E-\mu N)}{T}}\right] \ , \tag{2.4}$$

and using the "Kronecker delta" or rather the integral representation of the δ function,

$$\delta_{n,m} = \frac{1}{2\pi}\int_0^{2\pi} d\phi e^{i(n-m)} \ ,$$

we get the partition function with the total baryon number, B,

$$Z_B = \frac{1}{2\pi}\int_0^{2\pi} d\phi e^{-iB\phi} \exp(Z_p^1 e^{i\phi} + Z_{\overline{p}}^1 e^{-i\phi}) \ , \tag{2.5}$$

where

$$Z_p^1(T,V) = V\int \frac{d^3p}{(2\pi)^3} e^{-\frac{E_p}{T}} \ .$$

Thus the way of incorporating baryon quantum number conservation in statistical mechanics is to restrict the statistical trace to only those states having the required quantum number(s). This may be done by defining the Restricted Partition Function,

$$Z_B(T,V) = \frac{1}{2\pi}\int_0^{2\pi} d\phi \exp(-iB\phi)\overline{Z}(T,V,\phi) \ ,$$

where B refers to the fixed (exact) overall Baryon number the gas possesses and $\overline{Z}(T,V,\phi)$ is the function obtained by substituting $\phi = -i\beta\mu$ in the usual statistical trace. Here μ is the chemical potential conjugate to the conserved charge(s). For a brief review of the above result see for example [37] and [38].

$$\begin{aligned} Z_B &= \frac{1}{2\pi}\int_0^{2\pi} d\phi e^{-iB\phi} \sum_{n=0}^{\infty} \frac{(Z_p^1)^n e^{in\phi}}{n!} \sum_{m=0}^{\infty} \frac{(Z_{\overline{p}}^1)^m e^{-im\phi}}{m!} \\ &= \sum_{n=0}^{\infty} \frac{(Z_p^1)^n}{n!} \sum_{m=0}^{\infty} \frac{(Z_{\overline{p}}^1)^m}{m!} \frac{1}{2\pi}\int_0^{2\pi} d\phi e^{-iB\phi+in\phi-im\phi} \ . \end{aligned}$$

Replacing n by $m+B$ (recall $n-m=B$) we get,

$$\begin{aligned} Z_B &= \sum_{m=0}^{\infty} \frac{1}{m!(m+B)!} (Z_p^1)^{m+B} (Z_{\overline{p}}^1)^m \\ &= (Z_p^1)^B \sum_{m=0}^{\infty} \frac{1}{m!(m+B)!} (Z_p^1 Z_{\overline{p}}^1)^m \ . \end{aligned}$$

Using Eq. (9.6.10) of [20], i.e using Bessel Functions of the form ,

$$I_\nu(z) = \left(\frac{1}{2}z\right)^\nu \sum_{k=0}^{\infty} \frac{(\frac{1}{4}z^2)^k}{k!\Gamma(\nu+k+1)} \ ,$$

we can see that

$$I_B(z) = \left(\frac{z}{2}\right)^B \sum_{m=0}^{\infty} \frac{(\frac{1}{4}z^2)^m}{m!(m+B)!} \ .$$

and this allows us to write the general expression of Z_B in terms of I_B as

$$Z_B = (Z_p^1)^B \frac{I_B\left(2\sqrt{Z_p^1 Z_{\overline{p}}^1}\right)}{(Z_p^1 Z_{\overline{p}}^1)^{B/2}} \ , \tag{2.6}$$

where we have made use of

$$z = \sqrt{Z_p^1 Z_{\overline{p}}^1} \ .$$

Assuming $Z_p^1 = Z_{\overline{p}}^1$, we get

$$Z_B = I_B(2Z_p^1) \ . \tag{2.7}$$

2.3.1 Particle Number for the case B=0

We now want to find the number of particles in the canonical ensemble and compare this to the grand canonical case. Here the number of particles equals the number of anti-particles.

Canonical

We use Eq. 2.6 with $B = 0$ and introduce a chemical potential, which is set to zero after differentiation. Thus

$$Z_{B=0} = I_0\left(2\sqrt{Z_p^1 Z_{\overline{p}}^1 e^{\frac{\mu_p}{T}}}\right) .$$

The average proton number is then given by

$$< N_p >= T\frac{1}{Z_B}\frac{\partial Z_B}{\partial \mu_p}\bigg|_{\mu_p=0} . \tag{2.8}$$

We obtain the following expression after differentiation (and noting that $\frac{d}{dz}I_0(z) = I_1(z)$)

$$< N_p >= \sqrt{Z_p^1 Z_{\overline{p}}^1}\frac{I_1\left(2\sqrt{Z_p^1 Z_{\overline{p}}^1}\right)}{I_0\left(2\sqrt{Z_p^1 Z_{\overline{p}}^1}\right)} .$$

For $Z_p^1 = Z_{\overline{p}}^1$,

$$< N_p >= Z_p^1\frac{I_1(2Z_p^1)}{I_0(2Z_p^1)} . \tag{2.9}$$

Since $< N_p > - < N_{\overline{p}} >= B = 0$,

$$< N_p >=< N_{\overline{p}} > .$$

Grand Canonical

Considering the proton part for $B = 0$, the grand canonical partition function is given by,

$$Z_{GC} = \exp\left(V\int\frac{d^3p}{(2\pi)^3}e^{-\frac{E}{T}+\frac{\mu_p}{T}}\right) .$$

The mean number of protons is then

$$\begin{aligned} < N_p > &= T\frac{1}{Z_{GC}}\frac{\partial Z_{GC}}{\partial \mu_p} \\ &= V\int \frac{d^3p}{(2\pi)^3} e^{-\frac{E}{T}} . \end{aligned} \tag{2.10}$$

(Recall: $< N_p >=< N_{\overline{p}} > \Longrightarrow \mu_p = 0$.)

2.3.2 Particle Number for the case $B \geq 0$

This case implies that one is now dealing with the number of particles greater than the number of antiparticles.

Canonical

Again starting with the expression for Z_B,

$$Z_B = \sum_{m=0}^{\infty} \frac{(Z_p^1)^{m+B}(Z_{\overline{p}}^1)^m}{m!(m+B)!} ,$$

and introducing a chemical potential μ_p (which is set to zero after differentiations) in the expression, one finds the average number of protons evaluated as before by

$$< N_p >= T\frac{1}{Z_B}\frac{\partial Z_B}{\partial \mu_p}\bigg|_{\mu_p=0} ,$$

which gives

$$< N_p >= \sqrt{Z_p^1 Z_{\overline{p}}^1}\frac{I_{B-1}\left(2\sqrt{Z_p^1 Z_{\overline{p}}^1}\right)}{I_B\left(2\sqrt{Z_p^1 Z_{\overline{p}}^1}\right)} .$$

For $Z_p^1 = Z_{\overline{p}}^1$,

$$< N_p >= Z_p^1\frac{I_{B-1}(2Z_p^1)}{I_B(2Z_p^1)} . \tag{2.11}$$

Similarly, for antiprotons

$$< N_{\overline{p}} >= Z_p^1\frac{I_{B+1}(2Z_p^1)}{I_B(2Z_p^1)} .$$

Grand Canonical

For the case where $B \geq 0$, one has now baryon chemical potential μ_B. The average particle numbers are given by,

$$< N_p >= V \int \frac{d^3p}{(2\pi)^3} e^{-\frac{E}{T}+\frac{\mu_B}{T}} \quad , \tag{2.12}$$

$$< N_{\overline{p}} >= V \int \frac{d^3p}{(2\pi)^3} e^{-\frac{E}{T}-\frac{\mu_B}{T}} \quad , \tag{2.13}$$

where now μ_B is given by

$$\mu_B = T \sinh^{-1} \left(\frac{B}{2V \int \frac{d^3p}{(2\pi)^3} e^{-\frac{E}{T}}} \right) .$$

This result can be generalised not only for the gas of protons and antiprotons, but also for other non-strange baryons and mesons. The inclusion of non-strange mesons in addition to the proton-antiproton gas e.g pions would lead us to the partition function expression

$$Z = (Z_p^1)^B \frac{I_B\left(2\sqrt{Z_p^1 Z_{\overline{p}}^1}\right)}{(Z_p^1 Z_{\overline{p}}^1)^{B/2}} \cdot \exp(Z_\pi^1 e^{\frac{\mu_\pi}{T}}) \quad , \tag{2.14}$$

and as before,

$$\begin{aligned} < N_\pi > &= T \frac{1}{Z} \frac{\partial Z}{\partial \mu_\pi} |_{\mu_\pi = 0} \\ &= Z_\pi^1 \end{aligned}$$

which is nothing else but

$$= V \int \frac{d^3p}{(2\pi)^3} e^{-\frac{E_\pi}{T}} .$$

And if one adds the non-strange baryons e.g the deltas one has as the expression for the partition function

$$\begin{aligned} Z_B &= \frac{1}{2\pi} \int_0^{2\pi} d\phi e^{-iB\phi} \exp[(Z_p^1 + Z_\Delta^1)e^{i\phi} + (Z_{\overline{p}}^1 + Z_{\overline{\Delta}})e^{-i\phi}] \\ &= (Z_1)^B \frac{I_B\left(2\sqrt{Z_1 \overline{Z_1}}\right)}{(Z_1 \overline{Z_1})^{B/2}} \quad , \end{aligned} \tag{2.15}$$

where $Z_1 = Z_p^1 + Z_\Delta^1$ and $\overline{Z_1} = Z_{\bar{p}}^1 + Z_{\bar{\Delta}}^1$.

Continuing like this one can include all the non-strange baryons and mesons with

$$Z_1 = Z_p^1 + Z_\Delta^1 + Z_{\Delta^*}^1 + Z_{N^*}^1 + Z_n^1 + \cdots \text{, for non-strange baryons;}$$

$$\overline{Z_1} = Z_{\bar{p}}^1 + Z_{\bar{\Delta}}^1 + Z_{\bar{\Delta}^*}^1 + Z_{\bar{N}^*}^1 + Z_{\bar{n}} + \cdots \text{, for non-strange anti-baryons;}$$

$$Z_M = Z_\pi + Z_\rho + Z_\phi + \cdots \text{, for non-strange mesons;}$$

and we get the general expression

$$Z_{B+M} = (Z_1)^B \frac{I_B\left(2\sqrt{Z_1\overline{Z_1}}\right)}{(Z_1\overline{Z_1})^{B/2}} \exp(Z_M) \,. \tag{2.16}$$

Actually, the one particle partition function for a particle i is generally written as

$$Z_i^1 = g_i \int \frac{d^3p}{(2\pi)^3} e^{-\frac{\sqrt{p^2+m_i^2}}{T}} \,, \tag{2.17}$$

where g_i is the degeneracy and m_i is the mass of particle i, (e.g degeneracy for Δ is $4 \times 4 = 16$.)

The general expressions for the mean particle number in the canonical and grand canonical ensembles can be written as before.

In the Canonical ensemble

$$< N_{\substack{i \\ \bar{i}}} >= Z_i \frac{I_{B\mp1}(2Z_1)}{I_B(2Z_1)} Z_0 \,, \tag{2.18}$$

as before, Z_i is the one particle partition function for particle i, and Z_1 is the sum of all one particle partition functions for all particles of the same baryon quantum number as particle i (and in this case it implies all B_{+1} and S_0) and again since the one particle partition function depends on T, V, and the mass of the particle it is therefore the same for particles and antiparticles. Z_0 is the sum of all partition functions of particles with baryon quantum number 0 and strangeness 0 (i.e B_0 and S_0) which are the non-strange mesons. Thus we talk of all non-stange baryons and antibaryons of $B_{\pm1}$, where

$$Z_i = Z_{\bar{i}} \,,$$

and

$$Z_{\bar{1}} = \overline{Z_1} \,,$$

and where

$$Z_1 = \sum_{i \in B_{\pm 1}} g_i V \int \frac{d^3p}{(2\pi)^3} e^{-\frac{E_i}{T}} .$$

In the Grand Canonical ensemble

$$< N_i > = Z_i \cdot \exp\left(-\frac{\mu_B}{T}\right) Z_0 , \tag{2.19}$$

where now

$$\mu_B = T \sinh^{-1}\left(\frac{B}{2Z_1}\right) .$$

2.3.3 Results of Canonical vs Grand Canonical Ensembles

The results of the canonical versus grand canonical ensembles are shown in figures 2.1, 2.2 and 2.3. Figure 2.1 shows the ratio of the number of protons in the canonical ensemble $N_p^{B=0}$ to the number of protons in the grand canonical ensemble N_p^{GC} for the case of vanishing net baryon number as a function of the radius of the gas. One sees that as the volume grows, the ratio rises until it starts to saturate at the radius, $R \approx 7\ fm$. In nuclear collisions, the temperature and baryon chemical potential reached may vary depending on the conditions of the collisions. As figure 2.1 shows, the dependence on this variable is small. However, in

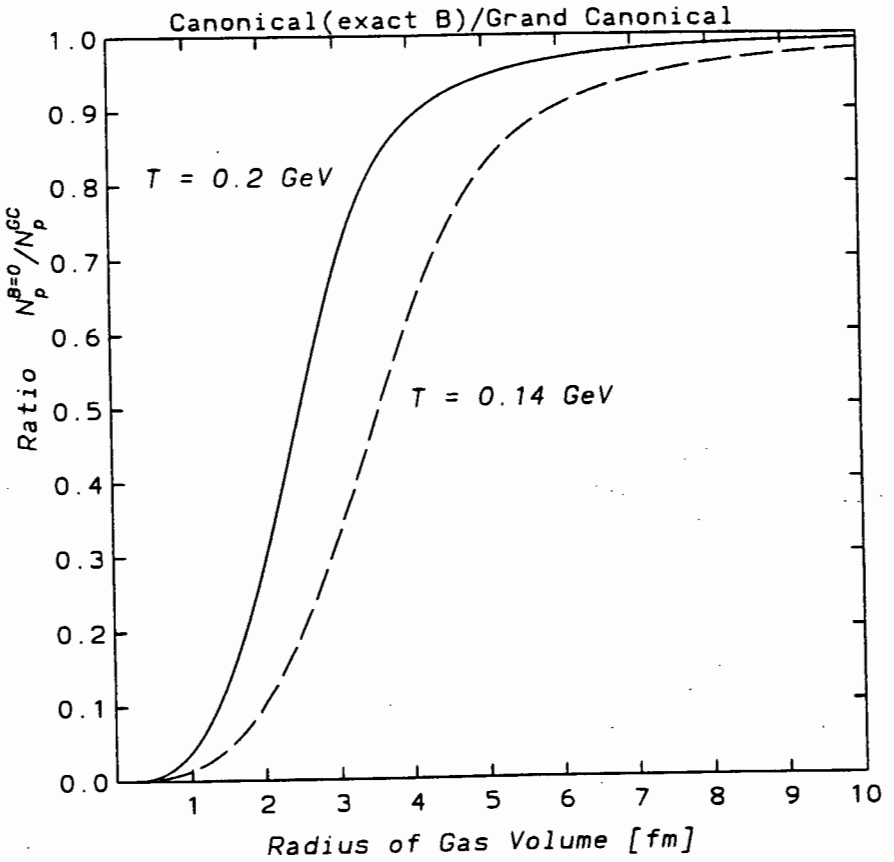

Figure 2.1: The ratio $\frac{N_p^{B=0}}{N_p^{GC}}$ as a function of the radius of the gas.

contrast, the dependence on the reaction volume is significant. Figure 2.2 shows the ratio $\frac{N_p^B}{N_p^{GC}}$ as a function of the radius of the gas for any B, and Figure 2.3 shows the ratio of the number of antiprotons in the canonical ensemble to the number of antiprotons in the grand canonical ensemble for any B. It can be seen that for smaller values of the gas volume and

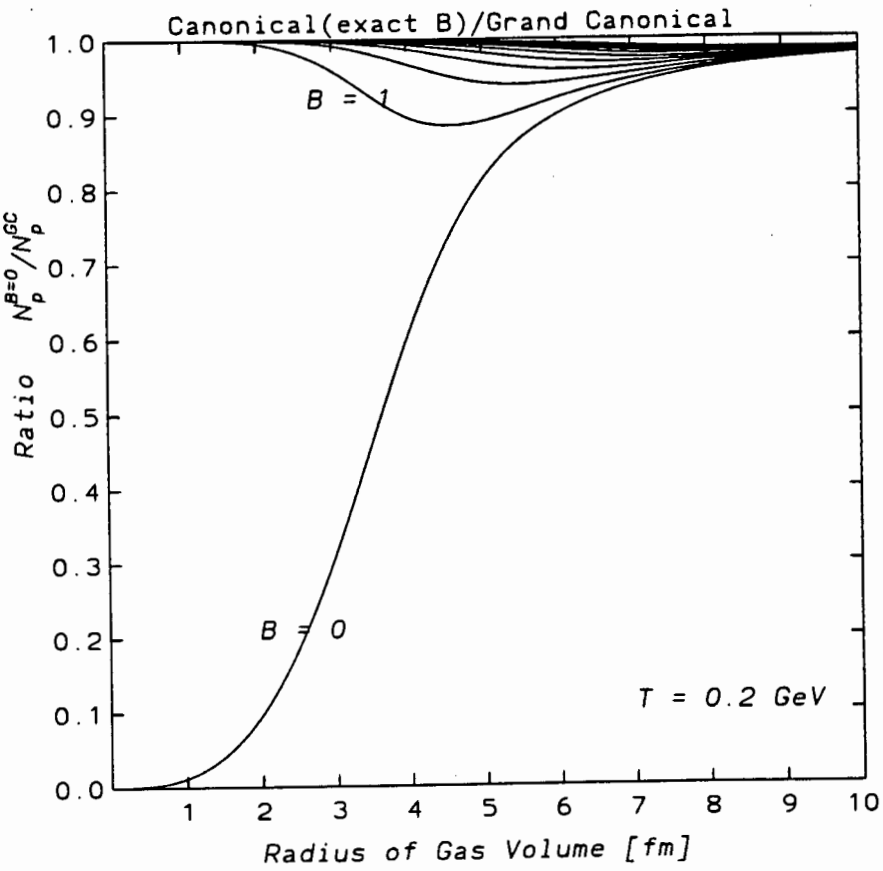

Figure 2.2: The dependence of $\frac{N_p^B}{N_p^{GC}}$ ratio on B is plotted as a function of the radius of the gas volume.

baryon number there are substantial deviations from the grand canonical ensemble. Here in Figs. 2.2 and 2.3, one notices that at smaller values of the radius, $R \leq 4\ fm$, the dependence of the ratios in B is very strong. However at large volumes, $R \approx 7\ fm$ the deviations are negligible. Thus when the radius of the gas is larger than about 7 fm and the baryon number B is larger than 30 (where the deviations to grand canonical are within the error of 5%), finite volume corrections are negligible and it is therefore justified to use grand canonical ensemble.

The behaviour of the figures 2.2 and 2.3 at the lower volume limit can be explained analytically. This is discussed below.

- The Small Volume Limit, $V \longrightarrow 0$

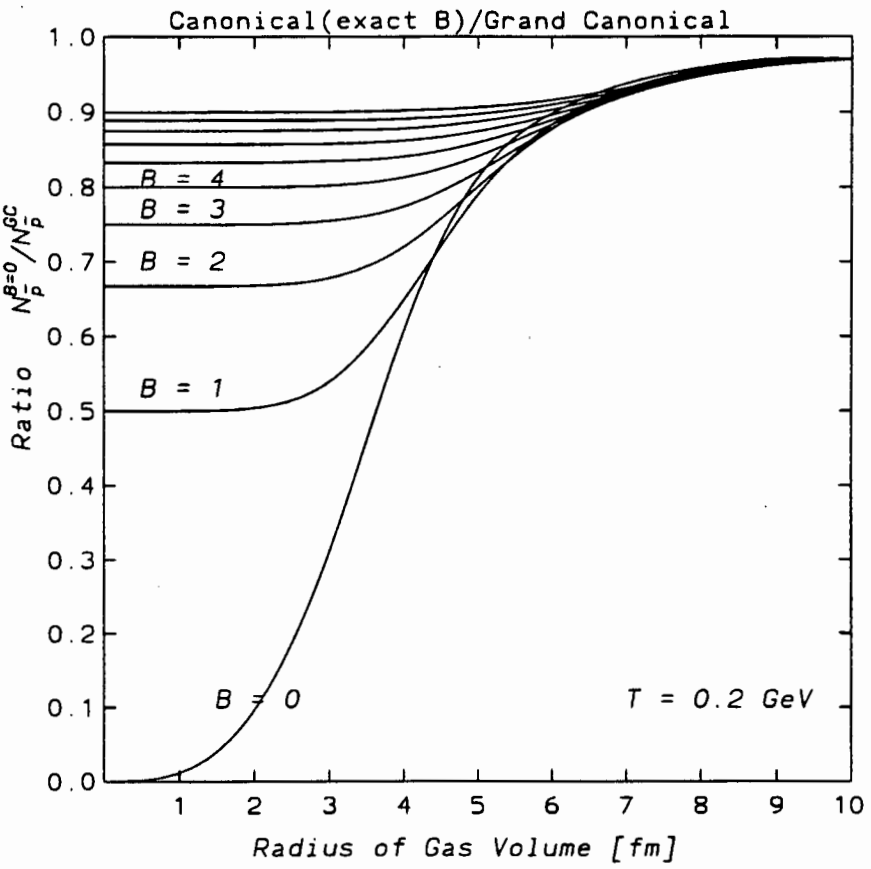

Figure 2.3: The dependence of $\frac{N_{\bar{p}}^{B}}{N_{\bar{p}}^{GC}}$ ratio on B is plotted as a function of the radius of the gas volume.

In the Canonical case we have for the protons and antiprotons

$$N_p^B = \frac{1}{2} x \frac{I_{B-1}(x)}{I_B(x)} \ , \tag{2.20}$$

$$N_{\bar{p}}^B = \frac{1}{2} x \frac{I_{B+1}(x)}{I_B(x)} \ , \tag{2.21}$$

where

$$x = 2\sqrt{Z_p^1 Z_{\bar{p}}^1} \ ,$$

and for

$$Z_p^1 = Z_{\bar{p}}^1 \ ,$$

we get

$$x = 2Z_p^1 \ .$$

Using Eq. 9.6.7 of [20] we have for a fixed B

$$\lim_{x\to 0} I_B(x) = \left(\frac{1}{2}x\right)^B /B! \ ,$$

and therefore

$$\lim_{x\to 0} N_p^B = \frac{1}{2}x\left[\frac{(\frac{1}{2}x)^{B-1}/(B-1)!}{(\frac{1}{2}x)^B/B!}\right] \ , \tag{2.22}$$

$$\lim_{x\to 0} N_{\bar{p}}^B = \frac{1}{2}x\left[\frac{(\frac{1}{2}x)^{B+1}/(B+1)!}{(\frac{1}{2}x)^B/B!}\right] \ . \tag{2.23}$$

In the standard Grand Canonical ensemble we have for the protons and antiprotons

$$N_p^{GC} = V\int \frac{d^3p}{(2\pi)^3} e^{-E_p/T+\mu_B/T} \ , \tag{2.24}$$

$$N_{\bar{p}}^{GC} = V\int \frac{d^3p}{(2\pi)^3} e^{-E_p/T-\mu_B/T} \ . \tag{2.25}$$

Recalling

$$N_p - N_{\bar{p}} = B = V\int \frac{d^3p}{(2\pi)^3} e^{-E_p/T}\left[e^{\mu_B/T} - e^{\mu_B/T}\right] \ ,$$

and using the identity $\frac{1}{2}[e^z - e^{-z}] = \sinh z$, where

$$\lim_{z\to\infty} \sinh z = \frac{1}{2}e^z$$

we get to the following expressions

$$\lim_{V\to 0}\left[e^{\mu_B/T} = \frac{B}{V\int \frac{d^3p}{(2\pi)^3} e^{-E/T}}\right] \ , \tag{2.26}$$

$$\lim_{V\to 0}\left[e^{-\mu_B/T} = \frac{V\int \frac{d^3p}{(2\pi)^3} e^{-E/T}}{B}\right] \ . \tag{2.27}$$

Thus in the small volume limit

$$\lim_{x\to 0} N_p^{GC} = B \ , \tag{2.28}$$

$$\lim_{x\to 0} N_{\bar{p}}^{GC} = \frac{1}{B}\left[V\int \frac{d^3p}{(2\pi)^3} e^{-E/T}\right]^2 \ , \tag{2.29}$$

and the ratios can be found from the following expressions

$$\lim_{V\to 0} \frac{N_p^B}{N_p^{GC}} = 1 \ , \tag{2.30}$$

$$\lim_{V\to 0} \frac{N_{\bar{p}}^B}{N_{\bar{p}}^{GC}} = \frac{B}{B+1} \ . \tag{2.31}$$

2.4 Exact strangeness (S) conservation

Strangeness conservation is also considered, especially in the case where one wants to treat baryon number grand canonically, and strangeness exactly (i.e treating strangeness canonically). This has been done for example by [39, 40].

2.4.1 Strangeness 0,±1

Let's start with the simple case where only particles carrying strangeness zero and ±1 are present. The partition function for this case is given by

$$Z_S^1 = \frac{1}{2\pi}\int_{-\pi}^{\pi} d\phi \exp(S_1 e^{i\phi} + S_{-1} e^{-i\phi} + S_0) \ , \tag{2.32}$$

where S_{-1} stands for the sum of all single-particle partition functions of all particles having strangeness -1 :

$$S_{-1} = Z_{\overline{K}} + Z_\Lambda + Z_{\overline{K^*}} + ... \quad ,$$

and S_1 stands for the sum of all single-particle partition functions of particle with strangeness $+1$:

$$S_{+1} = Z_K + Z_{\overline{\Lambda}} + Z_{K^*} + ... \quad ,$$

and S_0 is the sum of all single-particle partition functions of particles with strangeness zero. As an example, we quote the explicit form of Z_Λ assuming Boltzman statistics :

$$Z_\Lambda = \frac{V}{(2\pi)^3}\int d^3p \exp[(-E_\Lambda + \mu_B)/T] \ , \tag{2.33}$$

with μ_B being the baryon chemical potential. It is clear from the above equation that baryon number is being treated grand canonically. This is necessary because the baryon density is varying very strongly as a function of final state products. In the central rapidity region for example, it is known to be zero. To calculate the partition function in Eq. 2.32 more explicitly, we expand each term in the power series :

$$Z_S^1 = Z_0 \frac{1}{2\pi}\int d\phi \sum_{m=0}^{\infty}\sum_{n=0}^{\infty} \frac{1}{n!}\frac{1}{m!} \cdot S_1^m S_{-1}^n \exp(im\phi)\exp(-in\phi) \ , \tag{2.34}$$

where Z_0 is the standard partition function for all particles having zero strangeness. Performing the integration over ϕ we are left with :

$$Z_S^1 = Z_0 \sum_{n=0}^{\infty} \frac{1}{n!^2} (S_1 S_{-1})^n \ , \tag{2.35}$$

which is the result of [39] similar to that of [40].

In each term of Eq. 2.35 one sees explicitly strangeness conservation at work. This is so because each term in the sum is the product of strangeness $+1$ multiplied by strangeness -1. The series in Eq. 2.35 converges to a modified Bessel function

$$Z_S^1 = Z_0 I_0(x_1) \ , \tag{2.36}$$

where $x_1 \equiv 2\sqrt{S_1 S_{-1}}$. As an example, we quote the density of kaons deduced from the above expression

$$N_K = Z_K \frac{I_1(x_1)}{I_0(x_1)} \ .$$

Since the kaon contains an anti-strange quark, it has to be compensated by a hadron containing a strange quark. This is explicitly shown in Eq. 2.35 by the presence of the factor S_1, all other factors balance the number of anti-strange hadrons. The expression should be compared to the standard result in the grand canonical ensemble,

$$N_K = Z_K \exp(\mu/T) \ .$$

The difference being that one sees explicitly, that for every kaon produced, the system must also contain a particle with opposite strangeness, so as to conserve the overall zero strangeness of the system.

2.4.2 Strangeness ± 2

For a gas containing particles having strangeness $0, \pm 1$ and ± 2 the partition function becomes,

$$Z_S^2 = \frac{1}{2\pi} \int_{-\pi}^{\pi} d\phi \exp(S_0 + S_1 e^{i\phi} + S_{-1} e^{-i\phi} + S_2 e^{2i\phi} + S_{-2} e^{-2i\phi}) \ , \tag{2.37}$$

where S_2 stands for the sum of the single-particle partition functions of particles having strangeness $+2$,

$$S_2 = Z_{\overline{\Xi^-}} + Z_{\overline{\Xi^*}} + ... \quad ,$$

and correspondingly, S_{-2} is the sum of all single-particle partition functions of particles with strangeness -2 ,

$$S_2 = Z_{\Xi^-} + Z_{\Xi^*} + ... \quad ,$$

One sees that, in order to produce a Ξ hyperon one has to match it with two particles having strangeness -1, or with one anti-hyperon.

2.4.3 Strangeness ± 3

Finally, we consider here the most general case where particles with strangeness ± 3 are included in the hadronic gas. The partition function reads :

$$Z_S^3 = \frac{1}{2\pi}\int_{-\pi}^{\pi} d\phi \exp(S_0 + S_1 e^{i\phi} + S_{-1}e^{-i\phi} + S_2 e^{2i\phi} + S_{-2}e^{-2i\phi} + S_3 e^{3i\phi} + S_{-3}e^{-3i\phi}) \quad ,(2.38)$$

where S_3 stands for the sum of the single-particle partition functions of particles having strangeness $+3$:

$$S_3 = Z_{\overline{\Omega^-}} + ... \quad ,$$

and S_{-3} stands for the sum of the single-particle partition functions of particles having strangeness -3 :

$$S_{-3} = Z_{\Omega^-} + ... \quad ,$$

Proceeding similarly as in the previous example, one can calculate the particle number densities for different strange particles. For the results see for example [39, 40].

In the case where one considers a gas with arbitrary strangeness, the partition function given by Eq. 2.32 is generalized to the following form ,

$$Z_S^N = \frac{1}{2\pi}\int_{-\pi}^{\pi} d\phi \exp\left[\sum_{k=-N}^{N} S_k e^{ik\phi}\right] \quad , \qquad (2.39)$$

where S_k is the sum of the single particle partition functions having strangeness k. Using the symmetry properties of the integrand in the above equation, the partition function Z_S^N can be written as

$$Z_S^N = Z_0 \frac{1}{2\pi} \int_{-\pi}^{\pi} d\phi \exp\left[\sum_{k=1}^{N}(S_k - S_{-k}) \sin k\phi\right] \cdot \exp\left[\sum_{k=1}^{N}(S_k + S_{-k}) \cos k\phi\right] \quad . \qquad (2.40)$$

This form shows explicitly that Z_S^N is a real quantity. However, due to the cos terms under the integral, the numerical evaluation of the partition function and different particle numbers is not easy.

2.4.4 Strangeness in $p\bar{p}$ gas

Figure 2.4 shows the dependence of the correction factor η on the volume in units of V_h for different temperatures and associated chemical potential taken from [40]. It can clearly be seen that the behaviour is the same as for our results.

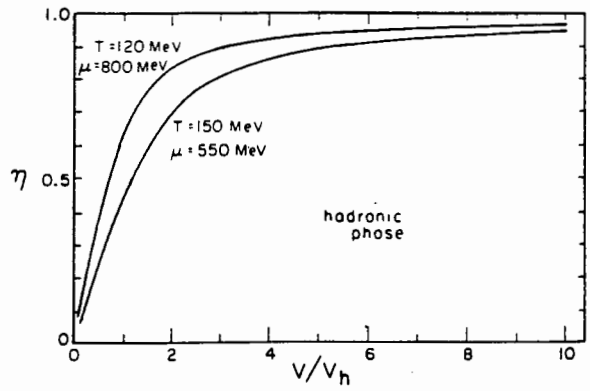

Figure 2.4: The quenching factor η as a function of the reaction volume in units of $V_h = \frac{4}{4}\pi(1fm)^3$, for two temperatures [40].

The correction factor (or the quenching ratio) is the coefficient of pair production, $< N_{\frac{p}{p}} >$, for $p\bar{p}$ where $< N_p >=< N_{\bar{p}} >$ in the canonical formalism as considered before. And in the case of [40] this quenching ratio, $\eta = I_1(\sqrt{4y})/I_0(\sqrt{4y})$, where $y = \lambda Z_p^1(T,V)Z_{\bar{p}}^1(T,V)$. Thus one quickly sees that $\sqrt{4y}$ is nothing else but the argument x of the Bessel function in our formalisms where x is explicitly defined. It is shown [40] that the relative strangeness

production is also suppressed by this quenching factor which depends on the reaction volume. Thus the reaction volume plays an important role in modifying the statistical thermodynamic predictions for strangeness production. One would therefore expect strangeness enhancement in heavy ion collisions relative to proton-proton collisions. Thus, in heavy ion collisions where we hope to achieve large volumes, the usual statistical result will be recovered. However for the reaction volumes of the order of hadronic size, substantial suppression of the production rates of particles is seen.

2.5 Simultaneous Baryon Number and Strangeness Conservation

The starting point of the analysis is the partition function for a free, pointlike gas, subject to the constraints of conserved baryon number B and strangeness S as presented by Hagedorn and Redlich [27]. The partition function differs from the one considered in the previous sections in that now two quantum numbers Q_1,Q_2 are conserved simultaneously and so two angles ϕ and ψ are required. We now have

$$Z_{Q_1,Q_2}(T,V) = \frac{1}{2\pi}\int_0^{2\pi} d\phi \exp(-iQ_1\phi)\frac{1}{2\pi}\int_0^{2\pi} d\phi \exp(-iQ_2\phi)\cdot \overline{Z}(T,V,\phi,\psi)\,.$$

The methods of exact overall quantum number conservation for the cases where the gas is composed of particles having baryon number ± 1 and strangeness $\pm 1, \pm 2, \pm 3$ will be investigated in this section. These quantum numbers correspond to the charges Q_1 and Q_2 above.

2.5.1 Baryon quantum number = ± 1 and Strangeness = ± 1

The canonical partition function $Z^1_{B,S}(T,V)$ (where the subscripts imply that B and S are exactly conserved and the superscript refers to the case where only particles with strangeness $= \pm 1$ are included) is given by;

$$\begin{aligned} Z^1_{B,S}(T,V) \;=\; & Z_0\frac{1}{2\pi}\int_0^{2\pi} d\psi e^{-iS\psi}\frac{1}{2\pi}\int_0^{2\pi} d\phi e^{-iB\phi} \\ & \cdot\exp[Z_K(\exp(i\psi)+\exp(-i\psi))] \\ & \cdot\exp[Z_N(\exp(i\phi)+\exp(-i\phi))] \\ & \cdot\exp[Z_Y(\exp(i(\phi-\psi))+\exp(-i(\phi-\psi)))]\,. \end{aligned} \tag{2.41}$$

Here $Z_i(T,V)$ is the sum of all the one particle partition functions having the same quantum numbers as i. Explicitly one has

$$\begin{aligned} Z_K &\equiv Z^1_K + Z^1_{K^*} + \cdots\,, \\ Z_N &\equiv Z^1_N + Z^1_\Delta + \cdots\,, \\ Z_Y &\equiv Z^1_\Lambda + Z^1_{\Lambda^*} + \cdots\,, \end{aligned}$$

where,

$$\begin{aligned} Z_i^1(T,V) &\equiv g_i V \int_{-\infty}^{\infty} \frac{d^3p}{(2\pi)^3} e^{\frac{-\sqrt{p^2+m_i^2}}{T}} \\ &= \frac{g_i}{2\pi^2} V m_i^2 T K_2(\frac{m_i}{T}) , \end{aligned} \tag{2.42}$$

and g_i is the degeneracy factor and $K_2(x)$ is the modified Bessel function of order 2. Thus one has for the partition function

$$\begin{aligned} Z_{B,S}^1(T,V) &= Z_0 \frac{1}{2\pi} \int_0^{2\pi} d\psi \exp(-iS\psi) \frac{1}{2\pi} \int_0^{2\pi} d\phi \exp(-iB\phi) \\ &\quad \cdot \exp[2Z_K \cos(\psi) + 2Z_N \cos(\phi) + 2Z_Y \cos(\phi - \psi)] . \end{aligned} \tag{2.43}$$

Z_0 is the partition function for all particles with zero baryon quantum number and strangeness quantum number, e.g pions.

The ϕ and ψ integrals in Eq. 2.43 do not factorize because the hyperons have both baryon quantum number and strangeness quantum number, hence the factor $\cos(\phi - \psi)$. To decouple the integrals, we introduce a new angle α defined to be $\phi - \psi$, and introducing a 1 in a form of a delta function

$$1 = \int_0^{2\pi} d\alpha \delta(\phi - \psi - \alpha) ,$$

the partition function then becomes

$$\begin{aligned} Z_{B,S}^1(T,V) &= Z_0 \frac{1}{2\pi} \int_0^{2\pi} d\psi e^{-iS\psi} \exp[2Z_K(T,V)\cos\psi] \frac{1}{2\pi} \int_0^{2\pi} d\phi e^{-iB\phi} \exp[2Z_N(T,V)\cos\phi] \\ &\quad \cdot \int_0^{2\pi} d\alpha \exp[2Z_Y(T,V)\cos\alpha] \delta(\phi - \psi - \alpha) . \end{aligned}$$

We make use of the following (Fourier expansion) representation of the delta function

$$\delta(x) = \frac{1}{2\pi} \sum_{n=-\infty}^{\infty} \exp(inx) .$$

Choosing the variable x to be $\phi - \psi - \alpha$ one obtains;

$$\begin{aligned} Z_{B,S}^1(T,V) &= Z_0 \frac{1}{2\pi} \int_0^{2\pi} d\psi e^{-iS\psi} \frac{1}{2\pi} \int_0^{2\pi} d\phi e^{-iB\phi} \\ &\quad \cdot \exp[2Z_K \cos\psi + 2Z_N \cos\phi + 2ZY \cos(\phi - \psi)] \\ &\quad \cdot \sum_{n=-\infty}^{\infty} \frac{1}{2\pi} \int_0^{2\pi} d\alpha \exp(in(\phi - \psi - \alpha)) . \end{aligned} \tag{2.44}$$

This can be rewritten as

$$\begin{aligned} Z^1_{B,S} &= Z_0 \sum_{n=-\infty}^{\infty} \int_0^{2\pi} d\phi e^{-iB\phi - in\phi} \exp[2Z_N(T,V)\cos\phi] \\ &\cdot \frac{1}{2\pi} \int_0^{2\pi} d\psi e^{-iS\psi + in\psi} \exp[2Z_K(T,V)\cos\psi] \\ &\cdot \frac{1}{2\pi} \int_0^{2\pi} e^{-in\phi} \exp[2Z_Y(T,V)\cos\alpha] \ . \end{aligned} \tag{2.45}$$

Using the integral representation of modified Bessel function of order n

$$I_n(x) = \frac{1}{2\pi} \int_0^{2\pi} d\theta \exp(x\cos\theta)\exp(-in\theta) \ ,$$

where we have made use of Eq. (9.6.19) of [20] which is

$$I_n(z) = \frac{1}{\pi} \int_0^{\pi} e^{z\cos\theta} \cos(n\theta) d\theta \ ,$$

the final expression for the partition function reads

$$Z_{B,S}(T,V) = Z_0 \sum_{n=-\infty}^{\infty} I_{S-n}(2Z_K) I_{B+n}(2Z_N) I_n(2Z_Y) \ . \tag{2.46}$$

Now that we have the canonical partition function for a gas with two conserved quantum numbers, what then left is to find the particle numbers. In the usual canonical formalism where these quantum numbers are not conserved, the particle numbers are fixed by construction. But in our case, the quantum numbers involved are fixed (i.e exact). The mean particle numbers are obtained by introducing an additional chemical potential for each particle sort and then making use of the grand canonical formalism to project them out. That is ,

$$< N_i >= \frac{T}{Z} \frac{\partial Z}{\partial \mu_i}\bigg|_{\mu_i=0} \ . \tag{2.47}$$

Thus to calculate the multiplicity of particle i we simply separate, for this species, the particle and anti-particle term, and multiply the relevant one by the chemical potential μ, differentiate and put $\mu = 0$ afterwards (this has to be done so that one remains in the canonical formalism). And since all other particles are not involved we leave their terms as they were.

This method leads to the following expression for the mean particle numbers :

$$
\begin{aligned}
< N_{\frac{K}{K}} > &= Z_0 \frac{Z_K^1(T,V)}{Z} \sum_{n=-\infty}^{\infty} I_{S-n\pm1}(2Z_K) I_{B+n}(2Z_N) I_n(2Z_Y) \\
< N_{\frac{N}{N}} > &= Z_0 \frac{Z_N^1(T,V)}{Z} \sum_{n=-\infty}^{\infty} I_{S-n}(2Z_K) I_{B+n\mp1}(2Z_N) I_n(2Z_Y) \\
< N_{\frac{Y}{Y}} > &= Z_0 \frac{Z_Y^1(T,V)}{Z} \sum_{n=-\infty}^{\infty} I_{S-n}(2Z_K) I_{B+n}(2Z_N) I_{n\pm1}(2Z_Y)
\end{aligned}
\tag{2.48}
$$

2.5.2 Baryon quantum number = ±1 and Strangeness = ±2

We now consider a gas which includes particles and antiparticles of strangeness quantum number ∓ 2 respectively, and in particular we now include Ξ and $\overline{\Xi}$.

In this case the partition function is given by

$$
\begin{aligned}
Z_{B,S}^2(T,V) &= Z_0 \frac{1}{2\pi} \int_0^{2\pi} d\psi e^{-iS\psi} \frac{1}{2\pi} \int_0^{2\pi} d\phi e^{-iB\phi} \\
&\cdot \exp[2Z_K \cos\psi + 2Z_N \cos\phi] \\
&\cdot \exp[2Z_Y \cos(\phi - \psi) + Z_\Xi (e^{i\phi - 2i\psi} + e^{-i\phi + 2i\psi})] \, .
\end{aligned}
\tag{2.49}
$$

The Z_Ξ term in the partition function now contains the angle 2ψ. The integrals in this expression can be reduced to the ones considered previously, by using the Generating Function of the modified Bessel functions I_n. That is, using Eq. (9.6.33) of [20] which is

$$
e^{\frac{1}{2}z(t+1/t)} = \sum_{k=-\infty}^{\infty} t^k I_k(z) \quad (t \neq 0) \, .
$$

We use the following notation :

$$
\exp\left[\frac{x}{2}(t + 1/t)\right] = \sum_{m=-\infty}^{\infty} t^m I_m(x) \, .
$$

Setting $x = 2Z_\Xi$ and $\exp(i(\phi - 2\psi)) = t$, the partition function above in Eq. 2.49 can be written as ,

$$
\begin{aligned}
Z_{B,S}^2 &= Z_0 \frac{1}{2\pi} \int_0^{2\pi} d\psi e^{-iS\psi} \frac{1}{2\pi} \int_0^{2\pi} d\phi e^{-iB\phi} \\
&\cdot \exp[2ZK \cos\psi + 2Z_N \cos\phi + 2Z_Y \cos(\phi - \psi)] \\
&\cdot \sum_{m=-\infty}^{\infty} I_m(2Z_\Xi) \exp(im(\phi - 2\psi)) \, .
\end{aligned}
\tag{2.50}
$$

Introducing the delta function to decouple ϕ and ψ again one obtains

$$\begin{aligned} Z^2_{B,S}(T,V) &= Z_0 \sum_{m=-\infty}^{\infty} I_m(2Z_\Xi) \\ &\cdot \sum_{n=-\infty}^{\infty} \frac{1}{2\pi} \int_0^{2\pi} d\psi e^{-i(S-n+2m)\psi} \exp[2Z_K \cos\psi] \\ &\cdot \frac{1}{2\pi} \int_0^{2\pi} d\phi e^{-i(B+n-m)\phi} \exp[2Z_N \cos\phi] \\ &\cdot \frac{1}{2\pi} \int_0^{2\pi} d\alpha e^{-in\alpha} \exp[2Z_Y \cos\alpha] \,, \end{aligned} \tag{2.51}$$

and thus the partition function in terms of Bessel functions I_n reads ,

$$Z^2_{B,S} = Z_0 \sum_{m=-\infty}^{\infty} I_m(2Z_\Xi) \cdot \sum_{n=-\infty}^{\infty} I_{S-n+2m}(2Z_K) I_{B+n-m}(2Z_N) I_n(2Z_Y) \,. \tag{2.52}$$

The mean particle numbers obtained from this function are given below :

$$\begin{aligned} < N_{\frac{K}{\bar{K}}} > &= Z_0 \frac{Z^1_K(T,V)}{Z} \sum_{m=-\infty}^{\infty} I_m(2Z_\Xi) \sum_{n=-\infty}^{\infty} I_{n\pm1-S-2m}(2Z_K) \cdot I_{n+B-m}(2Z_N) I_n(2Z_Y) \\ < N_{\frac{N}{\bar{N}}} > &= Z_0 \frac{Z^1_N(T,V)}{Z} \sum_{m=-\infty}^{\infty} I_m(2Z_\Xi) \sum_{n=-\infty}^{\infty} I_{n-S-2m}(2Z_K) \cdot I_{n+B-m\mp1}(2Z_N) I_n(2Z_Y) \\ < N_{\frac{Y}{\bar{Y}}} > &= Z_0 \frac{Z^1_Y(T,V)}{Z} \sum_{m=-\infty}^{\infty} I_m(2Z_\Xi) \sum_{n=-\infty}^{\infty} I_{n-S-2m}(2Z_K) \cdot I_{n+B-m}(2Z_N) I_{n\pm1}(2Z_Y) \\ < N_{\frac{\Xi}{\bar{\Xi}}} > &= Z_0 \frac{Z^1_\Xi(T,V)}{Z} \sum_{m=-\infty}^{\infty} I_m(2Z_\Xi) \sum_{n=-\infty}^{\infty} I_{n-S-2m\mp2}(2Z_K) \cdot I_{n+B-m\mp1}(2Z_N) I_n(2Z_Y) \end{aligned} \tag{2.53}$$

2.5.3 Baryon quantum number = ±1 and Strangeness = ±3

This is the most general case since now all the particles of the hadronic spectrum may be included in the gas. Here we also include the particles and antiparticles of strangeness quantum number ∓3, and in particular the Ω^- and $\overline{\Omega^-}$.

As before one has the expression of the partition function in its integral form

$$\begin{aligned} Z^3_{B,S}(T,V) &= Z_0 \frac{1}{2\pi}\int_0^{2\pi} d\psi e^{-iS\psi} \frac{1}{2\pi}\int_0^{2\pi} d\phi e^{-iB\phi} \\ &\cdot \sum_{n=-\infty}^{\infty} \frac{1}{2\pi}\int_0^{2\pi} d\alpha e^{in(\phi-\psi-\alpha)} \\ &\cdot \exp[2Z_K\cos\psi]\exp[2Z_N\cos\phi]\exp[2Z_Y\cos(\phi-\psi)] \\ &\cdot \exp[2Z_\Xi\cos(\phi-2\psi)+2Z_\Omega\cos(\phi-3\psi)] \ . \end{aligned} \tag{2.54}$$

Likewise the term Z_Ω contains the angle 3ψ. Performing the integrations like before one obtains for the partition function which includes particles of strangeness up to ± 3 ;

$$\begin{aligned} Z^3_{B,S}(T,V) &= Z_0 \sum_{l=-\infty}^{\infty} I_l(2Z_\Omega) \sum_{m=-\infty}^{\infty} I_m(2Z_\Xi) \\ &\sum_{n=-\infty}^{\infty} I_{S-n-2m-3l}(2Z_K) I_{B+n+m+l}(2Z_N) I_n(2Z_Y) \ . \end{aligned} \tag{2.55}$$

The expressions for particle numbers follow :

$$\begin{aligned} < N_{\frac{K}{\bar{K}}} > &= Z_0 \frac{Z^1_K(T,V)}{Z} \sum_{l=-\infty}^{\infty} I_l(2Z_\Omega) \sum_{m=-\infty}^{\infty} I_m(2Z_\Xi) \\ &\sum_{n=-\infty}^{\infty} I_{S-n-2m-3l\mp 1}(2Z_K) I_{B+n+m+l}(2Z_N) I_n(2Z_Y) \\ < N_{\frac{N}{\bar{N}}} > &= Z_0 \frac{Z^1_N(T,V)}{Z} \sum_{l=-\infty}^{\infty} I_l(2Z_\Omega) \sum_{m=-\infty}^{\infty} I_m(2Z_\Xi) \\ &\sum_{n=-\infty}^{\infty} I_{S-n-2m-3l}(2Z_K) I_{B+n+m+l\mp 1}(2Z_N) I_n(2Z_Y) \\ < N_{\frac{Y}{\bar{Y}}} > &= Z_0 \frac{Z^1_Y(T,V)}{Z} \sum_{l=-\infty}^{\infty} I_l(2Z_\Omega) \sum_{m=-\infty}^{\infty} I_m(2Z_\Xi) \\ &\sum_{n=-\infty}^{\infty} I_{S-n-2m-3l}(2Z_K) I_{B+n+m+l}(2Z_N) I_{n\pm 1}(2Z_Y) \\ < N_{\frac{\Xi}{\bar{\Xi}}} > &= Z_0 \frac{Z^1_\Xi(T,V)}{Z} \sum_{l=-\infty}^{\infty} I_l(2Z_\Omega) \sum_{m=-\infty}^{\infty} I_m(2Z_\Xi) \\ &\sum_{n=-\infty}^{\infty} I_{S-n-2m-3l\pm 2}(2Z_K) I_{B+n+m+l\mp 1}(2Z_N) I_n(2Z_Y) \\ < N_{\frac{\Omega}{\bar{\Omega}}} > &= Z_0 \frac{Z^1_\Omega(T,V)}{Z} \sum_{l=-\infty}^{\infty} I_l(2Z_\Omega) \sum_{m=-\infty}^{\infty} I_m(2Z_\Xi) \\ &\sum_{n=-\infty}^{\infty} I_{S-n-2m-3l\pm 3}(2Z_K) I_{B+n+m+l\mp 1}(2Z_N) I_n(2Z_Y) \end{aligned} \tag{2.56}$$

It is found that the series considered in Eqs. 2.48, 2.53 and 2.56 converges rapidly. Only a few terms of the index n, m, l were necessary to obtain accurate results. For a given value of B it was sufficient to sum from $-B-n_{max}$ to $B+n_{max}$, where n_{max} is the index n, m, l. It was seen that only $n_{max}=10$ was sufficient for the convergence when small values of B are used. However when B increases drastically to values of about 100 it was found that n_{max} becomes small for convergence and thus it was necessary to adjust n_{max} for convergence. This section concludes the derivation of the partition function and particle numbers in the exact baryon and strangeness formalism. The results will be used in the next Chapter(s) on Hadronic Gas Models where particle numbers and particle number ratios will be predicted.

Chapter 3

The Hadron Gas Model

3.1 Introduction

The Hadron Gas Model tries to model, amongst other things from the experiments performed at the accelerators, the particle numbers produced at certain projectile energies and chosen targets. In this model, one wants to describe the state of final interactions of the resulting fire-ball at freeze-out in a thermal and chemical equilibrium scenario. It should be noted, however, that we are dealing with processes occurring in very small volumes (of the order of a few nuclear volumes) and happening in a very short period of time. An interesting question would be whether one can really model the observed particle numbers in this equilibrium statistical picture. We expect the prediction of statistical mechanics to apply in the infinite volume limit. On the other hand trying to simulate nuclear collisions with nonequilibrium thermodynamics is not an easy task to handle, as one has to know the cross-section for each possible process in order to construct the rate equation. In this work, the equilibrium scenario will be assumed. By using the statistical modelling of particle production, we try to find whether the observed particle numbers can be accommodated in a thermodynamical picture of a free (or at least nearly free) relativistic gas, and to find out about the process itself (i.e temperature of the gas, and baryon density, etc). Information about the volume of the fireball system can be obtained from the interferometric method using particle correlations. The baryon chemical potential μ_B used in grand canonical models can be found by fixing

the net baryon number, B, or the baryon density B/V. The overall zero strangeness of the gas fixes the strange chemical potential μ_S. Thus, in principle, all the parameters needed for the free gas models are available from experiment. In this work, all parameters are fitted to reproduce the observed particle yields and ratios and none have been extracted from the experiment. The measured particle spectra made a great experimental support for the thermodynamic picture [41].

3.2 m_T scaling

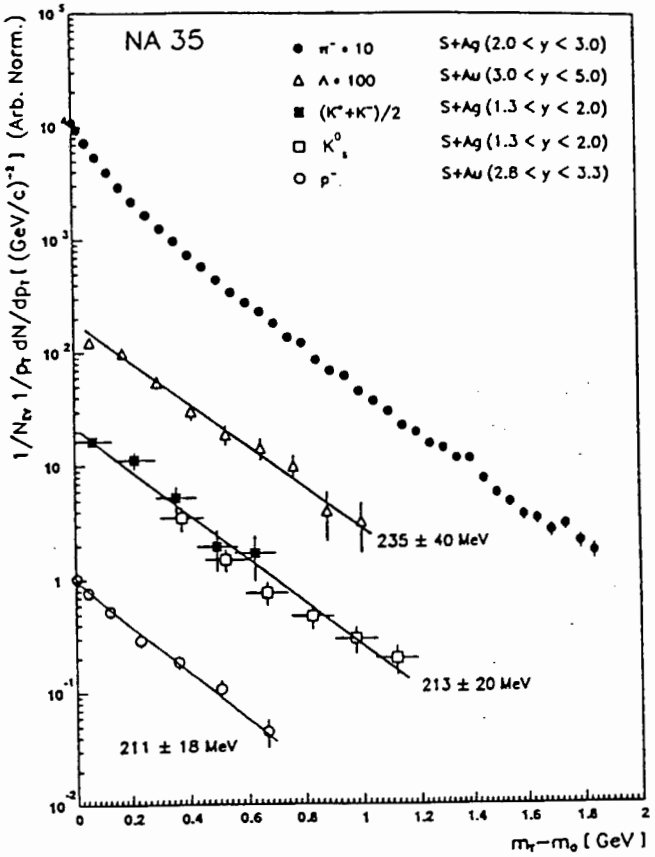

Figure 3.1: m_T scaling: plots of $1/p_T dN/dp_T$ as a function of $m_T - m_0$ [42]. Note that $1/p_T dN/dp_T$ is plotted because of the small rapidity intervals.

The plots of $m_T^{-3/2} dn/dm_T$ vs m_T, where m_T is the transverse mass normalized to $m_T = m$ for all particles, shows the exponentially decreasing trend as predicted by the differential Boltzmann equation, Fig. 3.1. If all particles from a thermalized source show the same

behaviour in their m_T spectra then this will be a good proof that thermal models provide a good approximation to the particle production rates observed in collisions and that a common temperature may be used to describe all the species in the gas. Also, an interesting plot will be a plot of $m_T^{-3/2} dn/dm_T$ vs $m_T - m_0$, and here too the behaviour of thermalisation is seen, except for pions which have a steeper tail at low p_T, indicating a lower temperature, Fig. 3.1. Note that when the rapidity window of the collected data is small we plot $dn/dydm_T$ vs m_T which behaves as $e^{\frac{-m_T}{T_{eff}}}$ with $T_{eff} = T/cosh(y - y_{FB})$. (See Appendix F).

3.3 The Hadron Gas Model

The formalism of the Hadron Gas Model was outlined in the previous Chapter. In statistical physics, there are three formalisms which one can use incorporating baryon number and strangeness conservation:

- grand canonical. Variables are μ_B, μ_S, T as used in [43];
- mixed canonical. Variables are μ_B, S, T as used in [39];
- canonical. Variables are B, S, T, V as used in [31];

where μ_B is the baryon chemical potential and μ_S the strange chemical potential. S is the overall strangeness of the gas, B is the net baryon number, V the volume of the gas and T the temperature of the gas at freeze-out. In this work the canonical formalism where baryon number and strangeness are exactly conserved will be considered and the result can always be compared to the grand canonical approach. The partition function is

$$Z = \mathrm{Tr}\left[e^{\frac{-(E-\mu N)}{T}}\right] . \tag{3.1}$$

The chemical potential governs only the conserved quantities and not the particle numbers as a whole. Thus the grand canonical formalism explicitly deals with conserved quantities of a given species. Pions do not carry either strangeness or baryon number (and hence are not assigned a chemical potential) and are produced proportional to the (temperature)^3. In this model, a basic assumption of equilibrium statistical mechanics is made. That is, the

relativistic chemical equilibrium exists. This means that chemical reactions are taking place at the same rate in both forward and reverse directions. Thermalisation means that the particles produced in the fireball have interacted sufficiently so that a common temperature may be used to describe all species in the gas. Also, for thermal equilibrium it will mean that the particles' momenta are distributed according to the equilibrium statistical mechanics and chemical equilibrium means that the abundances are dictated by the particle's statistical weights. The question whether thermalisation indeed has occurred has been addressed by [44, 45]. It was found that by using the equilibrium statistical model with hadronic interactions incorporated in a mean field way, the WA85 and NA35 data could be reproduced, except for the pions where the models predicted less than was observed. The thermalisation question has recently also been addressed by [46, 47], see Table 3.1, 3.2 and 3.3. These tables show how good the Hadronic Gas Model is in predicting the number of hadrons produced and the hadronic ratios in heavy ion collisions. For a review on the application of the hadronic gas model on $Si - Au$ collision, see [48].

Table 3.1: The abundances of Hadron Species in $Si - Au$ collisions at the AGS (Thermal parameters: $T = 110 \pm 5\ MeV$, $\mu_B = 540 \pm 20\ MeV$) [46].

Particle Species	Experimental Numbers	Thermal Numbers
nucleons	94	94
pions	120	133
kaons	14	17
hyperons	14	12
antikaons	3	4
Ξ's	2	1
ϕ's	2×10^{-1}	2×10^{-1}
antinucleons	4×10^{-2}	6×10^{-3}
antihyperons	3×10^{-2}	4×10^{-3}

The basic assumption of these models is that the system is described by a grand canonical ensemble of fermions and bosons in equilibrium at a freezeout temperature, T [47]. In addition to these models, the isospin symmetry of the initial state was taken into account

Table 3.2: Ratios of Hadron species in $Si - Au$ collisions at the AGS (Thermal parameters $T = 110 \pm 5\ MeV$, $\mu_B = 540 \pm 20\ MeV$) [46].

Particle Ratio	Experimental Ratio	Thermal Ratio
π^+/p	0.80 ± 0.08	0.87 ± 0.15
K^+/π^+	0.19 ± 0.02	0.21 ± 0.02
K^+/K^-	4.40 ± 0.40	4.51 ± 0.62
Λ/p	0.20 ± 0.04	0.16 ± 0.02
K^-/π^-	$0.035 \pm .005$	0.038 ± 0.006
Ξ^-/Λ	$(1.2 \pm 0.2) \times 10^{-1}$	$(4.9 \pm 0.5) \times 10^{-2}$
ϕ/π^+	$(4.5 \pm 1.2) \times 10^{-3}$	$(4.6 \pm 1.3) \times 10^{-3}$
$\bar{p}/p$	$(4.5 \pm 0.4) \times 10^{-4}$	$(7.2 \pm 6.3) \times 10^{-5}$
$\bar{\Lambda}/\Lambda$	$(2.0 \pm 0.8) \times 10^{-3}$	$(3.4 \pm 3.0) \times 10^{-4}$

[46]. These models were used to compare to the data from CERN-SPS and BNL-AGS. Finite size effects incorporated by modifying the phase space volume element to include surface and linear terms in the momentum distribution were found to be small because the volumes were of the order of $10^3\ fm^3$. That the system becomes thermalised seems to be a weaker requirement than the chemical equilibrium; the time scales for the two processes are very different. It seems plausible that thermal equilibrium is attained far more rapidly than chemical equilibrium. For thermal equilibrium one requires an interaction between particles of any type whereas for chemical equilibrium certain reactions are required for which there may not be enough time for the full equilibrium to be attained. However, the success of these models in predicting observables gives one faith in the statistical picture, provided that it includes the basic physical requirements: baryons are extended objects and volume corrections play an important role in fixing e.g. the baryon density (see Appendix H). It is unrealistic to use point-like particle expression when dealing with extended objects. For temperatures of the order of hundreds of MeV's, resonance production and decay into pions and kaons must be included as basic ingredients. It is important to note that because hadronic gas models presuppose equilibration, both chemical and thermal, all information

Table 3.3: Hadronic Ratios in $Si - Au$ Collisions at the AGS. (Thermal parameters: $T = 120\ MeV$, and $T = 140 \pm 5\ MeV$, $\mu_B = 540\ MeV$) [47].

Ratio	Thermal Model: 120 MeV	Thermal Model: 140 MeV	Experimental Ratio
$\pi/(p+n)$	1.29	1.34	1.05(5)
$d/(p+n)$	4.3×10^{-2}	5.8×10^{-2}	$3.0(3) \times 10^{-2}$
$\overline{p}/p$	1.47×10^{-4}	5.8×10^{-4}	$4.5(5) \times 10^{-4}$
K^+/π^+	2.3×10^{-1}	2.7×10^{-1}	$1.9(2) \times 10^{-1}$
K^-/π^-	5.0×10^{-2}	6.2×10^{-2}	$3.5(5) \times 10^{-2}$
$K^0{}_s/\pi^+$	1.4×10^{-1}	1.6×10^{-1}	$9.7(15) \times 10^{-2}$
K^+/K^-	4.6	4.3	4.4(4)
$\Lambda/(p+n)$	9.5×10^{-2}	1.1×10^{-1}	$8.0(16) \times 10^{-2}$
$\bar{\Lambda}/\Lambda$	8.8×10^{-4}	3.7×10^{-3}	$2.0(8) \times 10^{-3}$
$\phi/(K^+ + K^-)$	2.4×10^{-2}	3.6×10^{-2}	$1.34(36) \times 10^{-2}$
Ξ^-/Λ	6.4×10^{-2}	7.2×10^{-2}	$1.2(2) \times 10^{-1}$
$\bar{d}/\bar{p}$	1.1×10^{-5}	4.7×10^{-5}	$1.0(5) \times 10^{-5}$

about the early history of the fireball is lost. The predictive power of the models is restricted to the very last instance of the fireball's existence: the freeze-out. Information about the early history of the fireball is mediated by particles that do not interact with the secondaries and thus retain "memory" of the early period. The dileptons are such particles, but their interest is matched by the difficulty of their experimental detection and their spectrum (which is modified by the existence of fireball) is experimentally ambiguous [49]. (The main difficulty is the huge background of pairs from uncorrelated lepton tracks originating from the decay of hadronic particles and from conversions in the measurements of electron pairs. This background has a quadratic dependence on the multiplicity and strongly increases in the

low-mass and low-p_T regions). A strength of these models is that they allow calculation of densities other than the 4π value. This can be done by changing the spherically symmetrical momentum distribution $d^3p = 4\pi p^2 dp$ to a cylindrically symmetrical one (see Appendix G) corresponding to the experimental setup: $d^3p = 2\pi p_T dp_T dp_z$ (with $\mathrm{E} = \sqrt{m^2 + p_T^2 + p_z^2}$), and infinite integration over the longitudinal component of momentum (p_z) is understood. The lower bound on p_T can then be set to the experimental p_T cut. This is an advantage these models have; one can investigate the particle production in a specific dynamical window. Not only is the experimental data nor the 4π value, it is also measured in the specific rapidity window. This has an important consequence: the temperature obtained from the m_T spectrum is thus only an effective temperature applying to the particles at midrapidity – at first sight. However, if one invokes the Bjorken picture [1], the p_T spectrum of particles produced is independent of the rapidity y. It is clear that under this assumption, the experimental data measured in a specific window will differ from the y-integrated data by a constant factor. Given the overall success of the Bjorken model, let us see how these statistical formalisms perform when one attempts to reproduce the experimental data if one makes this assumption. We first look at the results of the Hadron Gas Model considered in this work.

3.4 Results of the Hadronic Gas Model

The motivation of the Hadronic Gas Model was presented in the previous sections. It remains a task to explore the final results of the previous chapter – Chapter 2. We shall try to study the behaviour of the particle production and the hadronic ratios as functions of baryon number and/or volume, and baryon density. Effects like the dependence on the cut-off mass and strangeness content will also be investigated.

3.4.1 Kaon Production

Kaons are light strange particles produced significantly in $p - p$ collisions and even more so in heavy ion collisions. This is so if one thinks of a greater interaction volume for the

gas as well as noting that the strange chemical potential increases rapidly with increasing baryon chemical potential. Kaons, especially K^+ due to its abundance over K^-, have been measured by many experiments. K^+ is mostly produced by the processes [16, 50] ;

$$\begin{aligned} pN &\longrightarrow NYK^+, \\ N\Delta^+ &\longrightarrow NYK^+, \\ \pi N &\longrightarrow YK^+, \\ \pi\Delta &\longrightarrow YK^+, \end{aligned} \tag{3.2}$$

with an associated production of a hyperon Y.

K^- is mostly produced by the processes ;

$$\begin{aligned} NN &\longrightarrow NNK^+K^- , \\ \pi\pi &\longrightarrow K^+K^- , \\ NN^* &\longrightarrow NNK^+K^- ; \end{aligned} \tag{3.3}$$

together with a K^+ (pair production). The K^- can be annihilated in a baryon rich environment through the strangeness exchange process

$$K^-N \longrightarrow \pi Y . \tag{3.4}$$

To expand our knowledge of strangeness production processes it is a good idea to study the kaon production in heavy ion collisions. Kaons have a longer mean free path than pions in a hadronic gas system, so they probe earlier stages of collisions [51]. This is supported by results from Hanbury-Brown-Twiss (HBT) interferometry measurements of kaon and pion pairs [52, 53, 54]. Because of its small rescattering, cross-section on baryons, K^+ is a

better probe than K^- in a baryon rich environment. The results obtained for kaon yield from the Hadron Gas Model using Strangeness = ± 1, ± 2, and ± 3 equations are presented in Figure 3.2. In this figure, we investigate the dependence of the kaon production on the strangeness content of the gas. The first feature to be deduced from this figure is

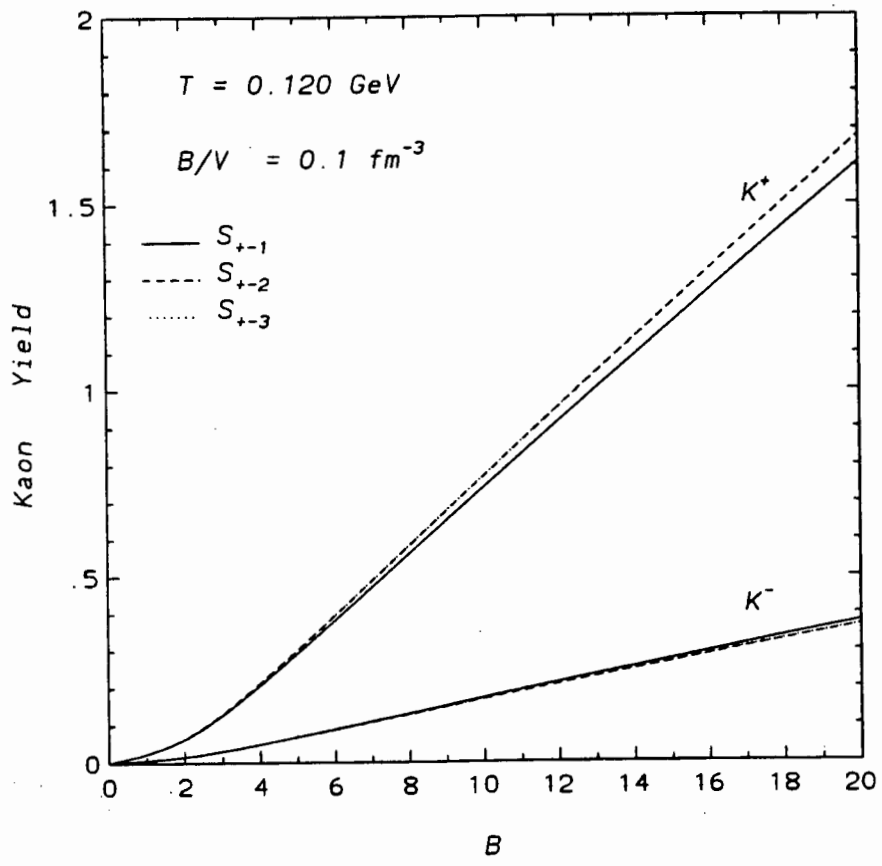

Figure 3.2: The Kaon Yield as a function of the baryon number, B. The fixed thermal parameters are the temperature $T = 120\ MeV$ and the baryon density $B/V = 0.1/fm^3$.

the dependence of the kaon yield on the net baryon number B. For small values of B the dependence of kaon production is quadratic. For small values of B there are few NN collisions and thus the kaon yield will be very small. However, for large values of B the quadratic dependence disappears and the kaon production increases linearly as a function of B. At large values of B we have more NN collisions which result in the higher kaon production. Because in this Hadron Gas model we fix the baryon density, B/V (n_B), the volume is determined by the net baryon number. This means, therefore, that the dependence of the kaon production on B implies a dependence on volume, V. Hence one should expect the same behaviour if one plots the kaon production as a function of V. For a fixed baryon density, $n_B = B/V$, with

$B, V \longrightarrow \infty$ one obtains the Grand Canonical results since particle fluctuations in the Grand Canonical Ensemble behave as $1/\sqrt{N}$, and in this case it will behave as $1/\sqrt{B}$. Based on the mechanisms of kaon production it is seen that the K^+ production is greater than the K^- production. Also it is easier to make K^+ than K^- because of strangeness conservation. The second feature from Figure 3.2 is the dependence of the kaon production on the components of the gas in terms of Strangeness composition. At small values of B (small volumes) the three curves's origins are similar (no distinctions) but at large values of B they show clear differences. Thus at small volumes the production of, e.g., Ω has to be accompanied by three kaons, and that of Ξ, by two kaons. There is no clear distinction between $S_{\pm 2}$ and $S_{\pm 3}$ curves for the particular chosen temperature. Thus the inclusion of Ω in our gas does not have a big effect. The inclusion of particles of $S_{\pm 2,3}$ increases the production of K^+ and decreases the production of K^- especially at high values of B. This is due to exact conservation of strangeness together with absorption. The main process responsible for this might be

$$K^- + N \longrightarrow K^+ + \Xi^- \,. \tag{3.5}$$

One sees immediately that K^+ will be enhanced to conserve the strangeness, while K^- will be absorbed for the same strangeness conservation. To have the effect of strangeness conservation large in K^+ as compared to K^-, one should recall that another process which enhances K^+ in the same environment is

$$\pi + Y \longrightarrow K^+ + \Xi^- \,, \tag{3.6}$$

where Y refers to the Λ or the Σ. And of course $\overline{N}N$ annihilation could lead to these effects, but which might favour K^+ at the expense of K^-. This happens at large values of B where one is having more of the nucleon-nucleon collisions. Comparing the $S_{\pm 1}$, $S_{\pm 2}$ and $S_{\pm 3}$ curves can be easily understood in the grand canonical formalism :

$$\begin{aligned} \frac{\Omega}{\Xi} &= \frac{\exp\left(-\frac{m_\Omega}{T} - \frac{3\mu_S}{T}\right)}{\exp\left(-\frac{m_\Xi}{T} - \frac{2\mu_S}{T}\right)} \\ &= \exp\left(-\frac{(m_\Omega - m_\Xi)}{T} - \frac{\mu_S}{T}\right) \\ &\approx \exp\left(-\frac{(m_\Omega - m_\Xi)}{T}\right) \,, \end{aligned} \tag{3.7}$$

and similarly

$$\frac{\Xi}{\Lambda} \approx \exp\left(-\frac{(m_\Omega - m_\Xi)}{T}\right) \,. \tag{3.8}$$

For the temperature considered here we have for Ω/Ξ ratio a factor of ≈ 0.05 and ≈ 0.3 for Ξ/Λ. Thus to see the difference between the $S_{\pm 2}$ and $S_{\pm 3}$ curves we should go for higher temperatures where we can produce the Ω's, and more clearly it will be seen at high values of B and/or volumes. We now investigate the effect of including particles of certain mass

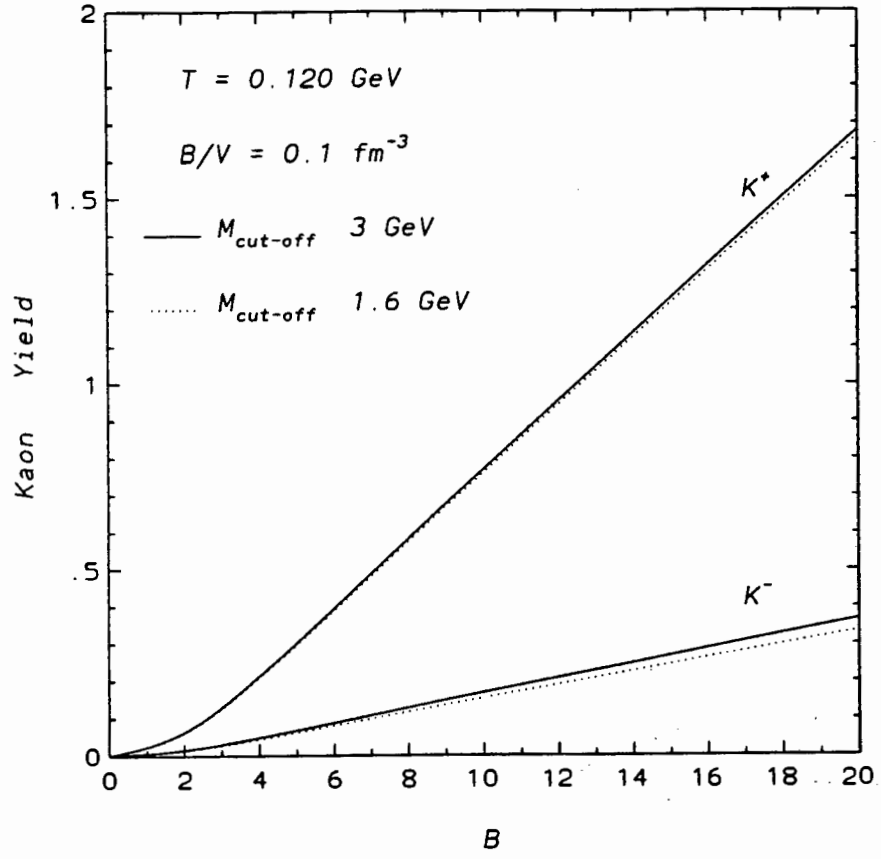

Figure 3.3: The dependence of Kaon Yield on the resonance composition (cut- off mass) of the gas is plotted as a function of the baryon number, B, at fixed T and B/V.

limit (referred to here as cut-off mass) in the gas, Fig 3.3. The K^+ production is slightly sensitive (or nearly insensitive to the composition of resonances in the gas (cut-off mass). The K^- production shows a clear sensitivity compared to K^+, on the composition of the gas especially for large volumes. One sees that including heavier resonances in the gas, increases the kaon production, especially the K^-. It means therefore that in order to see more of the K^-'s we need heavier resonances. But the K^+ is already produced by other mechanisms also. Thus, the K^+ does not rely much on the decay channels.

The K^+ production is sensitive to the baryon density B/V. For low baryon densities the

production increases, Figure 3.4. This effect of baryon density is also seen in the production of K^-. It is seen that for large values of B, the small values of B/V increase the K^+ production by an enormous amount as compared to K^- production. The $\bar{u}$ and $\bar{d}$ quarks are suppressed by the Pauli principle in high-baryon environment. However this is not true for $\bar{s}$ quarks. In a pure hadronic picture, a baryon rich system enhances the K^+ production through associated production with Λ's or Σ's and suppresses K^- due to its absorption through the exchange channels considered previously. It should be noted here that rather

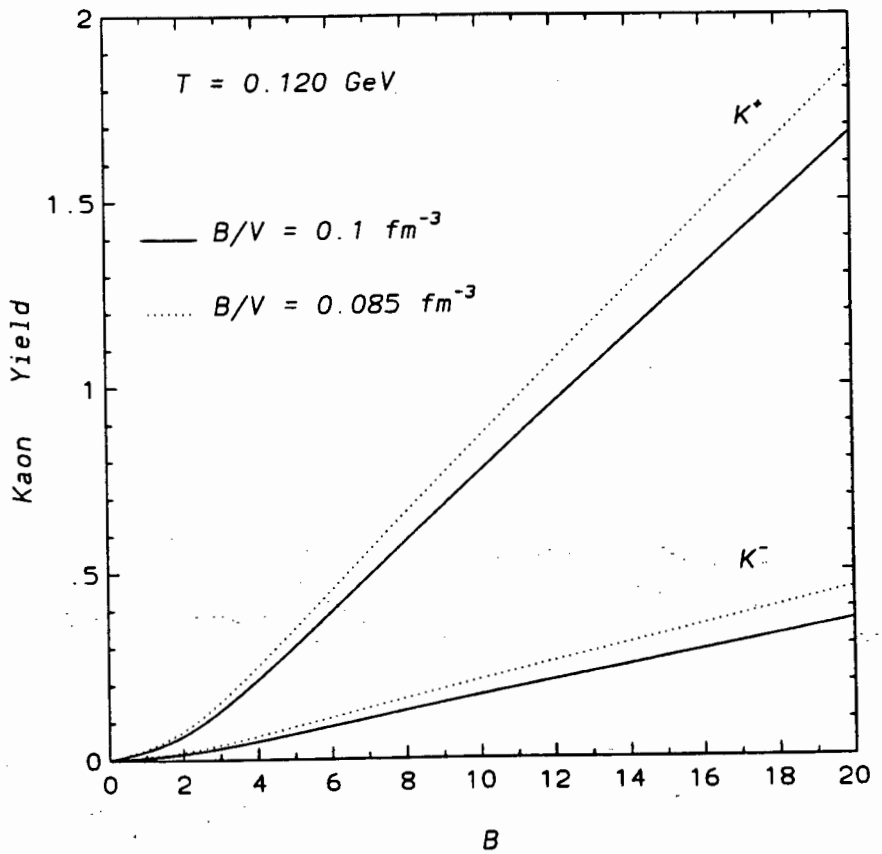

Figure 3.4: The dependence of Kaon Yield on baryon density is plotted as a function of the baryon number, B.

than the yield depending on the baryon density directly, it turns out that it depends much on the volume. This is so if one recalls that we are keeping the baryon density B/V fixed. Thus one quickly sees that at a particular value of B for a small B/V fixed we have larger volume than for high B/V fixed. Thus one expects a high yield since

$$Yield \propto V.$$

Since the mesons are not affected by the baryon chemical potential, the imbalance in strange and non-strange mesons can be attributed to the non-zero strange chemical potential (in the grand canonical). We impose zero net strangeness in the gas which does not necessarily mean that $\mu_S = 0$. Thus the difference in K^+ and K^- yields arises because it is energetically more favorable in baryon rich system to create anti-strange meson such as K^+ with strange baryons via

$$pp \longrightarrow K^+\Lambda p \ ,$$

than strange mesons such as K^- via

$$pp \longrightarrow K^+K^-pp \ .$$

3.4.2 Pion Production

Pions are very easy to create but are less interesting than kaons. They carry very little information from the early stages of collisions. Even if they are directly produced from interesting physics processes, the information they carry can be easily washed out by rescattering on the way out. Many particles and most resonances decay into pions, making them very diverse. Nevertheless, pions are important; for instance, to understand the K/π ratio, we have to first understand not only kaon production but also pion production. Figure 3.5 shows the particle m_T spectrum for rapidity range $0.< \delta y < 0.2$. The spectrum for the pions, especially for π^- is an interesting one in studying the pion production. Unlike kaons, there are clearly more pions at low m_T than one expects from exponential extrapolation from high m_T points. The bending up of low m_T points, the so-called low p_T enhancement (= enhancement over exponential predictions from high p_T points), is clearly seen in the spectrum. A single m_T exponential fit to the spectrum (from high m_T), would obviously fail at low m_T in Figure 3.5.

The low p_T enhancement for π^-'s can be more clearly seen with the guidance of the m_T exponential fit. Many other experiments (for example [56], etc.) have also seen this low p_T pion enhancement (for an overview see [57]). The enhancement was seen in early experiments too, such as those reviewed in [58]. The enhancement was thought to arise from contamination from decay resonances such as Δ's and N^*'s, probably together with weak

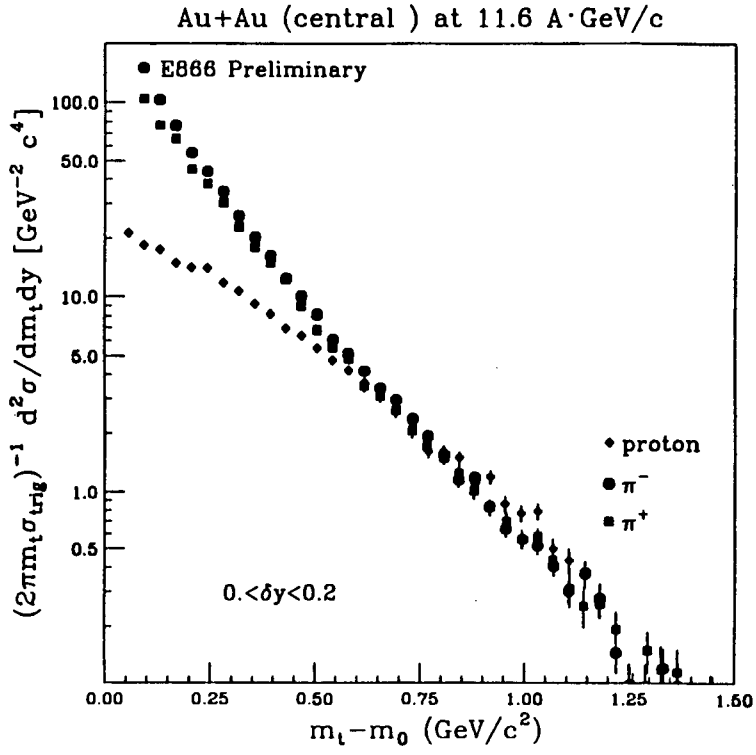

Figure 3.5: $\pi^{\pm}$ and proton m_T spectrum for the rapidity range $0.< y <0.2$ [55].

transverse flow [59, 60]. Decays producing low p_T pions [57] include the strong decays

$$\begin{aligned} N^* &\longrightarrow \pi N\ , \\ \Delta &\longrightarrow \pi N\ , \\ \rho^0 &\longrightarrow \pi^+\pi^-\ , \\ \rho^0 &\longrightarrow \pi^-\pi^0\ , \\ \omega &\longrightarrow \pi^+\pi^-\pi^0\ , \\ K^* &\longrightarrow K^+\pi^-\ , \end{aligned} \tag{3.9}$$

and weak decays

$$\begin{aligned} K_s^0 &\longrightarrow \pi^+\pi^-\ , \\ \Lambda &\longrightarrow p\pi^-\ , \\ \Sigma^0 &\longrightarrow p\pi^-\ , \\ \Sigma^- &\longrightarrow n\pi^-\ . \end{aligned} \tag{3.10}$$

Studies [32, 61], distinguishing between decay pions from Δ's and thermal pions indicate

that the dominant contribution of π^-s is from Δ. Low p_T enhancement was also observed in π^+ spectra, but not as much as for the π^- spectra. This is partially because there are more particles and resonances, as shown in the list above, which decay into π^- than into π^+. The result for pion production is shown in Figure 3.6. The first feature to notice is that the π^- is greater than the π^+ production especially as one goes to large values of B. This difference between the π^- and π^+ can be clearly seen from their ratios as shown in

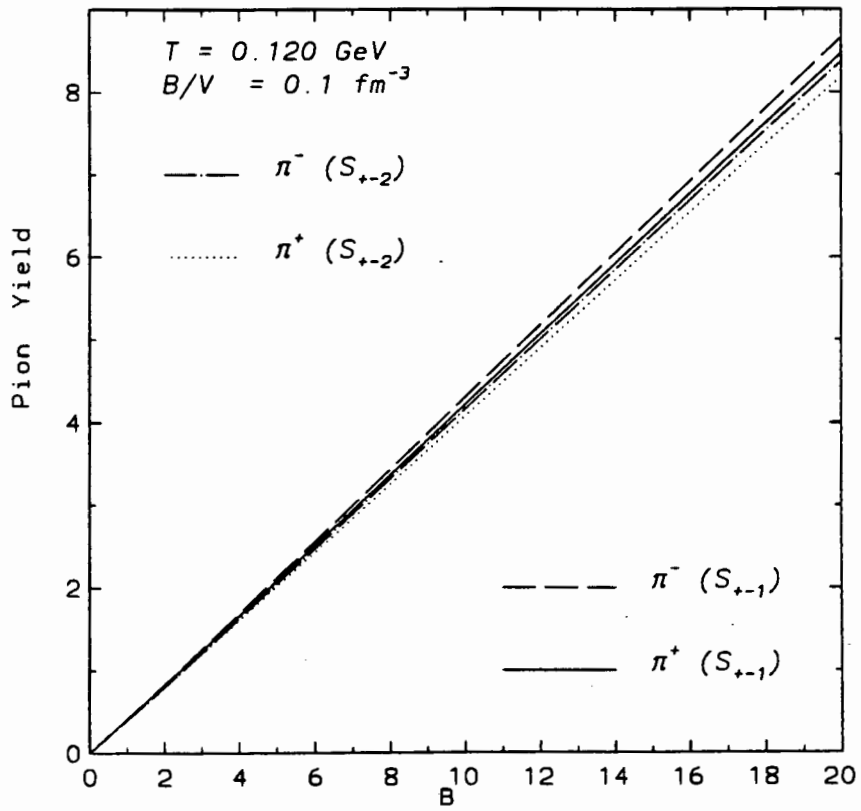

Figure 3.6: The Pion Yield as a function of the baryon number, B. The fixed thermal parameters are the temperature $T = 120\ MeV$ and the baryon density $B/V = 0.1/fm^3$.

Fig. 3.7. From this figure one notices the turning up at low m_T which indicates that some of the low m_T π^-'s are probably from physics processes and decays that do not contribute to π^+'s. Also to be noticed is the slight excess of π^- at high m_T which might be as a result of isospin asymmetry, and coulomb interaction. In heavy ion collisions like $Au - Au$ there should be coulomb (which favours the low m_T π^-'s because of the positive net charge) and isospin (which favours more π^- because of the neutron excess over protons in $Au - Au$ system) effects contributing to the difference between the π^- and π^+. The coulomb effect

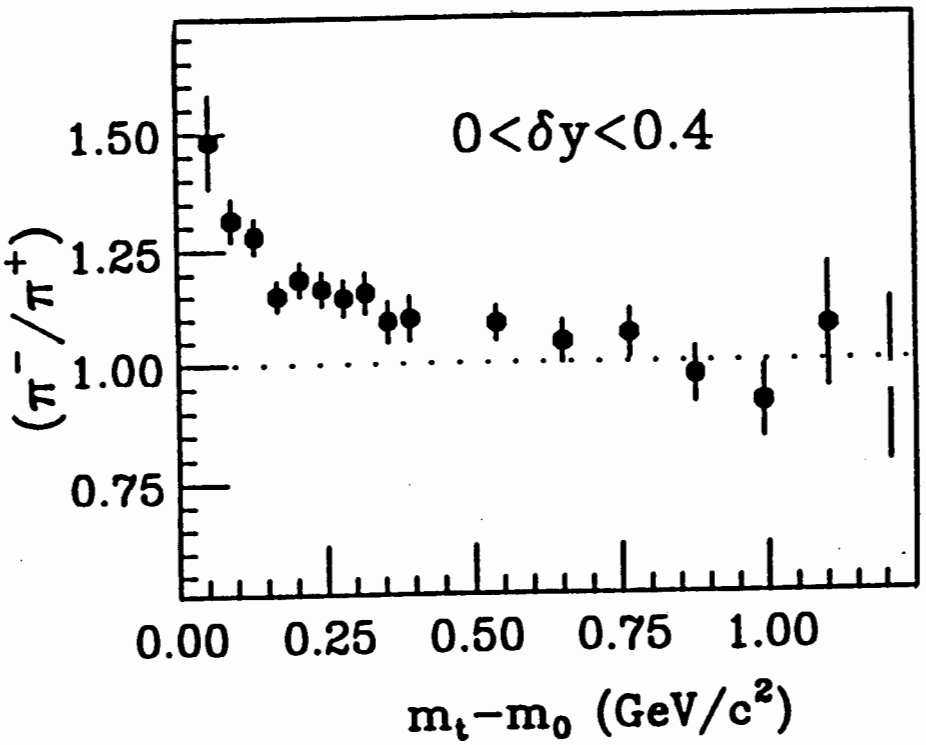

Figure 3.7: The m_T spectra of the π^-/π^+ ratio at different rapidities from $Au + Au$ [55].

has been investigated [62] using an oversimplified hadron gas model which shows perfectly the behaviour seen in experimental information. This difference was seen in nuclear collisions at Bevalac [63] and ISR [64].

The effect of introducing particles with strangeness = ± 2 is seen as decreasing the pion production, especially at large values of B. Similar to the situation of kaons this is due to strangeness conservation at the expense of pions through

$$\pi + Y \longrightarrow K + \Xi^- \ ,$$

and again Y is Λ or Σ. However pions, on average, will be at the forefront because of the existence of many decay channels. The pion production, however, seems to be linearly increasing with B even at the beginning (at small values of B), unlike the kaon production. The pions show a great sensitivity on the composition of the gas (cut-off mass), Figure 3.8. The inclusion of heavy resonances enhances the production of pions. This is an indication of many resonances decaying into pions. The production of pions increases with a decrease

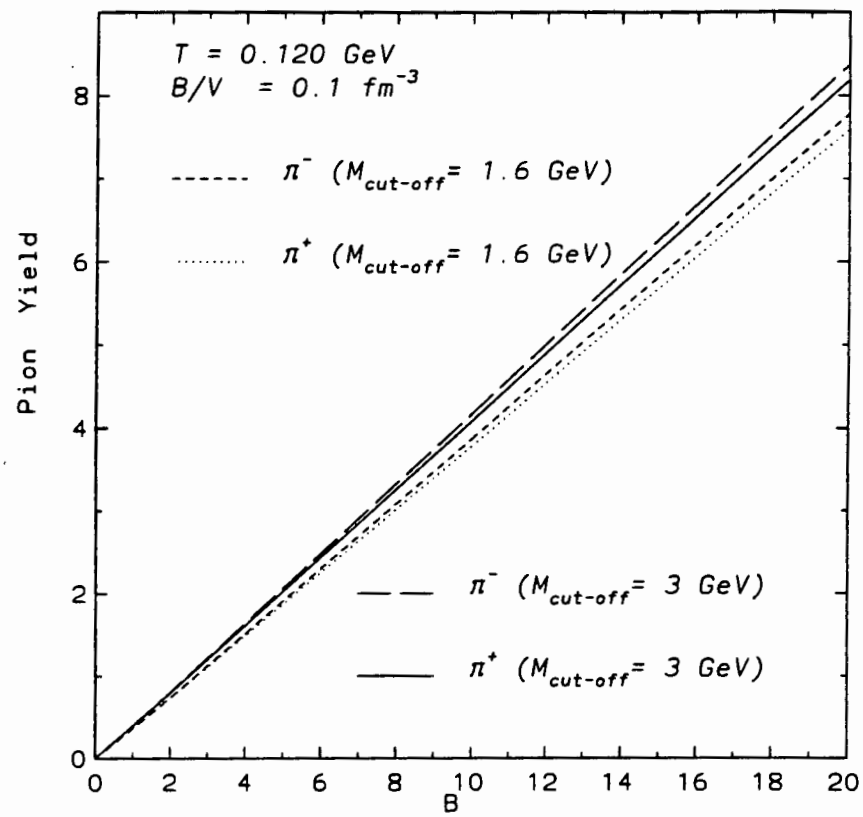

Figure 3.8: The dependence of the pion production on the cut-off mass is shown as a function of baryon number, B, at fixed T and B/V.

in baryon density, B/V. This is shown in Fig. 3.9. Like the kaon production, the pion yield also depends much on the volume, particularly at large values of B. This is so if one thinks that the pions are not affected by μ_B and μ_S in grand canonical, but are affected only by temperature, T, and volume, V. However, T is fixed here. Hence V is the major factor.

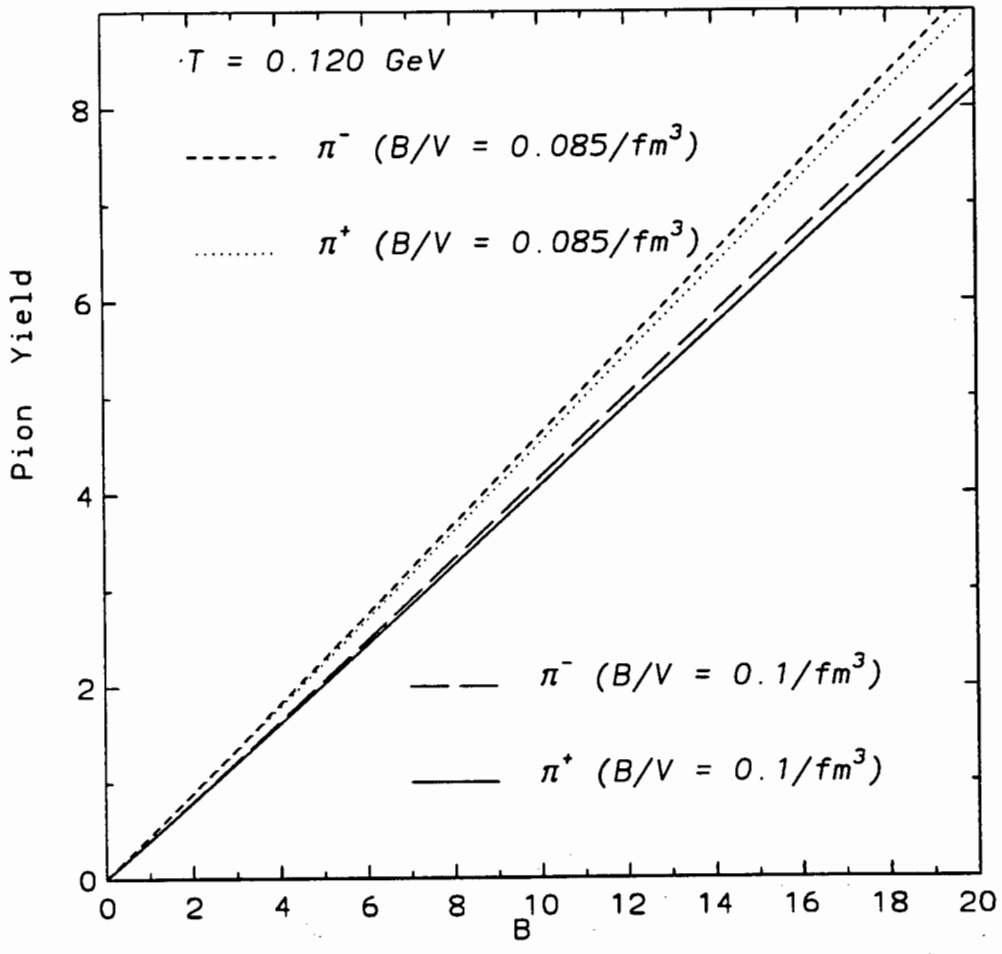

Figure 3.9: The dependence of the pion production on the baryon density is shown as a function of baryon number, B, at fixed T.

3.4.3 The K/π Ratio

The enhancement in K^+/π^+ ratio was originally proposed as a signature of QGP formation a few years ago. A fair amount of K^+ enhancement relative to π^+ has indeed been found in heavy ion experiments relative to *pp* collisions at similar collision energies per nucleon [65, 66]. However, the enhancement can also be explained in a hadronic picture without invoking QGP formation [67, 43]. Understanding the mechanisms responsible for the enhancement has been one of the primary goals in heavy ion physics. The enhancement might be due to the increased contribution of K^+'s in heavy ion collisions from particle rescattering processes. And these processes need closer attention to understand them. These processes are, however, negligible in light ion collisions. Thus the enhancement of K^+/π^+ ratio in heavy ion production needs to be approached by studying the individual particle production mechanisms, i.e. kaon and pion production mechanisms which are not well known. Many theoretical models [67, 43, 68, 69, 70], have shown, to some extent, that particle rescattering and hadronic gas models could explain the strangeness enhancement observed. The results obtained for K^+/π^+ and K^-/π^- ratios using strangeness ±1, ±2, ±3, are shown in Figure 3.10. The K^+/π^+ ratio increases more rapidly in Strangeness = $\pm$2,3 than in the Strangeness = ±1 case. However, there is no clear distinction between the $S_{\pm2}$ and the $S_{\pm3}$ curves. For the K^+/π^+, as values of B get high there is a clear distinction between $S_{\pm1}$ and $S_{\pm2,3}$. However, in the K^-/π^- ratio for $S_{\pm1}$, $S_{\pm2}$ and $S_{\pm3}$ there is almost no difference. The dependence on B for both K/π ratios seems to follow the same pattern. The ratios increase slowly from small values of B (small volumes) to a point where they begin to show some smooth levelling off. This indicates that as B approaches high values(large volumes) the ratios will be constant. Thus, it seems as if the mechanisms which are responsible for kaon production cease to generate the kaons. As B increases, we have a fast increase of light quarks and anti-quarks compared to strange quarks and anti quarks. Thus we expect to see a saturation behaviour at large values of B. The distinction due to the strangeness content factor arises solely from the kaon and pion yield due to the same factor.

One observes a slight decrease in the K^+/π^+ ratio, as calculated with resonances of cut-off mass of about 3 GeV when compared to a hadronic gas contained in resonances of cut-off mass of about 1.6 GeV. This can easily be explained by the fact that heavy resonances have more

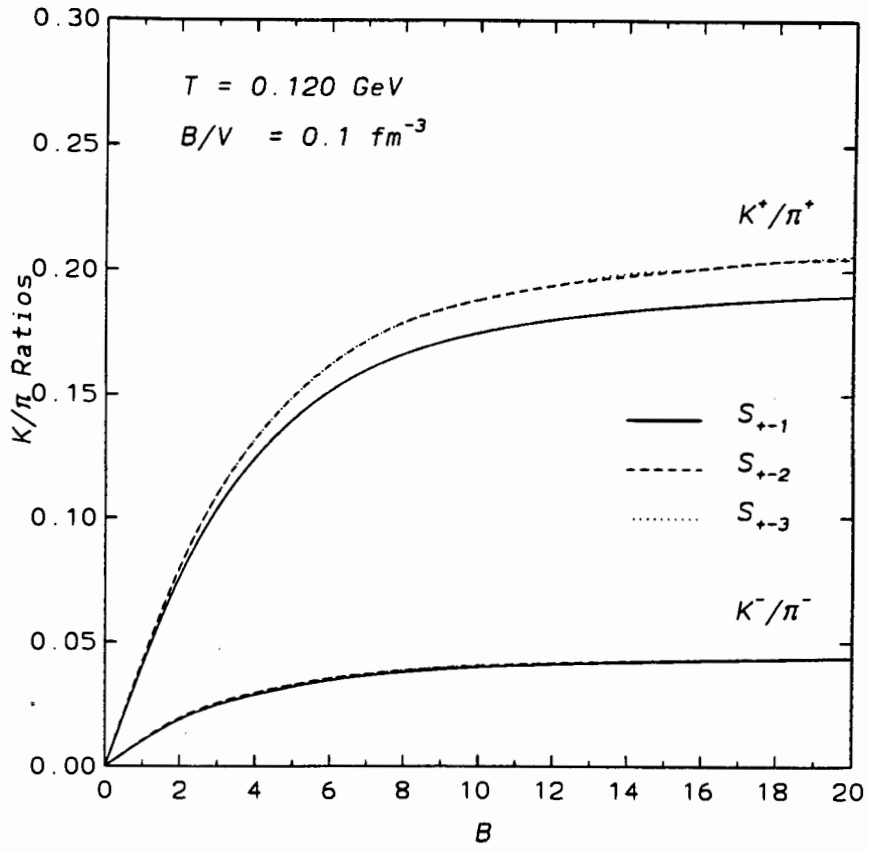

Figure 3.10: The K/π ratio as a function of the baryon number, B at fixed T and B/V.

pions than kaons in their decay products, thus reducing the K^+/π^+ ratio, Figure 3.11. But for K^-/π^- the change is even smaller (or almost not there) and vice-versa to the K^+/π^+ ratio. Both the K^+/π^+ and K^-/π^- ratios depend strongly on the baryon density. The K^+/π^+ ratio shows an increase with decreasing baryon density for a finite small B before converging for the different baryon densities. Thereafter at large B the ratio decreases for low B/V while for large B/V it has not yet shown a decrease. Thus it turns out that at large values of B the K^+/π^+ ratio will show minimal or no dependence on the baryon density. This is confirmed by the calculations done in the grand canonical formalism [46]. But for K^-/π^-, the effect of baryon density seems to show an increase of K^-/π^- ratio at low B/V's, Figure 3.12. At high baryon densities K^-/π^- is suppressed. The two ratios are also shown as a function of baryon density for a fixed B as shown in Figure 3.13. This is the same as fixing the volume or the radius of the gas. The situation of the two ratios depending on the baryon density can be clearly seen on the grand canonical scenario. In the quark level we

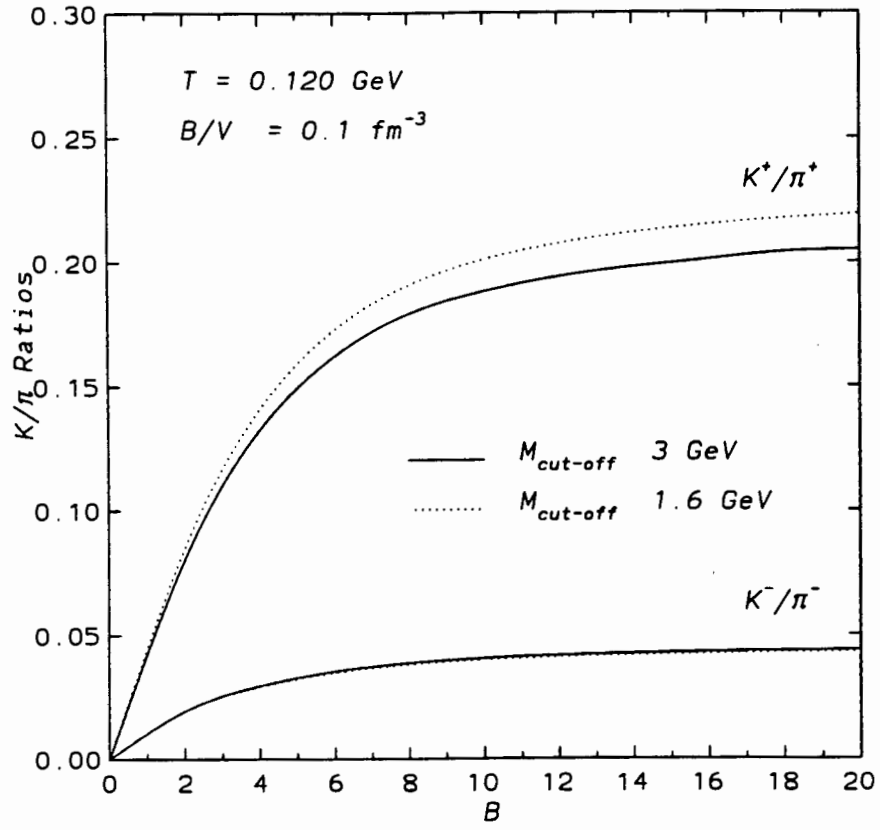

Figure 3.11: The dependence of K/π on the cut-off mass for a fixed T and B/V plotted as a function of baryon number, B.

have roughly

$$\begin{aligned} \frac{K^+}{\pi^+} &\sim \frac{\bar{s}u}{\bar{d}u} \\ &\sim \frac{\bar{s}}{\bar{d}} \\ &\sim \frac{\exp(-m_s/T)}{\exp(-\mu/T)} \ , \end{aligned} \tag{3.11}$$

while for K^-/π^- ratio one has

$$\frac{K^-}{\pi^-} \sim \frac{\exp(-m_s/T)}{\exp(\mu/T)} \ . \tag{3.12}$$

As one increases the baryon density, the chemical potential μ increases correspondingly. Thus one expects K^+/π^+ to increase and K^-/π^- ratio to decrease. Figures 3.14 and 3.15 are the K/π ratios obtained from a grand canonical hadron gas model with three hard-core radii and temperatures taken from [71]. As one can see, the K^+/π^+ ratio initially rises with

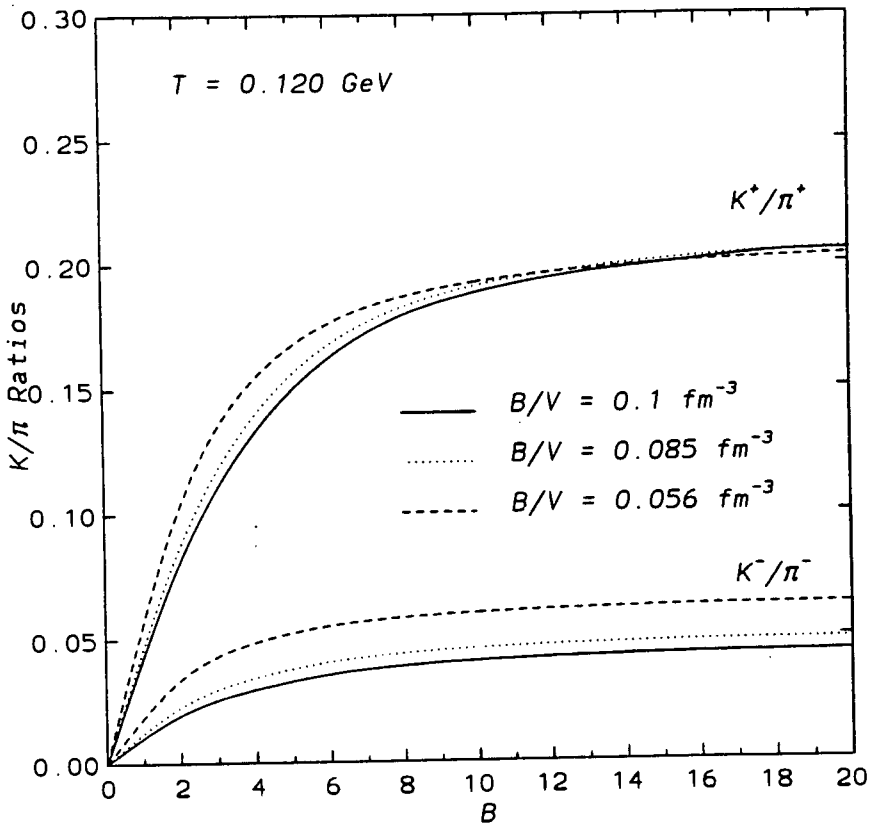

Figure 3.12: The dependence of K/π on the baryon density for a fixed T plotted as a function of baryon number, B.

increasing baryon density. It then reaches a plateau and starts decreasing. For moderate densities, the K^+/π^+ ratio is almost independent of the hard-core radius and after reaching a maximum, the ratio becomes very strongly dependent on the radius. The K^-/π^- ratio always decreases for increasing baryon densities. The decrease beyond $n_B = 0.1/\text{fm}^3$ is essentially caused by tilted baryon volumes (strong short-range repulsion between baryons). The two ratios are the same for a baryon free system, in agreement with $p\bar{p}$ collision data (vanishing baryon density) at CERN Intersecting Storage Rings (ISR) [72], [73], in which K^+/π^+ and K^-/π^- were both 11% at mid- rapidity.

Fig. 3.16 shows the dependence of the K/π ratio, both the K^+/π^+ and K^-/π^- ratios as a function of temperature. The same calculation is also done in the grand canonical ensemble, Fig. 3.17(b)[16]. As the temperature increases, the kaon density and the pion density increases. However, the kaon density increases at a more rapid rate as compared to pion

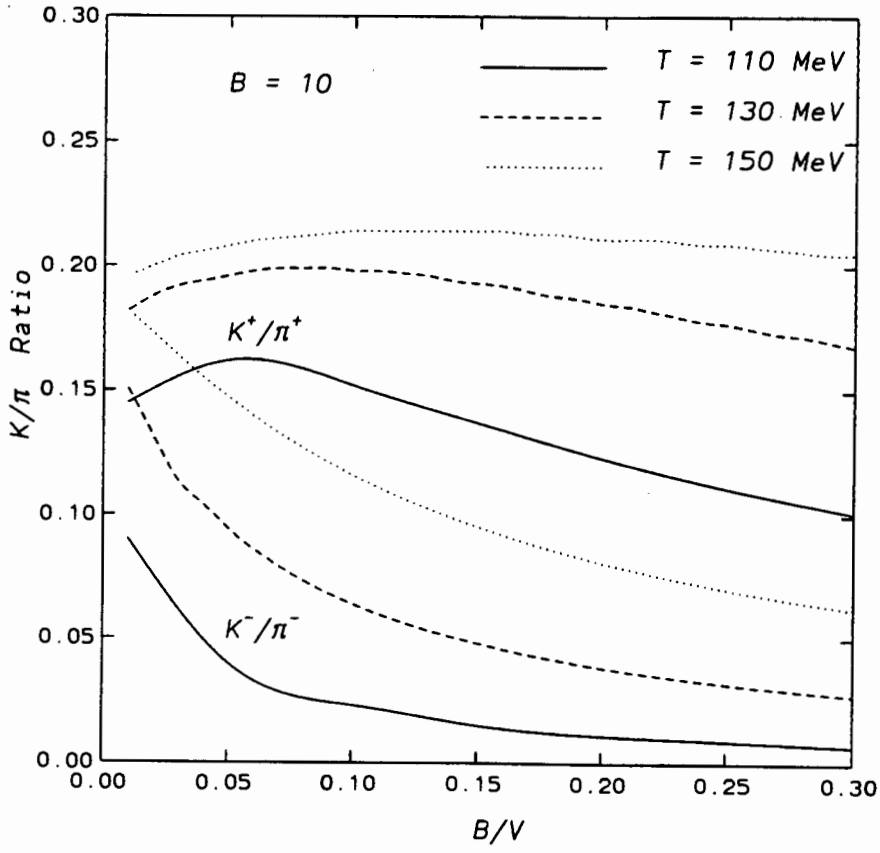

Figure 3.13: The K/π ratios are plotted as a function of the baryon density for three temperatures at a fixed baryon number, B.

density. Thus one will expect the ratio $n_{K+}/n_{\pi+}$ to increase as T increases. However in Fig 3.16, where we have fixed B, B/V and obviously V, we see that the ratio will reach a maximum at a particular temperature depending on the realistic choices of B and B/V, and as T increases the K^+/π^+ ratio starts to decrease slowly while the K^-/π^- ratio rises fast with temperature towards convergence with the K^+/π^+ ratio. In grand canonical at quark level the trend is clear :

$$K^+/\pi^+ \sim \frac{e^{-m_s/T}}{e^{-\mu/T}} \ ,$$

$$K^-/\pi^- \sim \frac{e^{-m_s/T}}{e^{+\mu/T}} \ ,$$

the exponential increase in the positive ratio is suppressed by an increase in T while it is enhanced for the negative ratio. This is due to difference in the signs of the quark chemical potential. At the hadron level one recalls that as temperature increases, the probability of

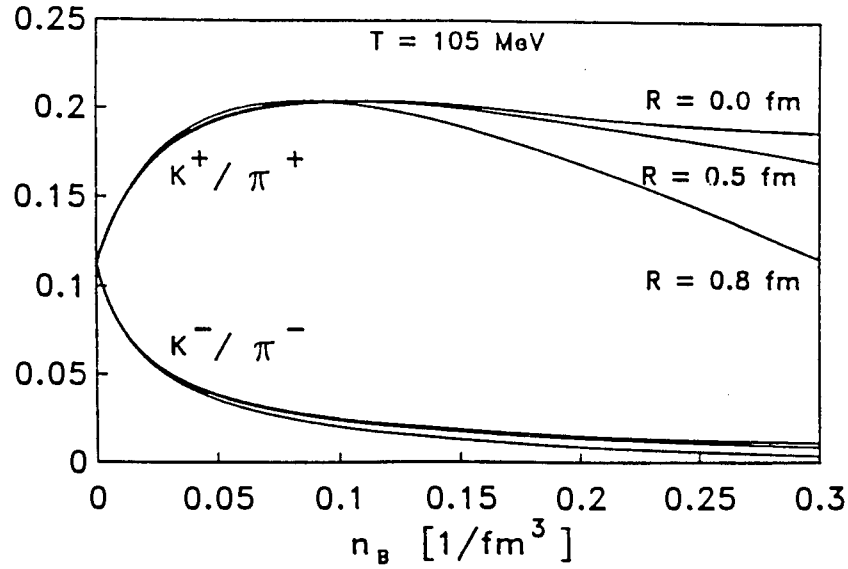

Figure 3.14: The dependence of the K/π ratios on the hard core radius R as a function of baryon density [71].

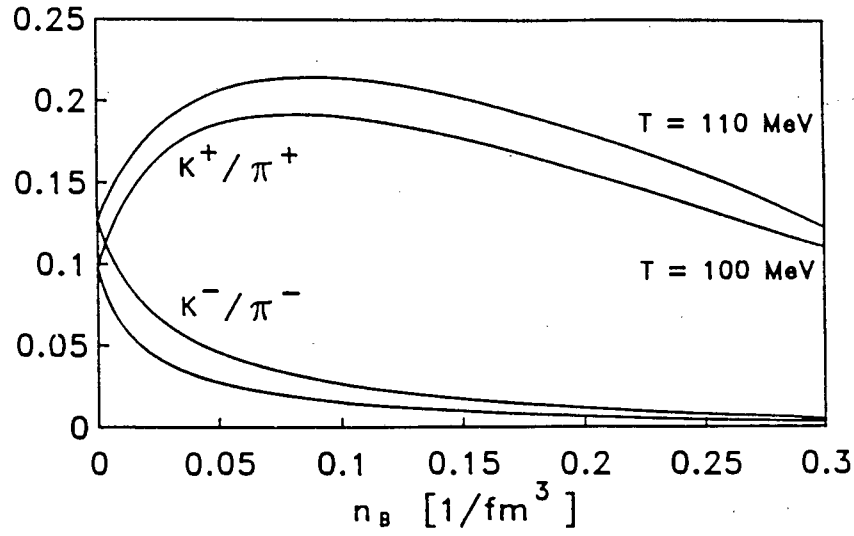

Figure 3.15: The dependence of the K/π ratios on the baryon density for different values of temperature T [71].

creating heavier resonances increases substantially, thereby increasing the decay channels, many of which favour pions and slightly the K^-. Thus we see that at large values of T both

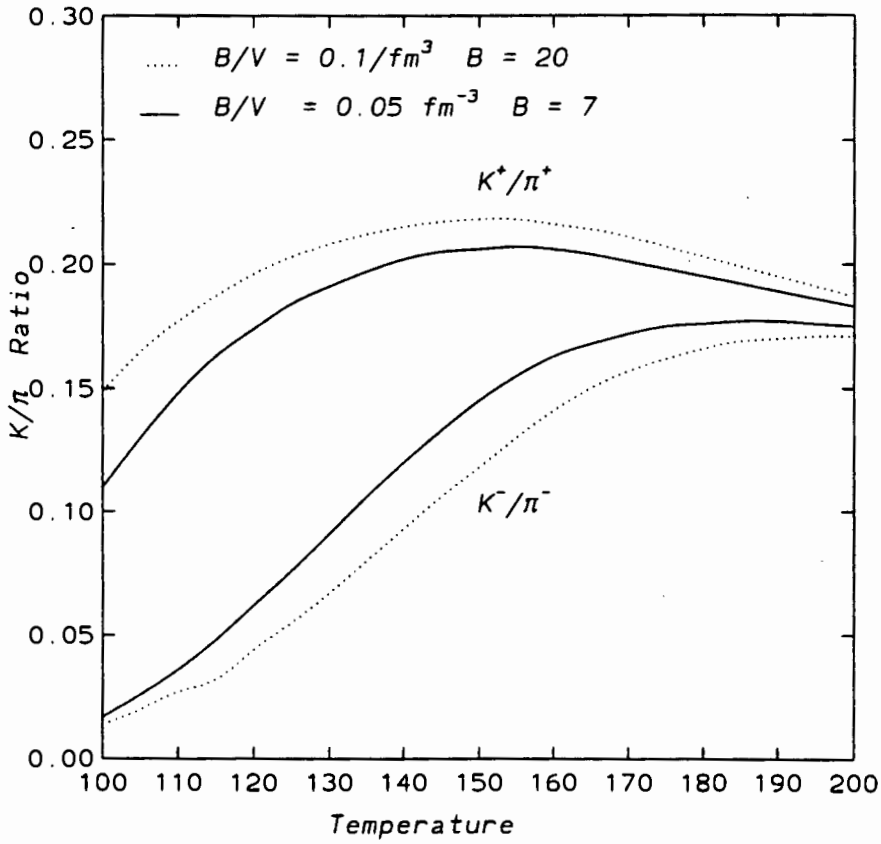

Figure 3.16: The dependence of the K/π ratio on the temperature.

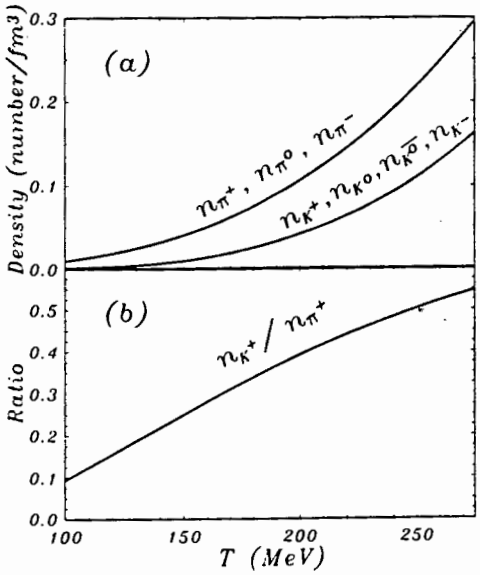

Figure 3.17: a) The pion and kaon densities as a function of temperature T. b) The ratio of K^+ density to π^+ density, as a function of temperature [16].

ratios start to decrease.

3.4.4 The K^+/K^- Ratio

Another important ratio in the study of the generating functions of the hadronic gas models is the K^+/K^- ratio. The inclusion of high strangeness particles in the gas will lead to the increase of the K^+/K^- ratio as indicated in Fig. 3.18. This is so since the high strangeness particles enhance K^+ and suppress K^-. However, the important feature here is the de-

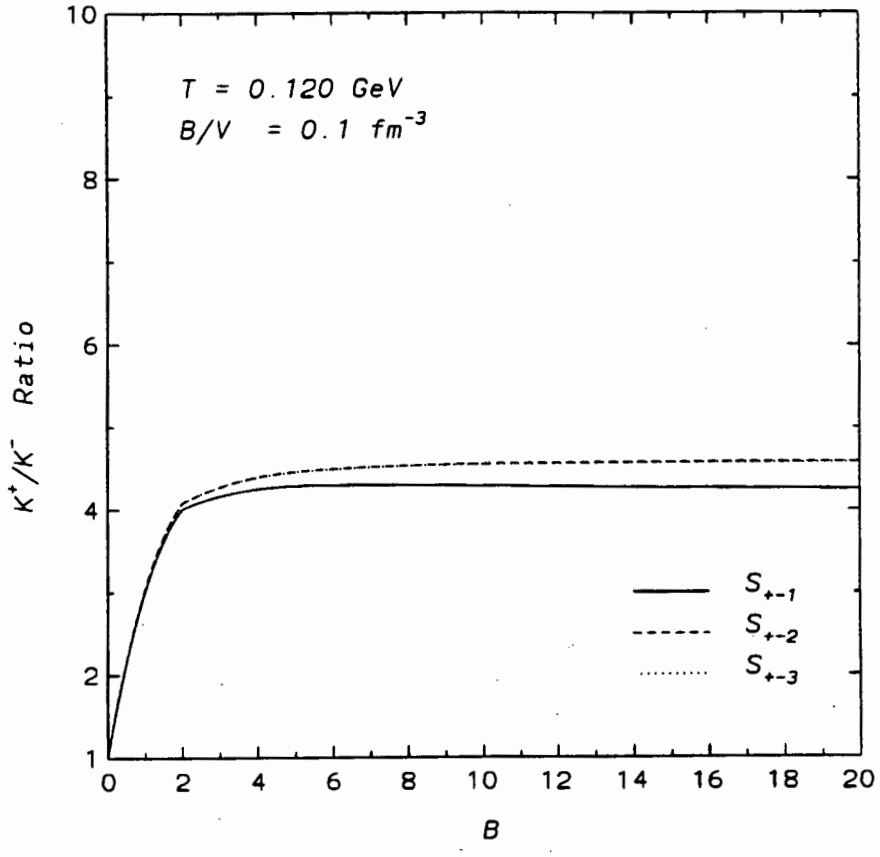

Figure 3.18: The K^+/K^- ratio as a function of baryon number, B.

pendence of the ratio on B. For small values of B the ratio increases very steeply before levelling off, and starts to be independent (or almost independent) of the volume for large values of B and thus remains flat on average. This is so irrespective of the difference in the K^+ and K^- yields. Thus one would expect that, at high values of B where we will have more K^-'s absorbed due to large K^-N inelastic cross-section, the ratio will be increased. This is not seen in this ratio. This might be because as B increases one produces more K^-'s than K^+'s. When one combines this with the fact that in the region of large B we also have large absorption of K^-'s, it will lead to the K^+/K^- ratio being insensitive to B (and/or

volume). For very large values of B the ratio drops slightly. This is due to more K^-'s being produced with respect to K^+'s, even though one would expect a larger fraction of K^-'s to be absorbed in large systems because of the large K^-N inelastic cross- section. This may make the K^+/K^- ratio drop at large volumes. The effect of resonances composition of the gas to the K^+/K^- ratio is shown in Figure 3.19. For small cut-off mass the ratio increases slightly. The low cut-off mass makes K^- decrease faster than K^+. Hence one would expect an increase in the K^+/K^- ratio when only low cut-off mass resonances are considered. The

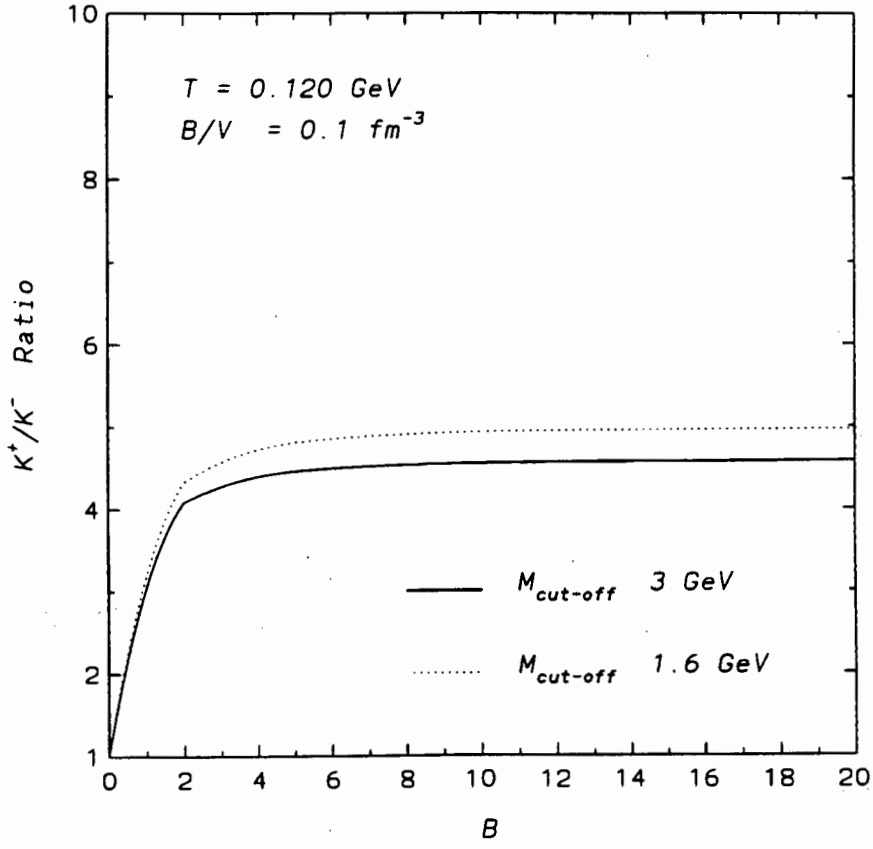

Figure 3.19: The dependence of the K^+/K^- ratio on the cut-off mass is plotted as a function of baryon number, B.

K^+/K^- ratio increases with increasing baryon density, Figure 3.20. The increase is independent of B. The increase in the K^+/K^- ratio as one goes high in baryon density B/V is an indication that this ratio is a good probe for the baryon density of the gas.

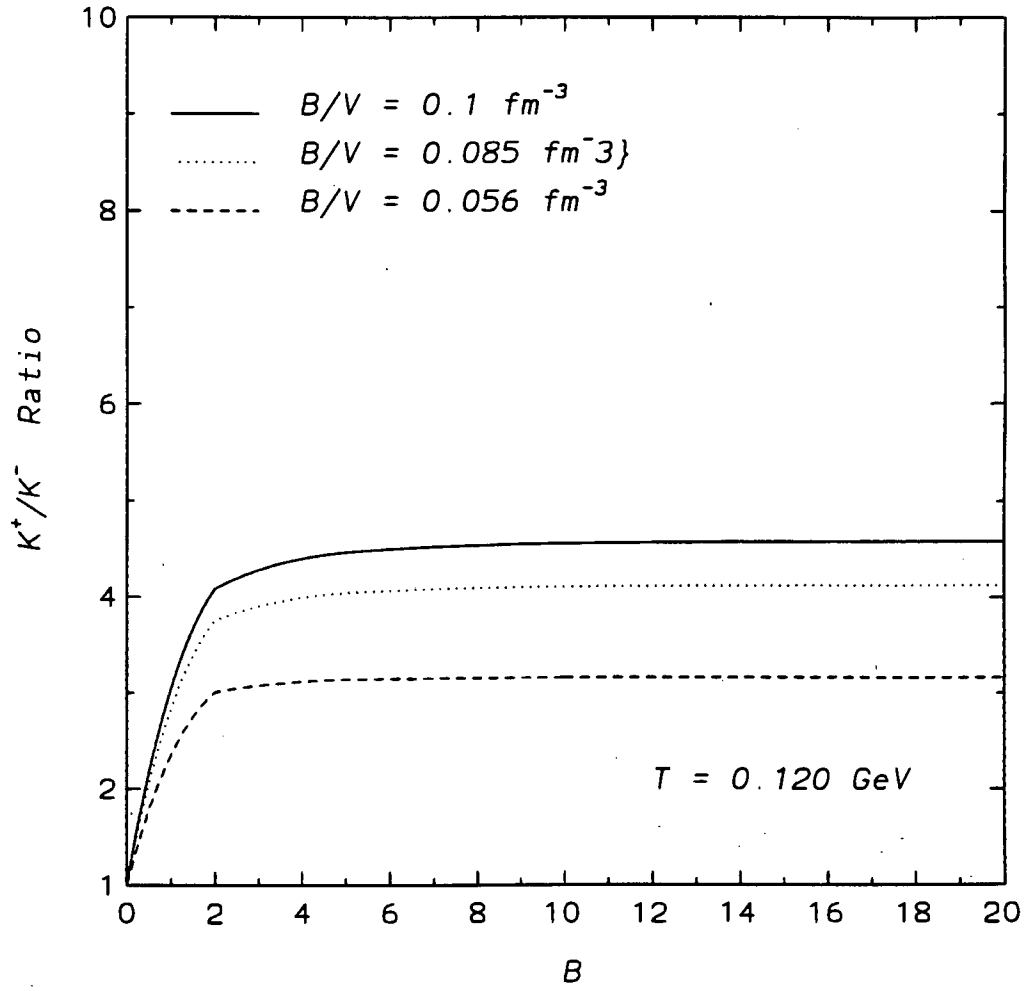

Figure 3.20: The dependence of the K^+/K^- ratio on the baryon density is plotted as a function of baryon number, B.

3.5 The Strange Baryons and Anti-Baryons

Multi-strange baryon and anti-baryon production is expected to be a useful probe in the search for Quark-Gluon Plasma formation since they are more difficult to produce in purely hadronic matter. And in particular, the enhancement of multistrange antibaryon yields relative to nucleon-nucleon interactions is expected in the case of QGP formation [74]. We thus model the production of these particles in our formalism. The production of Λ and Ξ is shown in Figs. 3.21, 3.22 respectively. The dependence of their production on the cut-off mass (i.e the composition of the resonances in the gas), is also shown. It can be seen that whereas including heavier particles(resonances) in the gas decreases the production of *baryons*, this, on the other hand, increases the production of $anti-baryons$. This is because when one increases the cut-off mass, the baryon density increases (if baryon chemical potential is fixed – in the grand canonical ensemble). In order to maintain the same baryon density, the baryon chemical potential must be decreased. This causes an increase in production of anti-baryons and a decreases in the production of baryons. The decreasing factor in Λ is small compared to the increasing factor in $\overline{\Lambda}$, while the decreasing factor in Ξ^- is large compared to the increasing factor in $\overline{\Xi^-}$. With respect to the production of these baryons : a Λ can be produced with one accompanying K while the $\overline{\Lambda}$ requires more accompanying particles to conserve strangeness as well as baryon number (eg. ΛK versus $\overline{\Lambda} N N \overline{K}$) and in the case of Ξ's, the $\overline{\Xi^-}$ can be compensated by two Λ's ($N\bar{\Lambda}\bar{\Lambda}$) while the Ξ^- can be compensated by two kaons ($N\bar{K}\bar{K}$).

The result of the ratios, $\overline{\Xi^-}/\Xi^-$ and $\overline{\Lambda}/\Lambda$, can be explained most easily in the grand canonical ensemble. By increasing the number of hadronic resonances from the cut-off mass of about 1.6 GeV to about 3 GeV, one also increases the net baryon number, B, since baryons have a greater statistical weight than anti-baryons as a result of the sign of the baryon chemical potential. The generating factor is related by,

$$\text{baryons} \sim \exp(-\frac{M}{T} + \frac{\mu_B}{T}) \ , \tag{3.13}$$

$$\text{anti-baryons} \sim \exp(-\frac{M}{T} - \frac{\mu_B}{T}) \ . \tag{3.14}$$

The ratios of $\overline{\Lambda}/\Lambda$ and $\overline{\Xi^-}/\Xi^-$ are both shown in Fig. 3.23. The $\overline{\Lambda}/\Lambda$ ratio is less than the

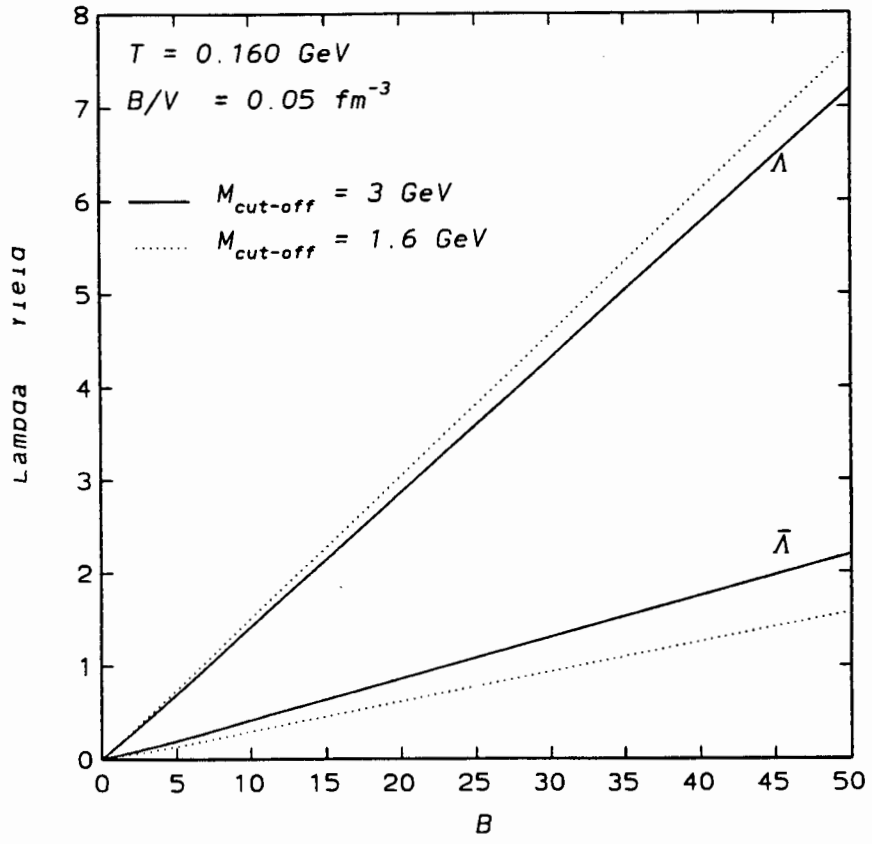

Figure 3.21: The dependence of Λ Yield on the cut-off mass is shown as a function of baryon number, B, at fixed T and B/V.

$\overline{\Xi^-}/\Xi^-$. One can see that there is a strong effect of the cut-off mass in both the ratios. The effect on the $\overline{\Xi^-}/\Xi^-$ ratio is large compared to that on the $\overline{\Lambda}/\Lambda$ ratio. This might make it difficult for the calculation of these ratios in this hadronic gas model. Thus the number of the hadronic resonances changes the results in a crucial way. The two ratios stay almost constant and therefore show almost no dependence on B and/or volume. This behaviour resembles the one in the K^+/K^- ratio. In Fig. 3.24 the effect of cut-off mass is shown for the ratios Ξ^-/Λ and $\overline{\Xi^-}/\overline{\Lambda}$. It can be seen that the effect is more pronounced in the strange anti-baryons ratio. Including heavier resonances in the gas lowers these ratios. Here we see that the ratios grow steeply before reaching saturation at large values of B. However, at small values of temperature and large values of B/V, the anti-baryons ratio rises smoothly until it shows some saturation at large values of B while the baryons ratio starts from a finite value at $B = 0$ and rises with a very small sharp slope and then starts to show some saturation or rather levelling-off, see Fig 3.25.

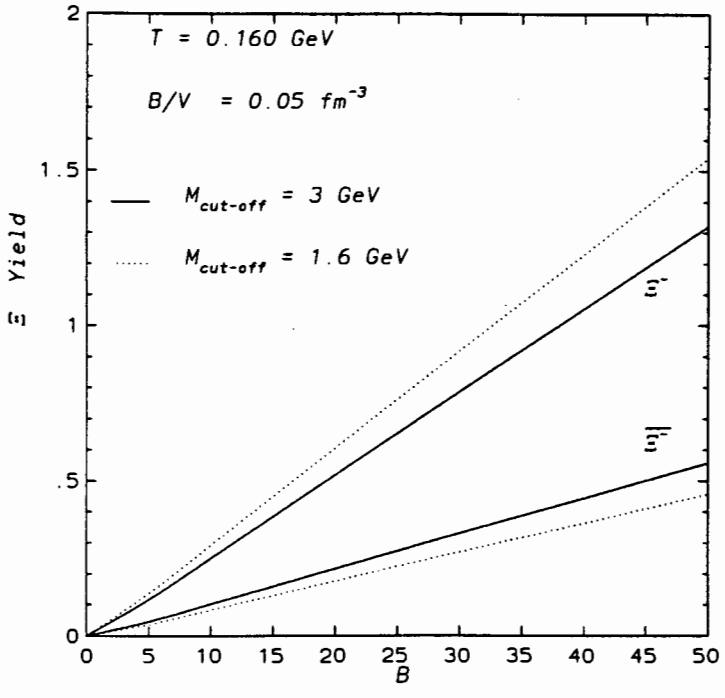

Figure 3.22: The dependence of Ξ Yield on the cut-off mass is shown as a function of baryon number, B, at fixed T and B/V.

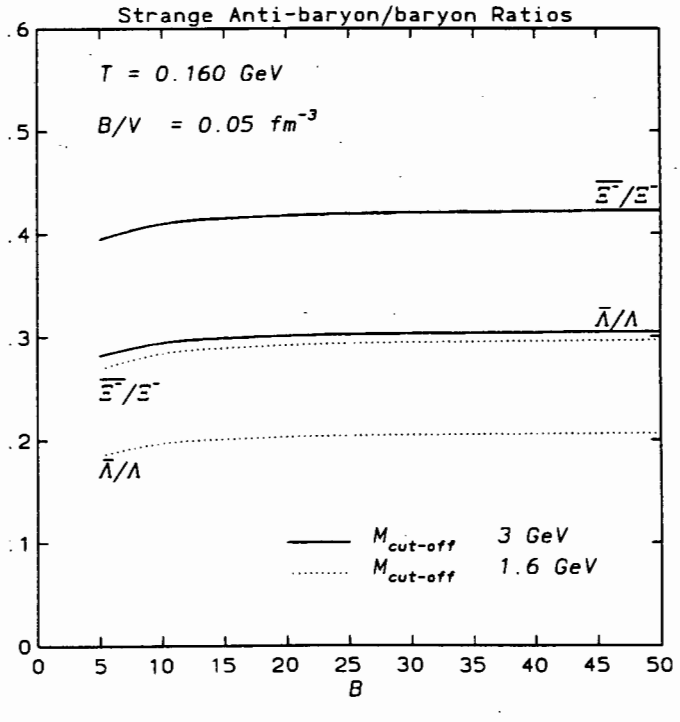

Figure 3.23: The $\overline{\Xi^-}/\Xi^-$ and $\overline{\Lambda}/\Lambda$ ratios as a function of baryon number, B.

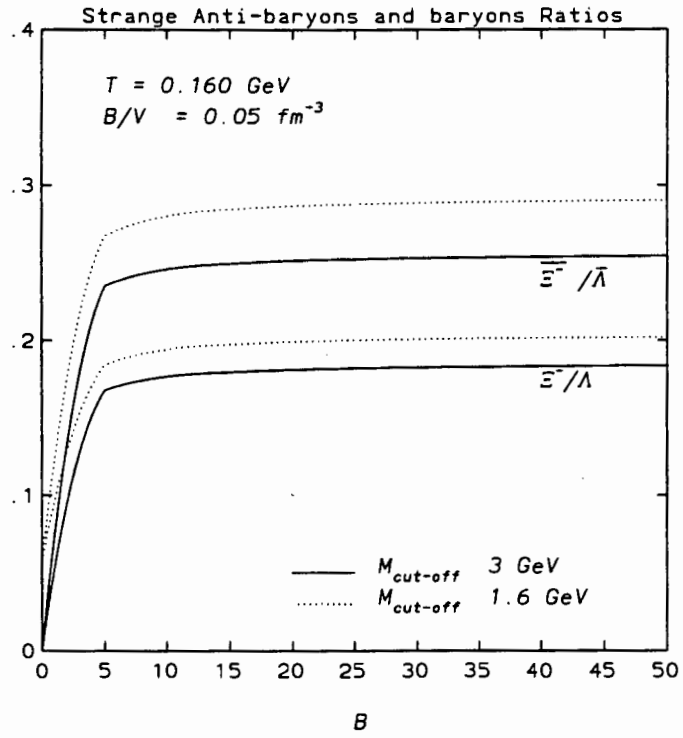

Figure 3.24: The dependence of $\overline{\Xi^-}/\overline{\Lambda}$ and Ξ^-/Λ ratios on the cut-off mass is shown as a function of baryon number, B.

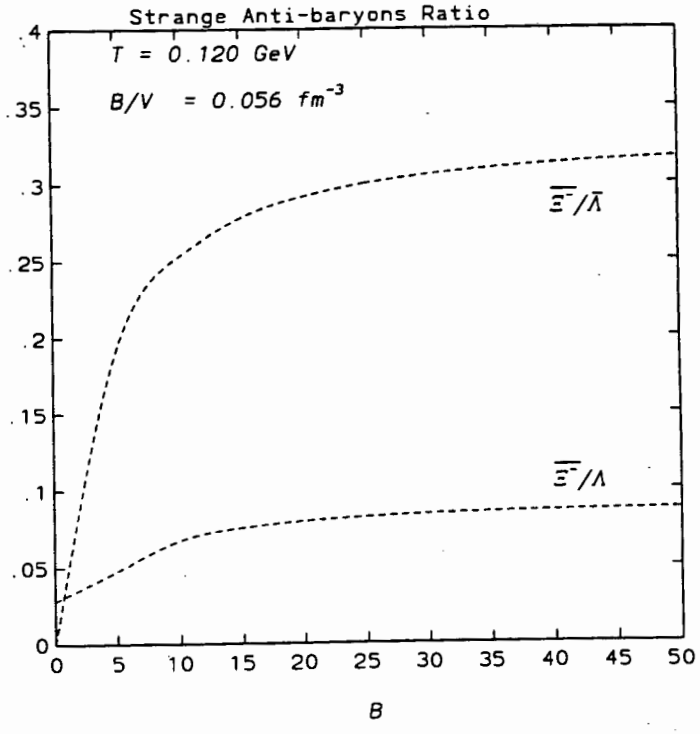

Figure 3.25: The $\overline{\Xi^-}/\overline{\Lambda}$ and Ξ^-/Λ ratios as a function of baryon number, B.

The production of these strange baryons and antibaryons strongly depends on the baryon density. The baryon density can only remain fixed if one lowers the chemical potential μ_B in the grand canonical formalism and this in turn will lead to the enhancement in the $\overline{\Lambda}/\Lambda$ and $\overline{\Xi^-}/\Xi^-$ ratios. In quark level language we have

$$\begin{aligned} \frac{\overline{\Lambda}}{\Lambda} &\sim \frac{\bar{s}\bar{u}\bar{d}}{sud} \\ &\sim \frac{\bar{u}\bar{d}}{ud} \\ &\sim \frac{\exp(-2\mu/T)}{\exp(+2\mu/T)} \\ &= \exp(-4\mu/T) \ , \end{aligned} \tag{3.15}$$

and

$$\frac{\overline{\Xi^-}}{\Xi^-} \sim \frac{\bar{d}\bar{s}\bar{s}}{dss} \ . \tag{3.16}$$

In hadronic level language:

$$\begin{aligned} \frac{\overline{\Lambda}}{\Lambda} &\sim \frac{\exp\left[(-\mu_B+\mu_S)/T\right]}{\exp\left[(+\mu_B-\mu_S)/T\right]} \\ &= \exp\left[(-2\mu_B+2\mu_S)/T\right] \ , \end{aligned} \tag{3.17}$$

while for Ξ's we have

$$\frac{\overline{\Xi^-}}{\Xi^-} \simeq \exp\left[(-2\mu_B+4\mu_S)/T\right] \ . \tag{3.18}$$

Thus we will also expect

$$\frac{\overline{\Xi^-}}{\Xi^-} > \frac{\overline{\Lambda}}{\Lambda} \ . \tag{3.19}$$

This will lead to the enhancement of the baryons and anti baryons ,

$$\overline{\Lambda}/\Lambda \sim \exp(-2\mu_B/T) \ , \tag{3.20}$$

$$\overline{\Xi^-}/\Xi^- \sim \exp(-2\mu_B/T) \ , \tag{3.21}$$

as compared to the Ξ/Λ (like K/π) ratio since it is less sensitive to μ_B:

$$\Xi/\Lambda \sim \text{constant}$$

$$(K/\pi \sim \text{constant}) \ .$$

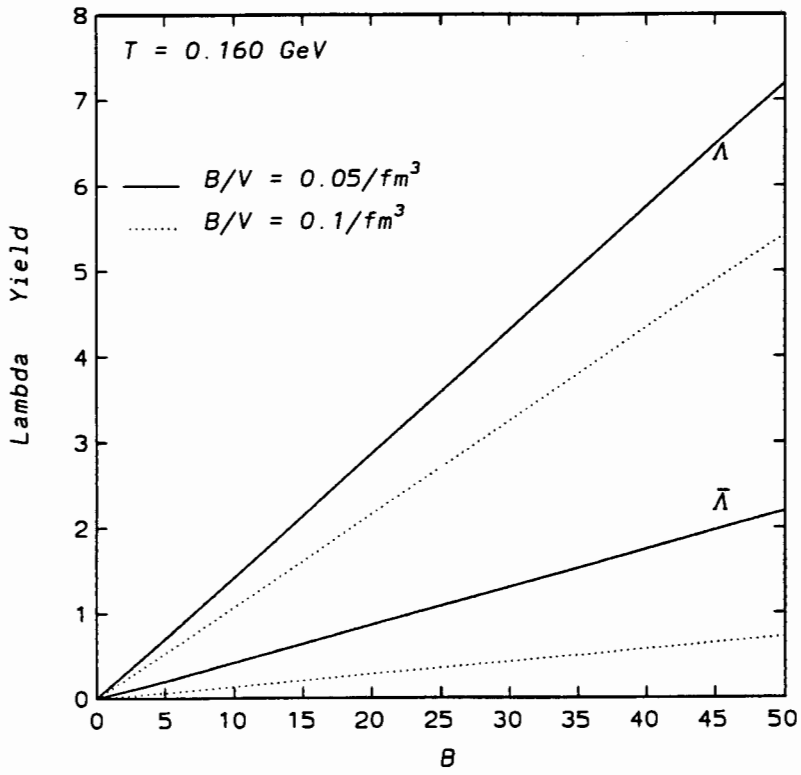

Figure 3.26: The dependence of Λ Yield on the baryon density is shown as a function of baryon number, B.

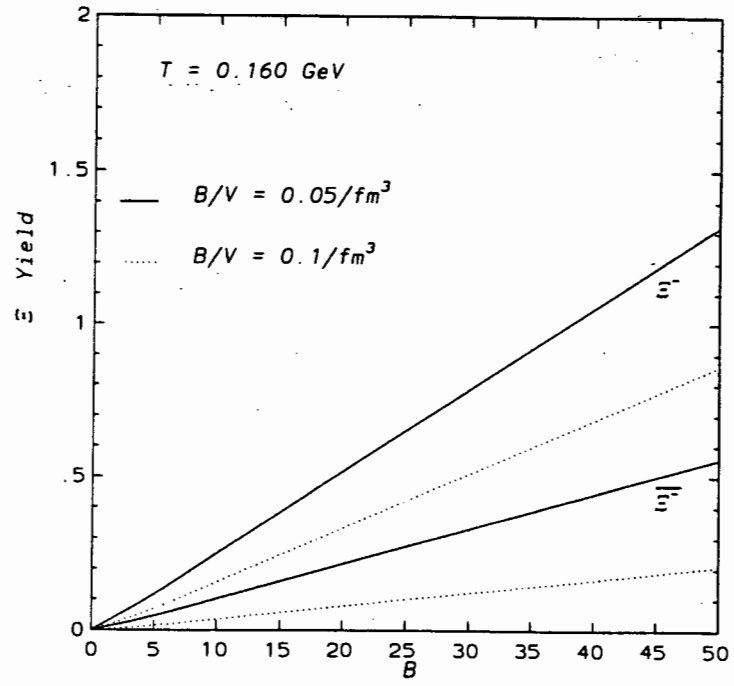

Figure 3.27: The dependence of Ξ Yield on the baryon density is shown as a function of baryon number, B.

Fig. 3.26 shows the dependence of Λ and $\overline{\Lambda}$ production on the baryon density, and it can be seen that an increase in B/V lowers their production. The same effect is seen to be also strong in $\overline{\Xi^-}$ and Ξ^- production. This is shown in Fig. 3.27. Again one sees that the volume is an important factor in determining the yields of these particles.

The dependence on B/V is again seen for the ratios $\overline{\Lambda}/\Lambda$ and $\overline{\Xi^-}/\Xi^-$ and it is seen strongly in both ratios, even though there is slight difference in suppression factor as one increases B/V, Fig. 3.28. This difference depends strongly on the choice of temperature. However, for the ratios Ξ^-/Λ and $\overline{\Xi^-}/\overline{\Lambda}$, the situation looks a bit different: for the strange baryons, the increase in B/V lowers the ratio, whereas for the anti-strange baryons, the increase in B/V increases the ratio by a large factor compared to the lowering one on strange baryons, Fig. 3.29.

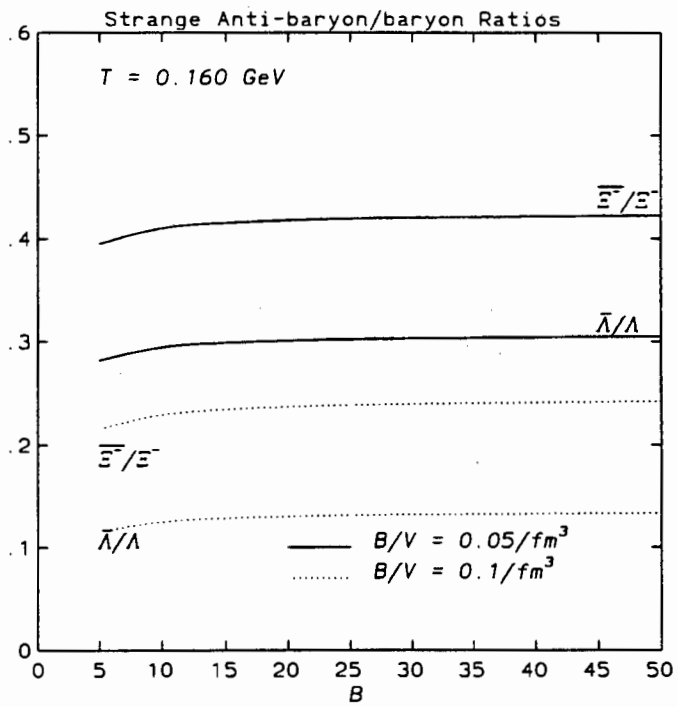

Figure 3.28: The dependence of the $\overline{\Lambda}/\Lambda$ and $\overline{\Xi^-}/\Xi^-$ on the baryon density is plotted as a function of baryon number B.

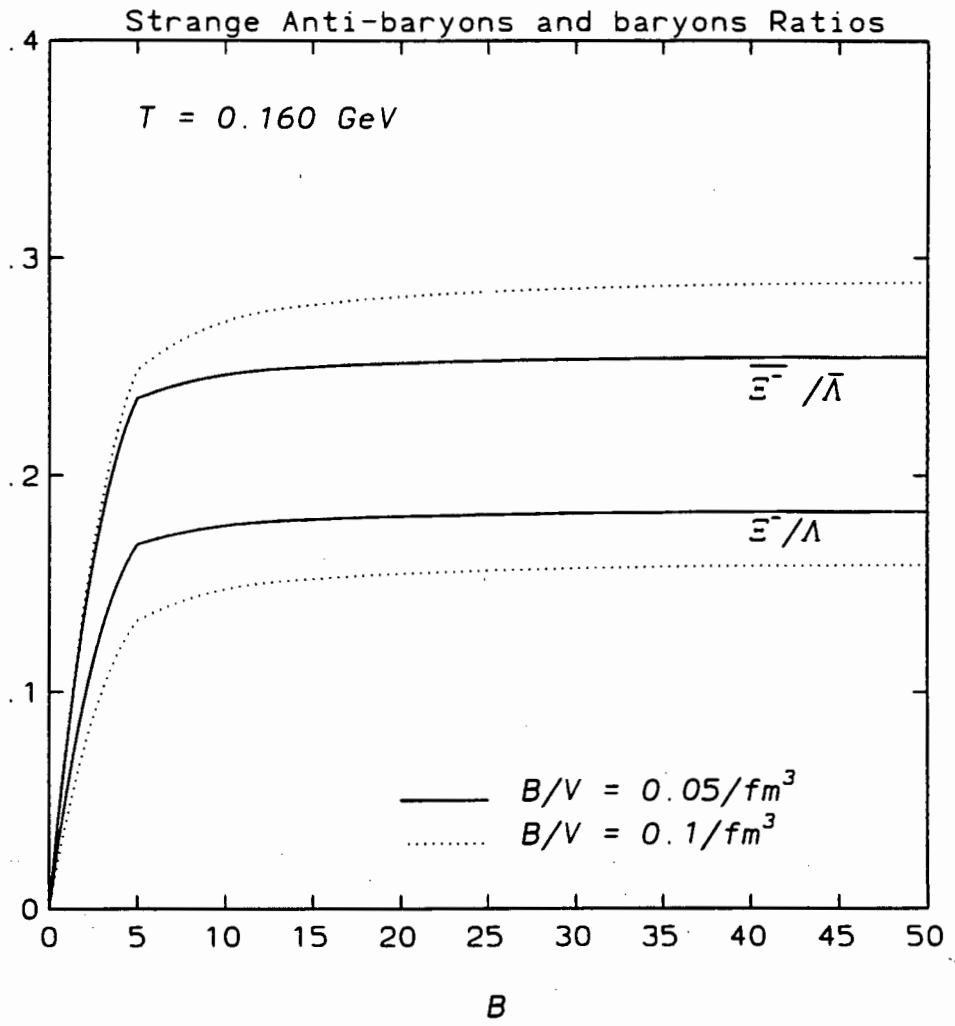

Figure 3.29: The dependence of the Ξ^-/Λ and $\overline{\Xi^-}/\overline{\Lambda}$ on the baryon density is plotted as a function of baryon number B.

The WA85 experiment at CERN-SPS provides data on multistrange baryon and anti-baryon production in SW collisions at 200 A GeV. This experiment has measured $\Lambda, \overline{\Lambda}, \Xi^-, \overline{\Xi^-}, \Omega^-$, and $\overline{\Omega^-}$ yields. For a review of the recent experimental data on multistrange baryon and anti-baryon see for example [75, 76]. These data have been analysed independently by two different groups [77, 78] and [79, 80] with mutually consistent results. The studies by the WA85 Collaboration on the hyperon production in SW and pW interactions indicates that the inverse slopes of the m_T distributions for $\Lambda, \overline{\Lambda}, \Xi^-$ and $\overline{\Xi^-}$ decays for pW data, are lower than those from central SW interactions. The $\overline{\Lambda}/\Lambda$ and $\overline{\Xi^-}/\Xi^-$ ratios are consistent in both sets of the data; there is however an increase of up to 40% in the ratios Ξ^-/Λ and $\overline{\Xi^-}/\overline{\Lambda}$ when going from pW to SW interactions. The experimental results are summarized in Table 3.4 and 3.5 below.

Table 3.4: Relative hyperon yields in pW and SW interactions ($m_T > 1.9GeV$) [81].

Ratio	pW interaction	SW interaction
$\bar{\Lambda}/\Lambda$	0.19 ± 0.02	0.20 ± 0.01
$\overline{\Xi^-}/\Xi^-$	0.48 ± 0.07	0.41 ± 0.05
Ξ^-/Λ	0.13 ± 0.001	0.19 ± 0.01
$\overline{\Xi^-}/\bar{\Lambda}$	0.31 ± 0.03	0.41 ± 0.05

The WA94 have measured these ratios for sulphur-sulphur(SS) interactions. These ratios are shown in Table 3.6. It is interesting to note that the central SS results of strangeness yield ratios are very similar to those obtained in (SW) interactions obtained by the WA85 in the equivalent centre of mass rapidity [82]. Figure 3.30 shows the ratios Ξ^-/Λ and $\overline{\Xi^-}/\overline{\Lambda}$ for SS interactions (WA94) and SW interactions (WA85), together with those from other processes. It is noted that the ratios $\overline{\Xi^-}/\overline{\Lambda}$ is $3\frac{1}{2}$ times larger in sulphur induced reactions than the value (0.06 ± 0.02) obtained by the AFS Collaboration in pp interactions [83].

Table 3.5: Relative hyperon yields in pW and SW interactions ($2.3 < y_{LAB} < 3.0, 1.2 < p_T < 3.0 GeV/c$) [81].

Ratio	pW interaction	SW interaction
$\bar{\Lambda}/\Lambda$	0.19 ± 0.02	0.20 ± 0.01
$\overline{\Xi^-}/\Xi^-$	0.47 ± 0.06	0.45 ± 0.05
Ξ^-/Λ	0.064 ± 0.005	0.095 ± 0.06
$\overline{\Xi^-}/\bar{\Lambda}$	0.15 ± 0.02	0.21 ± 0.02

Table 3.6: Relative hyperon yields in SS interactions $2.5 < y < 3.0$ [84].

Ratio	$1.2 < p_T < 3.0$ GeV/c	$1.0 < p_T < 2.0$ GeV/c	$m_T > 1.9$ GeV/c
$\bar{\Lambda}/\Lambda$	0.23 ± 0.01	0.24 ± 0.01	0.22 ± 0.01
$\overline{\Xi^-}/\Xi^-$	0.55 ± 0.07	0.58 ± 0.07	0.54 ± 0.06
Ξ^-/Λ	0.09 ± 0.01	0.08 ± 0.01	0.18 ± 0.01
$\overline{\Xi^-}/\bar{\Lambda}$	0.21 ± 0.02	0.20 ± 0.02	0.44 ± 0.04

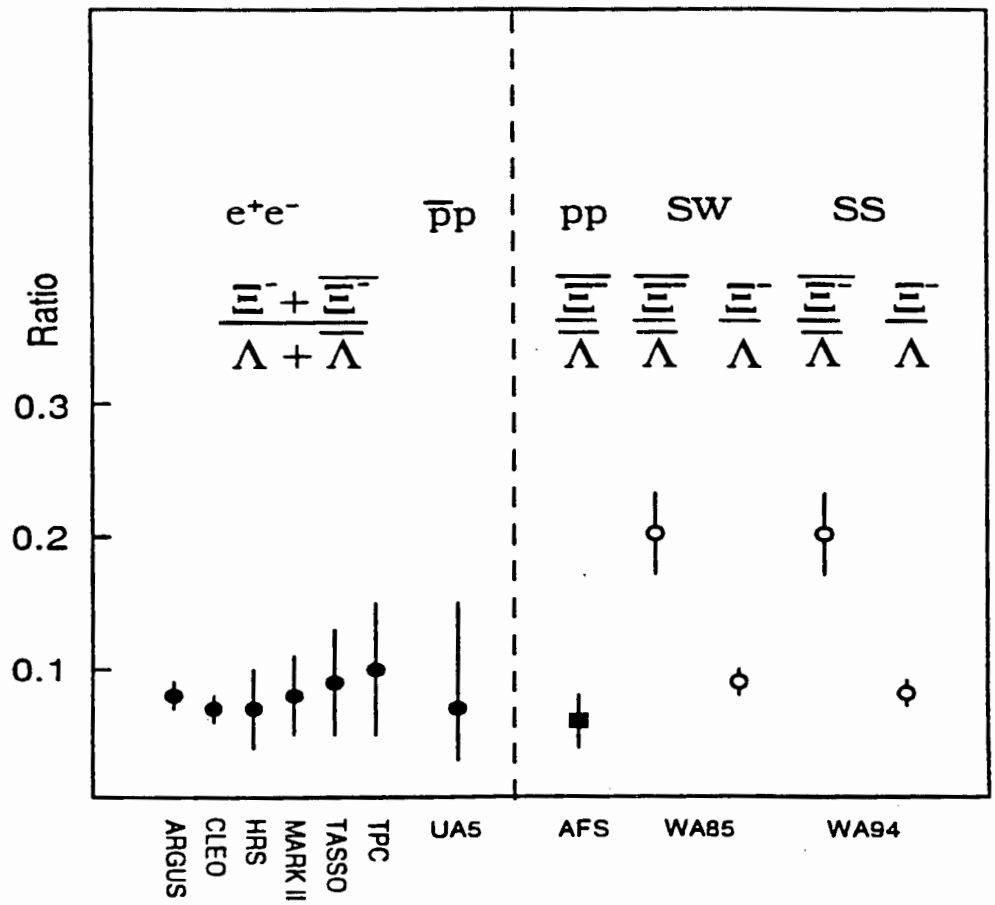

Figure 3.30: Hyperon yield ratios Ξ^-/Λ and $\overline{\Xi^-}/\overline{\Lambda}$ for $e^+e^-, \bar{p}p$ and ion induced processes in the p_T range $1 < p_T < 2GeV/c$ [84].

3.6 Summary and Conclusion

The results of the hadronic gas model have been presented and discussed throughout the Chapter. The results have been presented as a function of the net baryon number, B. This corresponds to the total number of participating nucleons in the collisions. The concept of the number of participants will be reflected in detail in the next Chapter when we will be comparing the model results to the experimental information. The model was used for fixed T and B/V. Fixing B/V means that talking about B implies talking about V and hence the size of the system at freeze-out. It has been seen that the particle yields generally increase linearly with B, but at small values of B, the kaon yield shows a quadratic dependence. Pions did not show this quadratic behaviour at small values of B. Moving to strange baryons and anti-baryons we still find the linear dependence on B. Considered at the same T and B/V as for the light particles, the Ξ yield shows a quadratic dependence at small B as compared to Λ. For the chosen values of T and B/V, the quadratic behaviour disappears. Note that the temperature and baryon density for the strange baryons and anti-baryons have been chosen so as to provide large scale information on these particles and especially their anti-particles.

The hadronic ratios show a different behaviour to the particle yields. The kaon/pion ratio grows smoothly from zero towards saturation as B increases showing that at very large values of B one should expect total saturation of the ratio. Thus we have the constant kaon yield at large B. However the K^+/π^+ ratio increases more than K^-/π^- which shows only a very small increase. The ratio of positive kaons to negative kaons rises steeply and then becomes almost flat as B increases. The ratio stay almost constant and independent of B . The strange anti-baryon to baryon ratios show an increase from small values to large values of B by a very small factor, with the Ξ ratio greater than the Λ ratio. For the same temperature considered for the light particles, the strange anti-baryons ratio increases smoothly from zero towards saturation while the strange baryons ratio increases steeply and starts to level off with a small increase, with increasing B. For the temperature and baryon density shown, the two ratios grow steeply and then level off. The behaviour of the hadronic ratios involving strange baryons and anti-baryons is also seen in experimental results (also reviewed here). It has been found that the strange anti-baryon to baryon ratios are consistent with both sets of data (pW and SW), while there is a large increase in the strange anti-baryons and

strange baryons ratios when going from pW and SW interaction. This increase in the latter ratios is, of course, so because in moving from pW to SW, we are increasing the size of the system and/or the number of the participating nucleons, which is consistent with our model.

Compared to the light particles, the effect of cut-off mass (composition of the gas in terms of resonances) is found to have a great impact on strange baryons and anti-baryons. This is mainly reflected in the strange anti-baryon to baryon ratios.

The effect of the baryon density B/V on the particle yields seems to be well understood when one recalls that for a particular value of B for different values of B/V, one will have large volumes at small baryon densities, and this favours the particle yields. Thus it turns out that rather than depending on the baryon density directly, the particle yields depend on the volume. However, coming to the dependence of different hadronic ratios on baryon density, it is the baryon density which is influencing the observed hadronic ratios. It has been seen that the baryon density increases some ratios and decreases others. The ratio of the positive to negative kaons is found to be an interesting one under the aspect of baryon density, since its dependence on baryon density and an almost independence on the net baryon number can tell us more about the properties of a hadronic matter produced in collisions. Compared to light particles, the effect of the baryon density is again seen to be dominant in the strange baryons and anti-baryons, especially the ratios considered here.

The K^-/π^- and the $\overline{\Lambda}/\Lambda$ ratios do not show significant increase with B but the K^+/π^+ ratio does. The production of strange baryons in a small volume is not favoured since, first, these are relatively heavy particles ($\sim$ 1 GeV) and secondly, they have to be accompanied by an anti-strange baryon, making the total expenditure in energy not less than 2 GeV. As the interaction volume increases, it becomes easier to produce these particles and one can explain the observed increase in anti-strange baryons to strange baryons as one collides heavier nuclei in this way.

The final state of a relativistic heavy ion collision has been described by a hadronic gas. It has been found that for large values of baryon numbers and/or interaction volumes, a description using the grand canonical ensemble could be justified. For a small system, however, corrections arising solely from the exact conservation of baryon number and strangeness are

important and cannot be neglected. This is particularly relevant if one wants to compare results from $p - p$ collisions with those from heavy ion collisions. The particle yields rises linearly (or almost linearly) from zero with an increasing B, and most of the particle ratios increase smoothly from zero for small values of B towards the value obtained in grand canonical ensemble. Due to the dependence on the precise composition of the hadronic gas, i.e. the number of resonances kept, it turns out that the strange antibaryon to baryon ratios cannot be evaluated in a reliable manner if one applies the model as it is.

Chapter 4

Review of Strangeness Production in Heavy Ion Collisions

4.1 Strangeness in Relativistic Heavy Ion Collisions

It is generally held that all matter which is known to exist is made of u and d quark flavors. The third quark known as the strange s quark is found in strange particles which are produced during ion collisions. We recall that in Chapter 2 we used strangeness conservation in our calculations. This has been possible because strangeness is conserved by strong interactions. Because of the absence of the strangeness content in the initial state of ion collisions, strangeness production could tell us more about the properties and the dynamics of the newly made hadronic matter formed in collisions. During the collisions, $u\bar{u}$, $d\bar{d}$ and $s\bar{s}$ pairs are produced. The strange quark and antiquark subsequently combine with neighbouring quarks and antiquarks to form strange particles. Strangeness was proposed a long time ago as a signature of quark-gluon plasma [85, 74, 86, 87]. However, this proposal was weakened when it was also realized that strangeness enhancement can also be produced by hadronic interactions [88, 89]. One of the main reasons that made strangeness yield an attractive subject is that strange particles have a much lower production threshold in the QGP than in a hadronic gas. The threshold for creating strange hadrons in a hadron gas is given by the mass difference between the centre-of-mass energy of the two colliding hadrons (with zero

strangeness) and the combined mass of the lightest strange hadron pair. In the quark-gluon plasma, on the other hand, the threshold is given by the rest mass of the strange-antistrange quark pair. In the QGP with deconfined quarks, the energy needed to create an $s\bar{s}$ pair is only $2m_s$, which is twice the strange quark mass, m_s. Assuming a strange quark current mass of 180 MeV, the threshold for strangeness production in QGP is only 360 MeV. On the other hand, in a hadronic gas, creating a strange hadron pair (with zero net strangeness) through processes such as $\pi\pi \longrightarrow K\overline{K}$ and $NN \longrightarrow NK\Lambda$ needs at least 700 MeV. Another reason why strangeness production is an attractive subject is the fact that strangeness production processes are much faster in the QGP than in hadronic systems. The strangeness production time constant in the QGP is of the order of 10^{23} s (about 1 fm)[85], while in HG it is 10 to 30 times slower [74]. In the plasma, strange quarks and anti quarks can be produced by collisions among the constituents of the plasma. There are two processes by which $s\bar{s}$ pairs can be produced: by light quark and antiquark collisions through the reactions

$$u + \overline{u} \longrightarrow s + \overline{s} \tag{4.1}$$

and

$$d + \overline{d} \longrightarrow s + \overline{s}\,, \tag{4.2}$$

they can also be produced by the collisions of the gluons in the plasma through the reaction

$$g + g \longrightarrow s + \overline{s}\,. \tag{4.3}$$

Gluons are expected to be abundant in QGP and they play an important role in strangeness yield. The high density of strangeness in QGP will enhance multi-strange particles through hadronization as well, while in the hadronic gas, multi-strange particles have to be made by successive collisions. For QGP in chemical equilibrium at high baryon density, an enhancement of anti-strangeness production is expected with respect to anti-baryons, as argued in [85, 19] using the Boltzmann approximation

$$\frac{n_{\bar{s}}}{n_{\bar{u}} + n_{\bar{d}}} = \frac{m_s^2}{4T^2} K_2\left(\frac{m_s}{T}\right) e^{\mu_B/3T}\,, \tag{4.4}$$

where K_2 is a modified Bessel function. At high baryon density, light anti-quarks $(\bar{u}, \bar{d})$ are suppressed because they have to be created together with light quarks (u, d), whose Fermi energy levels are already high. On the other hand, $\bar{s}$ quarks are created along with s quarks, enhancing anti-strangeness over anti-baryons in such systems.

4.2 Kaon Production and the K/π Ratio

In a quark-gluon plasma with a net baryon content, there are many u and d quarks, however the $\bar{u}$ and $\bar{d}$ are suppressed and the s and $\bar{s}$ quarks are less than the light quarks but more than the light antiquarks for $\mu_{u,d} \neq 0$. In this environment of a dense baryon-rich quark-gluon plasma, which may occur in collisions in the stopping regime, it is likely for the $\bar{s}$ quark to find a u quark or a d quark to form a K^+ meson or a K^0 meson. It is, however, not easy for the $\bar{s}$ quark to find a $\bar{u}$ or a $\bar{d}$ quark to form a K^- or a $\overline{K^0}$ meson. Thus one will expect the number of K^+ to be larger than the number of K^-. However this can be expected without the assumption of the baryon rich QGP, as reflected in Chapter 3.

The K/π ratio has received much attention because its enhancement, and especially the enhancement of K^+/π^+, can be interpreted as a signature of quark gluon plasma [91, 92]. However the enhancement has also been discussed in terms of thermal models [43, 93, 94] and rescattering models [67]. The quark production rate in a strong field has been shown [16] to be proportional to $e^{-\pi m_q^2/\kappa}$. With constituent masses of u, d and s quarks of 325 MeV, 325 MeV and 450 MeV respectively, and a string tension, κ, of 1 GeV/fm, one obtains a relation of $\bar{s}s/u\bar{u}d\bar{d}$ to K^+/π^+ which is

$$\frac{s+\bar{s}}{u+\bar{u}+d+\bar{d}} = \frac{K^+/\pi^+}{1.5+K^+/\pi^+} , \tag{4.5}$$

where we made use of the rate of production of quarks:

$$\frac{R_{s\bar{s}}}{R_{u\bar{u}}} = 0.214 \tag{4.6}$$

and

$$\frac{R_{s\bar{s}}}{R_{q\bar{q}}} = 0.107 . \tag{4.7}$$

Recall the density n_i of particle i with rest mass m_i at temperature T is given by

$$\begin{aligned} n_i &= \frac{1}{(2\pi)^3}\int_0^\infty \frac{4\pi p^2 dp}{e^{\sqrt{p^2+m_i^2}/T}-1} \\ &= \frac{Tm_i^2}{2\pi^2}\sum_{k=1}^{\infty}\frac{1}{k}K_2(\frac{km_i}{T}) , \end{aligned} \tag{4.8}$$

where K_2 is the modified Bessel function of order 2. See Appendix C. For hadron gas in thermal and chemical equilibrium, at temperature of 200 MeV we have

$$\frac{n_{K^+}}{n_{\pi^+}} = 0.3792 , \tag{4.9}$$

and the ratio of strange quark density to nonstrange quark density is

$$\begin{aligned} \frac{n_s + n_{\bar{s}}}{n_u + n_{\bar{u}} + n_d + n_{\bar{d}}} &= \frac{n_{K^+}/n\pi^+}{1.5 + n_{K^+}/n_{\pi^+}} \\ &= 0.2018 \, . \end{aligned} \tag{4.10}$$

Therefore, for a hadron gas in thermal and chemical equilibrium at $T = 200$ MeV the K^+/π^+ ratio is about 0.38 and the strangeness content is about 0.2. So far, it has not been determined whether hadron matter produced in nucleus-nucleus collisions can react sufficiently frequently to reach chemical equilibrium within the time available during the collision process. An early detailed analysis [74] indicated that if one starts with a hadron matter with non-strange particles at $T \sim 200\ MeV$, the reaction rate is not fast enough for the hadron gas to approach chemical equilibrium, because of the large threshold energy for strange hadron pair production compared to the temperature of the hadron gas. However many models have been put forward to describe additional strangeness enhancement due to the lowering of the strange particle masses as the temperature approaches the phase transition temperature [93, 95], $\Delta - \Delta$ interactions [96], and (higher meson resonance) - nucleon interactions [97], and thermal models [43].

4.3 Experimental Information on Strangeness Production

Relativistic heavy-ion beams available at the BNL Tandem-AGS Complex and CERN-SPS provide an opportunity for studying nuclear matter at high baryon density. In what follows, we look at the trend which goes from $p-p$ to $p-A$ to $p-B$ to $A-B$ and finally to $A-A$ or $B-B$ collisions. Here A and B refer to the two nuclei in collision while p refers to the nucleon. $A-A$ and $B-B$ are heavy nuclei collision systems with the $B-B$ system greater than the $A-A$ system which follows from $A-B$ collisions, where $A < B$. The main reason of following this trend is to see, following the expectations of the previous Chapter, how the particle yields and particle ratios depend on the size of the system. The motive being that one wants to see how strangeness production is affected by the size of the system.

4.3.1 $p-p$ Collisions

In pp collisions, kaons are primarily produced through the channels

$$\begin{aligned} & pp \longrightarrow K\overline{K} + X \\ & (\text{e.g. } pp \longrightarrow ppK^{-}K^{+}) \ , \end{aligned} \tag{4.11}$$

$$\begin{aligned} & pp \longrightarrow KY \\ & (\text{e.g. } pp \longrightarrow ppYK^{+}) \ , \end{aligned} \tag{4.12}$$

where X denotes anything and Y indicates one of the hyperons, Λ or Σ. One sees here that strangeness is conserved in both the channels. From the experiment of Bøggild et al., [98, 99] the cross-sections of the above processes are estimated to be $\sigma_{KY} = 2.6\ mb$ and $\sigma_{K\bar{K}} = 1.3\ mb$, assuming $\sigma_{K^+}/\sigma_{K^-} = 3$ [100]. Based on these results, they further estimated the average numbers of various particles per inelastic pp collision to be $N_{\pi^+} = 1.6$, $N_{\pi^-} = 1.0$, $N_{K^+} = 0.06$ and $N_{K^-} = 0.02$. The difference in the above cross-sections was also seen from the experiment by Fesefeldt et al. [101], where it was found that the process $pp \longrightarrow KYX$ has much larger cross section than the process $pp \longrightarrow K\overline{K}X$. The difference might well be as a result of the difference in the thresholds of the two reactions. In studying the kaon production, as one moves away from the $p-p$ to $p-A$ to $A-A$ collisions, it is

interesting to see how kaons interact with nucleons. Figures 4.1 and 4.2 show the total and elastic cross sections for positive and negative kaons incident on protons [102]. From these two figures one can deduce that the total cross section of K^+p is about 10-20 mb and for the K^-p about 30-40 mb.

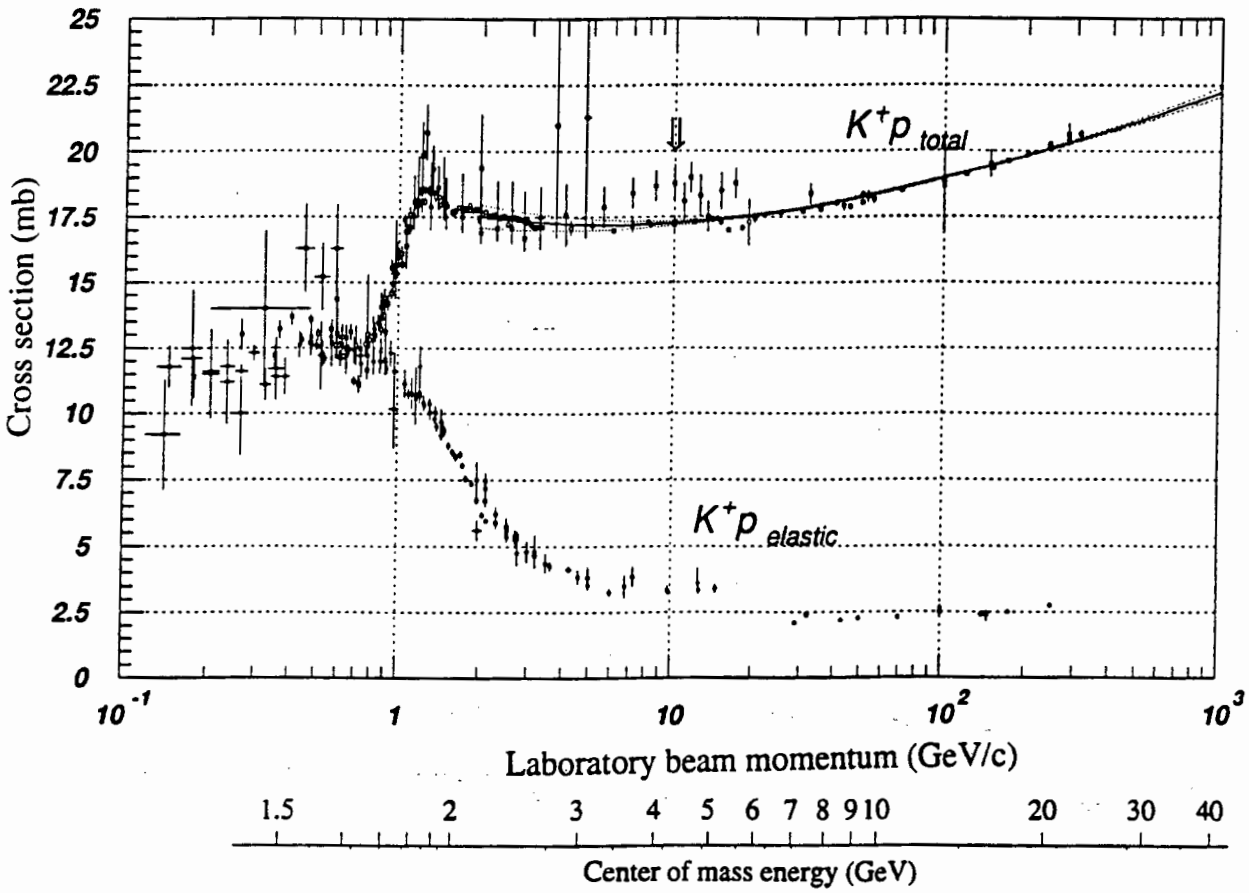

Figure 4.1: K^+p cross section and elastic cross section as a function of incident momentum and as a function of s [102].

There is, however, not much data on the rare particle production in pp collisions close to AGS energies. Kaon data with the nearest energy to the AGS comes from bubble chamber measurements of pp collisions at 12 GeV/c [101, 103] at the CERN proton synchrotron (PS). The reported numbers of K^+ and K^- per inelastic pp collision were 0.05 and 0.008 respectively. The observed K^+/π^+ ratio in pp collision is $\approx (4-8)\%$ and the $K^-/\pi^- \approx (2.4 \pm 2.0)\%$ [98][104][105]. For the AGS energies, the K^+/π^+ ratio is found to be 4% and K^-/π^- ratio is 2% [106, 65].

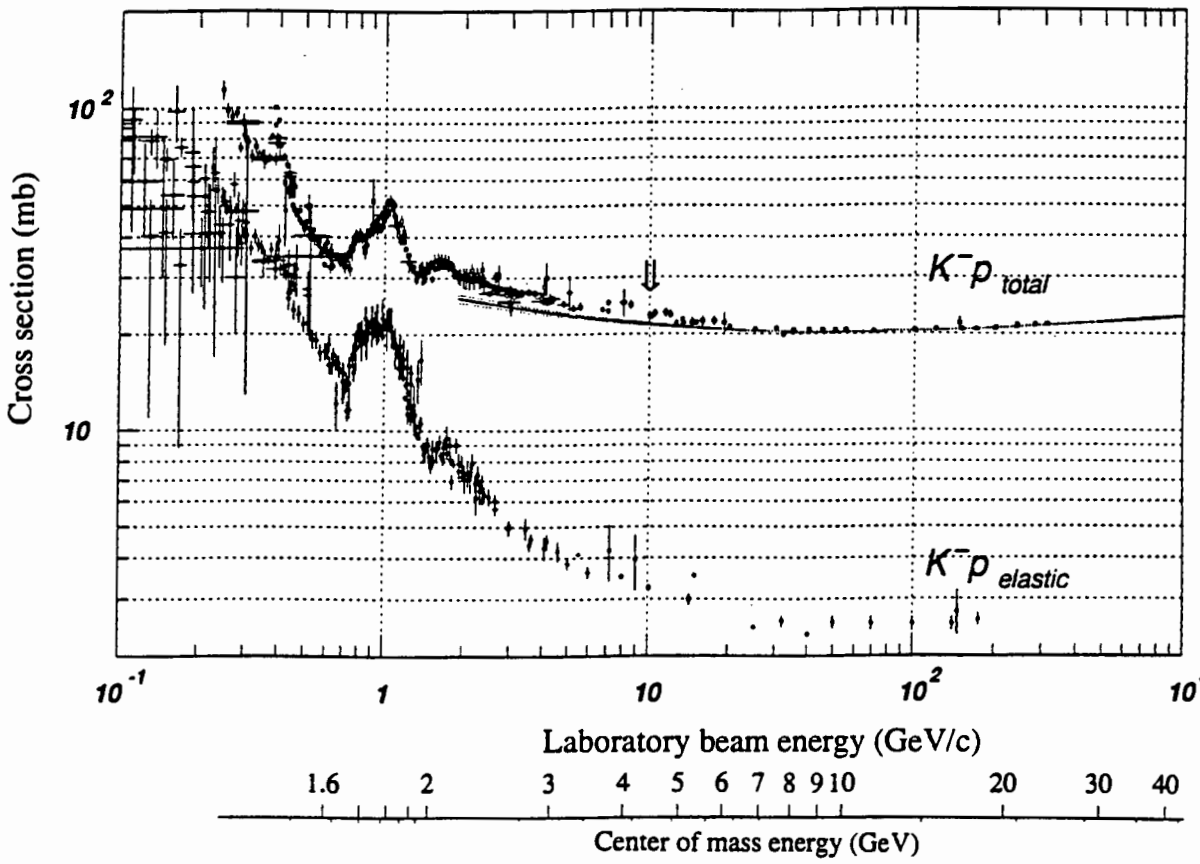

Figure 4.2: K^-p cross section and elastic cross section as a function of incident momentum and as a function of s [102].

4.3.2 $p-A$, $p-B$ and $A-B$ Collisions

In going from $p-p$ to $p-A$ to $A-A$ collisions, we are at the same time increasing the size of the interacting system. The big difference starts to emerge when going from $p-p$ to $p-A$ collisions, since in $p-A$ collisions we begin to have more interactions, i.e more NN collisions. Thus one will have, in addition to the primary production mechanisms discussed in $p-p$ collisions, new processes appearing, including, for example

$$\begin{aligned} N\Delta &\longrightarrow N\Lambda K^+ , \\ N\Delta &\longrightarrow NNK^+K^- , \\ NN^* &\longrightarrow N\Lambda K^+ , \\ NN^* &\longrightarrow NNK^+K^- , \end{aligned} \tag{4.13}$$

and there are absorption effects to consider for the K^-'s, through processes like $K^-N \longrightarrow \pi Y$. Thus the yield of K^+ increases as one moves to heavier systems, and there seems to be

a similar trend in the K^-, as we shall see later.

Proton-nucleus $(p-A)$ interactions can be thought of as a pile up of several pp collisions, in that one nucleon undergoes several collisions with several other nucleons. In proton-nucleus interactions the total cross-section can be reasonably well described by a power law, $\sigma_{pA}^{inel} \propto A^{\alpha}$ where $\alpha = 0.71 \pm 0.05$ [107, 108]. Proton induced reactions at 14.6 GeV/c on Be, Al, Cu and Au targets, have been measured at the BNL AGS with the E802 spectrometer [65]. Figure 4.3 shows the rapidity distributions of various particles produced in different pA collisions [65] at the AGS. As indicated from the trends, there are gradual changes in both

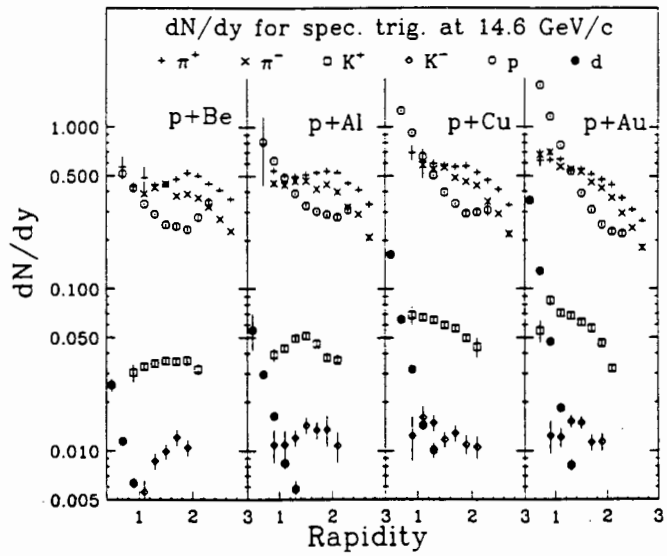

Figure 4.3: $\pi^{\pm}, K^{\pm}$, proton and deutron dn/dy distributions in $p+Be$, $p+Al$, $p+Cu$ and $p+Au$ collisions [65].

the magnitude and the shape of the rapidity distribution. The shape of particle distributions as a function of rapidity changes from $p+Be$ to $p+Au$ reactions (from a small to a large system), with more particles, especially K^+, produced at lower rapidity and fewer particles produced towards projectile rapidity for heavy targets. It is found [65] that while the inverse slope parameters of protons and kaons increase systematically with increasing target mass, the parameter for pions is constant from $p+Be$ to $p+Au$. Fig. 4.4 shows the K/π ratios as a function of rapidity for $p+Be$, $p+Al$, $p+Cu$ and $p+Au$. For comparison, K/π ratios for central $Si+Au$ are also included, this being an example of $A-B$ collisions. From Figure 4.3 the pion yield remains roughly constant while the K^+ yield increases substantially.

This causes the K^+/π^+ ratio to increase for heavier targets, as indicated in Fig. 4.4. The K^-/π^- ratio remains approximately constant. In contrast to pA collisions, which can be

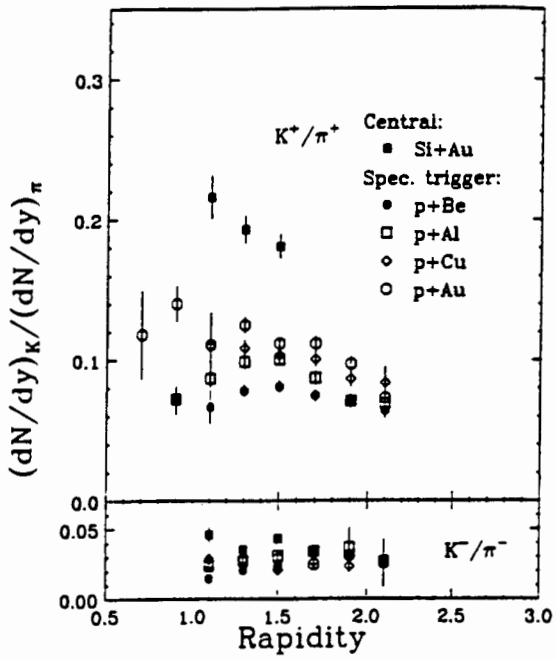

Figure 4.4: K/π ratio as a function of rapidity for $p+Be$(solid circle), $p+Al$ (open square), $p+Cu$ (diamond), and $p+Au$ (open circle) and $Si+Au$ (solid square). The upper and lower panels show ratios for K^+/π^+ and K^-/π^- respectively [66].

thought of as an assembling of several pp collisions, nucleus-nucleus ($A-B$ and $A-A$ or $B-B$) collisions, and especially heavy ion collisions, cannot be thought of simply as a pile up of many nucleon-nucleon collisions. This is so if one thinks that one is now dealing with many nucleon-nucleon interactions and there are also large particle rescattering effects in heavy ion collisions [109]. The rescattering effects, both in theoretical models [67, 68] and experimental data, are found to be important in particle production. Heavy ion collisions can be well characterized by the participant-spectator picture, in which as two nuclei pass each other, the overlapping regions are left behind and the other parts (spectators) continue flying in the same directions as if nothing happened [110]. Kaon and pion production in central $Si+Au$ collisions at 14.6 GeV/c has been measured by the E802 Collaboration [106]. This is an example of an $A-B$ collision, where A is the projectile and B is the target, and $A<B$. An enhanced K^+/π^+ ratio of $19.2\pm3\%$ was observed [106][65][90][66] in the central rapidity region ($1.2<y<1.4$). By comparison, for the pp interactions in the same rapidity interval and at roughly the same incident energy, the K^+/π^+ ratio is 5%. The K^-/π^- was found to be $3.6\pm0.8\%$, in comparison to pp value of $2.4\pm2.0\%$. Table 4.1 summarizes the

K/π ratios measured by the E802 Collaboration. What one reads from this table is nothing less than the increase in the K^+/π^+ ratio as one goes from a small system to a large system. Kaon production was also studied as a function of rapidity by D.Morrison for his PhD. thesis

Table 4.1: K/π ratios in different collision systems measured by the E802 Collaboration in the rapidity interval $1.2 < y < 1.4$.

System	K^+/π^+	K^-/π^-
$p + Be$ [65]	$7.8 \pm 0.04\%$	—
$p + Al$ [65]	$9.9 \pm 0.5\%$	—
$p + Cu$ [65]	$10.8 \pm 0.6\%$	—
$p + Au$ [65]	$12.5 \pm 0.6\%$	—
$Si + Au$ [106]	$19.2 \pm 3\%$	$3.6 \pm 0.8\%$

[111]. The E859 had enough data to perform the similar rapidity study for both K^+ and K^- [112]. A selection of rapidity distributions dN/dy are shown in Figure 4.5. Comparisons of $Si + Al$ and $Si + Au$ indicate that the yield peaks at lower rapidity in central $Si + Au$ than in $Si + Al$. The peak depends on the centrality of the collision and in particular, the impact parameter. The peripheral interaction in $Si + Au$ is almost close to that in $Si + Al$. As one increases the size of the system or the impact parameter, the width of the rapidity distribution is seen to narrow. The similarity between the trends in the K^+ and K^- distributions is shown in Fig. 4.6. This figure shows the ratio of K^+ yield to that for K^- as a function of rapidity. At all rapidities, the ratio is almost independent of the system within 10%. It will be interesting to study this ratio because, besides the ratio rising at the low rapidity, it does not change much with the size of the system at a particular rapidity.

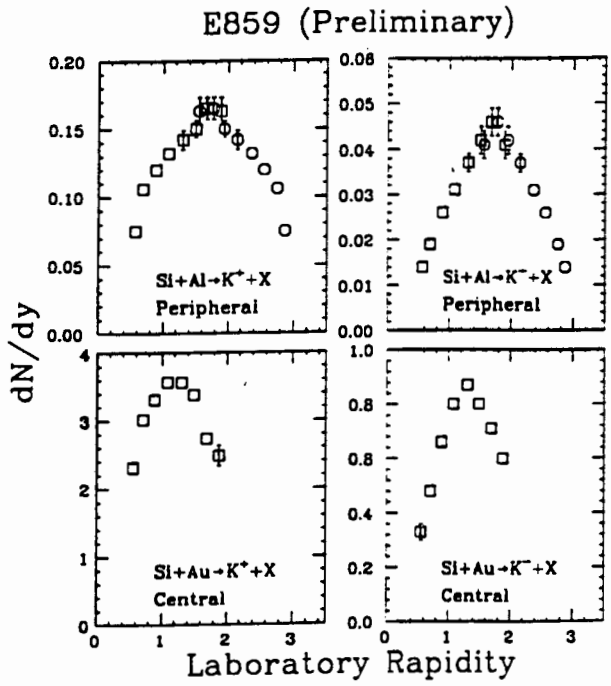

Figure 4.5: A sample of rapidity distributions of the yield of charged kaons in Si induced reactions at 14.6 A.GeV/c [112].

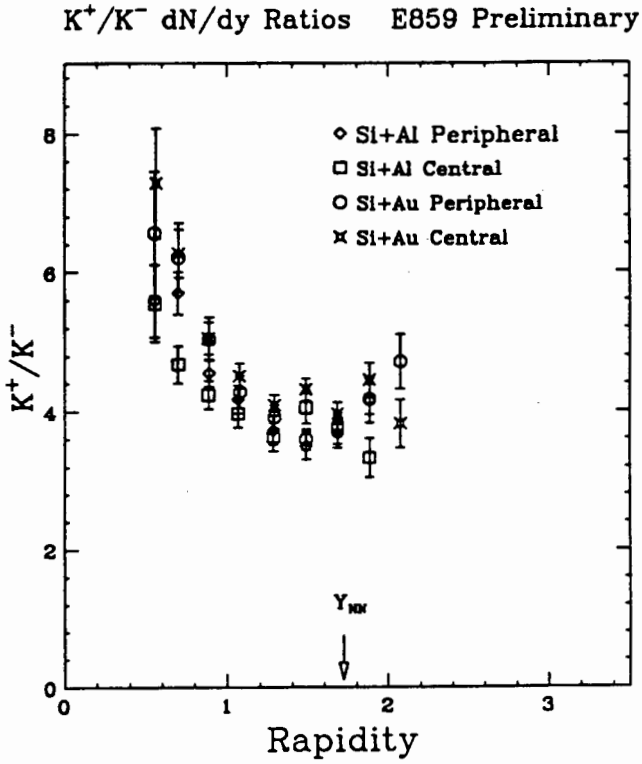

Figure 4.6: The ratio of the yield of K^+ over K^- is plotted as a function of rapidity in Si induced reactions as at 14.6GeV/c [111].

4.3.3 Kaon Production and the K/π ratio *vs* $N_{participants}$

We have seen how the K^+/π^+ ratio depends on the mass of the colliding nuclei. It will be interesting to see how this ratio depends on the number of participants ($N_{participants}$) in the reaction. The E802 has also studied the kaon and pion multiplicities as a function of the number of participants and the first study was done particularly for the number of projectile participants(N_{Part}^{Proj}) [113]. Figure 4.7 shows the observed π^+ and K^+ multiplicities plotted as a function of the nucleon number of projectile participants (N_{Part}^{Proj}), measured at BNL-AGS [113]. For a small system like $Si + Al$, the production of both K^+ and π^+ increases almost linearly with respect to N_{Part}^{Proj}. However, as one goes to large systems like $Si + Cu$ and $Si + Au$, the increase is greater than linear or rather it shows quadratic behaviour. This is seen more clearly for K^+ than for π^+. If the extrapolation can, however be done on the last three data points, one will expect the intercept to be at a value different from zero and furthermore this value will depend on the size of the system. This picture of quadratic dependence seems to originate from pure geometry of the collisions. It is also seen that the increase in kaons exceeds that of pions, as shown by the number of ΔK^+ to the number of $\Delta\pi^+$ versus $< N_{Part}^{Proj} >$, in Figure 4.8.

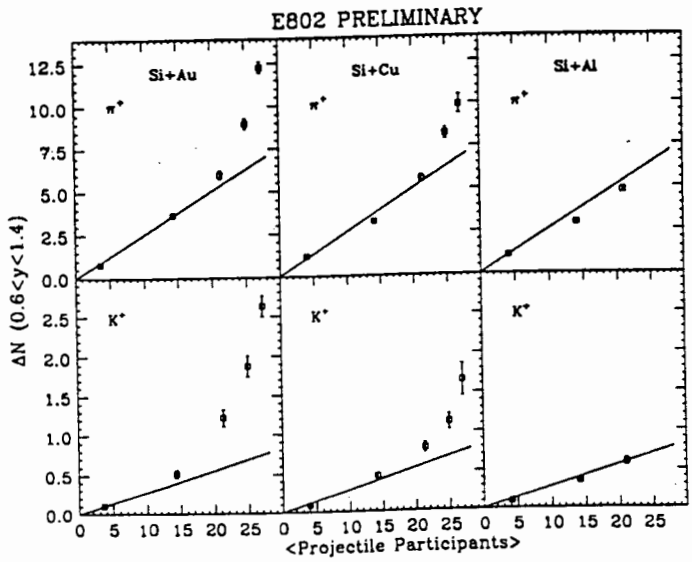

Figure 4.7: The number ΔN of π^+'s and K^+'s produced in the rapidity range $0.6 < y < 1.4$ for ^{28}Si incident on Al, Cu and Au targets versus the number of projectile participants [113].

The kaon and pion production was first studied as a function of N_{Part}^{Proj} by [114]. It was found that the K^+ yield also rises linearly with the number of projectile participants in $Si + Al$ but as one goes to $Si + Au$, deviations from the linear dependencies were seen. This happens as one goes from peripheral to central collisions. This is because in moving from peripheral to central we increase the number of NN collisions which enhance K^+ yield. Figure 4.8 shows the ratio $\Delta n(K^+)/\Delta n(\pi^+)$ plotted against $< N_{Part}^{Proj} >$. The K^+/π^+ ratio increases with the increase in the number of projectile participants for Cu and Au, and the two central values for $Si + Au$ are distinctly larger than for $Si + Al$ and $Si + Cu$. For peripheral interactions, the two systems ,$Si + Al$ and $Si + Cu$, give K^+/π^+ at 9%, close to $p + p$ value [98, 104, 105] of $\approx 6\%$. In view of the above, it is noted that the high K^+/π^+ ratio is due to the increase in the size of the system. For a particular system, it becomes a question of an increase of the size as one goes from a peripheral to a central collision. The kaon yield is also studied

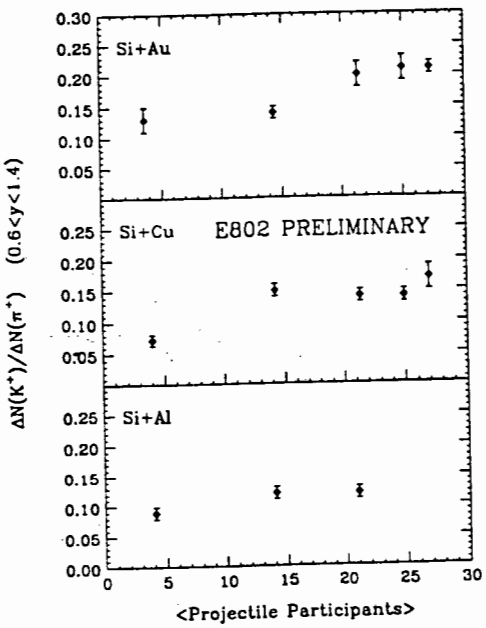

Figure 4.8: The $\Delta n(K^+)/\Delta n(\pi^+)$ as a function of number of Projectile Participants $< N_{Part}^{Proj} >$ [114].

as a function of the total number of nucleons participating in the reaction. Figure 4.9 shows the positive and negative kaons plotted as circles and triangles, respectively, while open and closed symbols are used for $Si + Al$ and $Si + Au$. It can be seen from Figure 4.9 that the yields of both K^+ and K^- behave in a similar way (which exhibit some similarity of the two kaon species) with system size, except for an overall multiplicative difference. From this

figure, one can also see that although the number of particles rises roughly linearly with the number of participants, the intercepts of straight line fits (dotted lines) are not at zero. This is an indication that for very small systems, we will have a smaller kaon production [112]. This figure will again appear at the end when we make comparisons with the hadronic gas model.

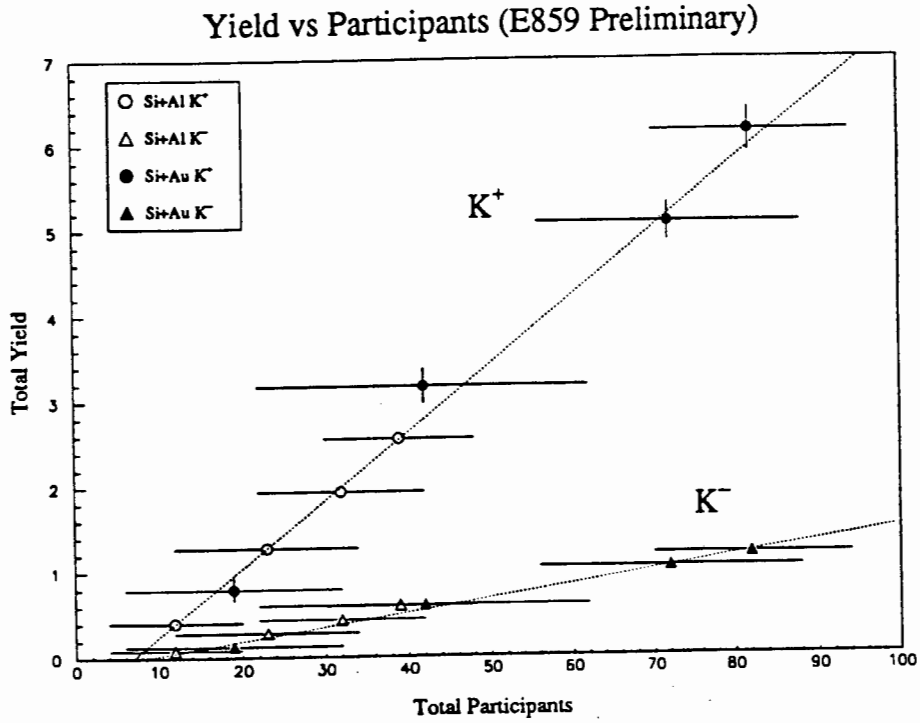

Figure 4.9: The total yield of both positive and negative kaons is plotted as a function of the system size in Si induced reactions at 14.6 A.GeV/c [112].

Figure 4.10 shows the K^+/π^+ ratio as a function of the number of projectile participants for $Si+Al$ and $Si+Au$ collisions. The ratio rises smoothly from a value near 0.05 then begins to saturate towards a $Au+Au$ value 5 times the most peripheral value in $Si+Al$. We have learnt that the kaon and pion production increases roughly linearly with the number of projectile participants. However, the kaon dependencies appear to have a quick saturation tendency in small systems where the number of particles per participant changes significantly. This results in the smooth rising of the K/π ratio as a function of the system size in $Si + A$ collisions. For the large systems, the tendency towards a saturation point at a small value of the number of participants, becomes less important and the K/π reaches an asymptotic

value at a rather large value of the number of participants. The K^+/π^+ ratio has also been examined as a function of the transverse neutral energy [114]. This corresponds to the total number of participants (i.e target + projectile) in the reaction. The ratio versus transverse energy for $Si + Al$ and $Si + Au$ collisions is shown in Figure 4.11. It is noted that the dependence of the K^+/π^+ is more linear when plotted against transverse energy produced in the collisions than when plotted against $< N_{Part}^{Proj} >$, and that the ratio for $Si + Al$ and $Si + Au$ is roughly the same at a given value of the transverse energy. This behaviour is different from what we have seen in the case of the dependence of the ratio on the size of the system or the number of participants. The increase in the ratio with transverse energy is an indication that the ratio is correlated with the degree of nuclear overlap. The greater the degree of overlap of the two nuclei, the greater the ratio. It is because of this result that it is predicted that the central $Au - Au$ collision will have a slightly lower value of K^+/π^+ than the observed one in central $Si - Au$ [113].

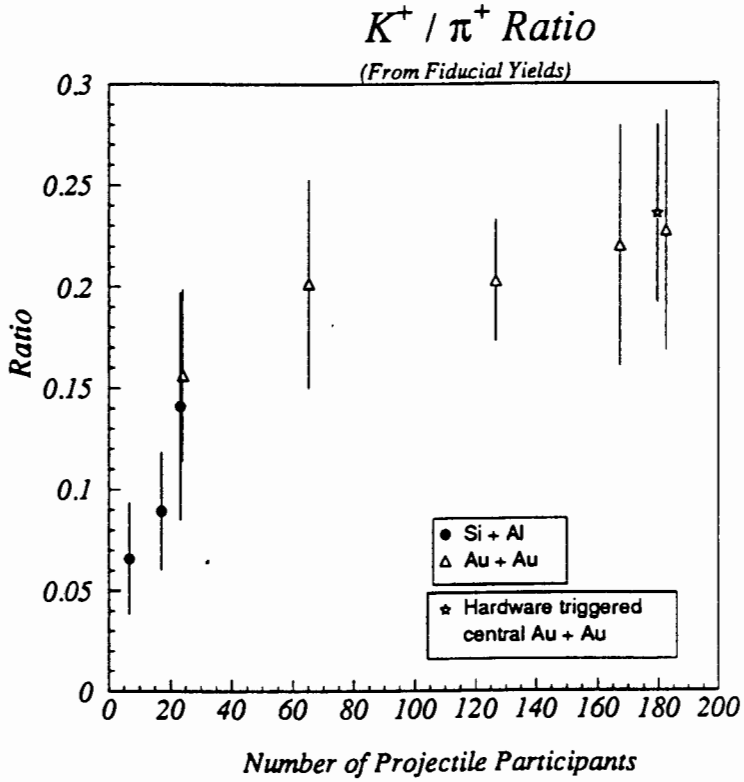

Figure 4.10: The ratio of the total yield of K^+/π^+ is plotted as a function of the number of projectile participants for $Si + Al$ at 14.6GeV/c and $Au + Au$ at 11.5 A.GeV/c [112].

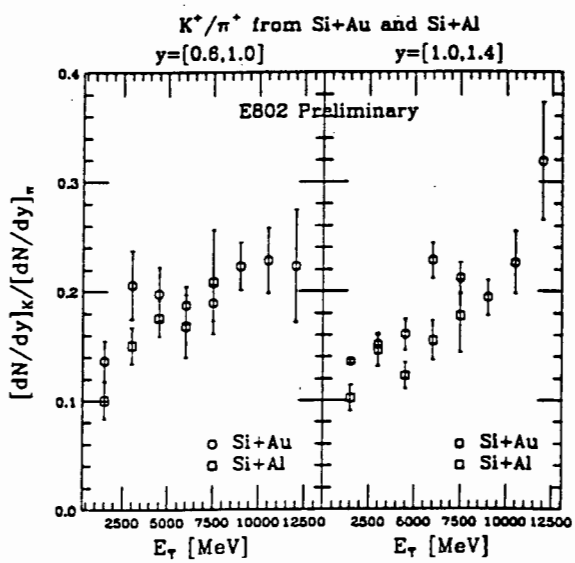

Figure 4.11: The K^+/π^+ ratio for two different rapidity intervals versus the transverse energy in $Si + Al$ (open squares) and $Si + Au$ (open circles) collisions [113].

4.3.4 Summary

The E802 Collaboration has studied the K^+/π^+ ratio as a function of the projectile mass (from p to Si and presently Au), target mass(from Be to Au) and the degree of centrality. It is found that the K^+/π^+ ratio increases when any of these three parameters is increased. The analysis of the kaon yields indicates that the processes that were enhancing kaon production (relative to pion production) may have saturated. This is also clearly shown by the K^+/π^+ ratio from the results of the hadronic gas model in this work. The linear dependence which is seen in our hadronic gas model is seen in both the kaon and pion yields with the number of total participants. The quadratic behavior seen in the experimental data, was also seen in the hadron gas model, at a value of the of number of participants which is close to zero. However, the model predicted that on the large scale of the total number of participants, the quadratic behaviour will disappear. It has been seen that dependence of the kaon yield on the system appears to have some sort of threshold which is quick in small systems where the number of particles per participant changes significantly. This threshold results in the smoothly rising K/π ratio as a function of the system of size especially in $Si - A$ collisions. This is also seen in our hadron gas model. But it was shown [118] that on the large scale of the number of participants, the smoothly rising behaviour will disappear. Thus for a very large system , the effect of the threshold at a small number of participants becomes less important and the K/π ratio reaches an asymptotic value very quickly.

4.3.5 The AA Collisions

The E802 Collaboration has studied the particle production in $Au + Au$ collisions at 11.6 GeV/c from the BNL E866 experiment [55]. Amongst the studied particles are the $K^{\pm}$ and $\pi^{\pm}$. The particle yields and the particle ratios are studied as a function of centrality in the mid-rapidity, particularly the dependence of particle yields and particle ratios on the number of projectile participants.

Fig. 4.12 shows the dependence of particle yields as a function of centrality. One notices that the kaon yield increases faster than the pion yield with centrality. The particle ratios

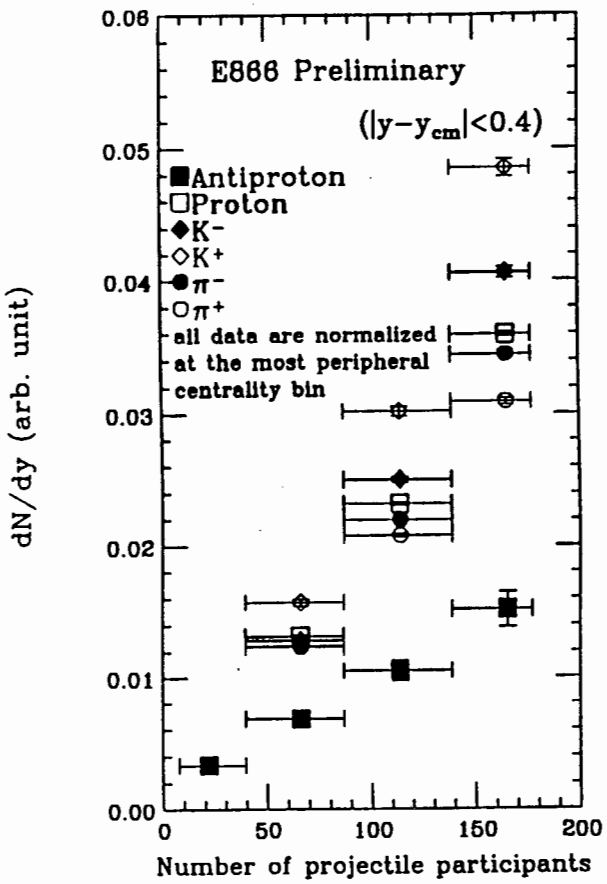

Figure 4.12: Particle yields dN/dy for $K^{\pm}, \pi^{\pm}$, proton and antiproton versus the number of projectile participants [55].

are dealt with in the next section. We have noted that the data is still preliminary. We also note the following about the data: The K^+/π^+ ratio shows a strong dependence on the centrality. It increases with the collision centrality and it seems to reach saturation in the central collisions. This ratio reaches (18 ± 2) % at mid-rapidity for central collisions. The K^-/π^+ ratio shows a similar dependence on the centrality of the collision, (since π^+ and π^- yields are almost the same, the ratios K^-/π^+ and K^-/π^- are almost the same), however the ratio does not increase much because it is still close to the value of K^-/π^- obtained in pp collisions. The K^+/K^- ratio does not seem to depend on the centrality because it stays almost the same on average, from peripheral to central collisions.

4.4 Hadronic Gas Model in Action.

4.4.1 Hadron Gas Model Revisited

The chemically and thermally equilibrated hadron gas model describes the final state of relativistic heavy ion collisions in terms of statistical distributions (Fermi-Dirac or Bose-Einstein). Strong interactions conserve net baryon number and strangeness which can either be achieved in grand canonical ensemble by introducing corresponding chemical potentials ([43, 44, 45], etc..) or in canonical ensemble ([37, 27, 115, 31], etc...). Most people like to work with the grand canonical ensemble because of its computational simplicity. However, the grand canonical formalism has limitations for small systems, which should be taken into consideration. In addition to the two chemical potentials μ_B and μ_S, corresponding to the conservation of baryon number and strangeness respectively, one can also have the third chemical potential, μ_Q, corresponding to isospin or charge conservation [46]. Since in heavy ion collisions hadrons are strongly interacting, certain effects on these interactions (for example, finite volume effects) should be taken into account. The excluded volume approximation, in which the hadrons are given a hard-core volume, has been considered in [129, 43, 30, 116]. For $Au + Au$ system, finite volume effects will be negligible since we are already dealing with a system of the volume of the order of $10^3\ fm^3$, therefore we will not include them in our application. Of the three parameters, the temperature T, the baryon chemical potential μ_B, and the strangeness chemical potential μ_S, one needs only two to describe the final state of the hadronic matter in collisions: since the third one, eg. μ_S, is fixed by the requirement of vanishing overall strangeness, the two remaining parameters are, T and μ_B. The grand canonical partition function of the hadron gas can be written [77] as

$$\ln Z(T, \mu_B, \mu_S) = \sum_i [W_i^m + (\lambda_B^{B_i} \lambda_S^{-S_i} + \lambda_B^{-B_i} \lambda_S^{S_i}) W_i] \ . \tag{4.14}$$

Here the first term refers to non-strange mesons and the second term to particles which carry baryon numbers B_i and strangeness S_i. The fugacities related to the baryon number and strangeness are $\lambda_B \equiv \exp(\mu_B/T)$ and $\lambda_S \equiv \exp(\mu_S/T)$. Including charge conservation we can write the general expression given by [46]

$$\ln Z(T, \mu_B, \mu_S, \mu_Q) = \sum_i \lambda_B^{B_i} \lambda_S^{S_i} \lambda_Q^{Q_i} W_i \ . \tag{4.15}$$

where W_i is the phase space factor for hadrons of species i (mesons, baryons and their antiparticles), with Q_i denoting the charge of the hadron in question and $\lambda_Q = \exp(\mu_Q/T)$ is the fugacity for charge. The phase space factors are given by

$$W_i = \frac{d_i m_i^2 VT}{2\pi^2} K_2(m_i/T) \ , \tag{4.16}$$

with d_i denoting the spin degeneracy, m_i the mass of hadron species i, V the volume of the system and K_2 is the Bessel function of the second type. The thermal contribution of the particle multiplicity $N_i = W_i$ has to be added by resonance contributions to get the particle multiplicity

$$N_i = W_i + \sum_j Br(j \longrightarrow i) W_j \ . \tag{4.17}$$

Here $Br(j \longrightarrow i)$ is the branching ratio of the decay of resonance j to particle i. For a final state of interaction, which is in both thermal and chemical equilibrium (unique freeze-out), all hadronic ratios should be determined using the values of T and μ_B which can be fixed by at least two ratios.

In this work we will use canonical formalism of which we can compare the results to the ones obtained in the grand canonical formalism at the end. The motivation for using canonical description for hadronic interactions comes from the work of R.Hagedorn [25]. In such a model one assumes that a thermal system is being produced, which expands until freeze-out is reached, and the hadronic resonances decay into the lightest stable particles. The observed particle yields reflect the properties of the system at freeze-out. We learnt from Chapter 2 that the use of grand canonical in small volumes is not justified, and instead one should use the canonical ensemble. As an example, in the grand canonical ensemble we have for the density of kaons [117]

$$n_{K^+} = \int \frac{d^3p}{(2\pi)^3} \exp(-\frac{E_{K^+}}{T} + \frac{\mu_S}{T}) \ , \tag{4.18}$$

while in the canonical ensemble for a small system one has

$$n_{K^+} = \left[\int \frac{d^3p}{(2\pi)^3} \exp(-\frac{E_{K^+}}{T})\right] V \int \frac{d^3p}{(2\pi)^3} \exp(-\frac{E_{K^-}}{T}) \ . \tag{4.19}$$

One sees explicitly that strangeness is conserved because for each K^+ one needs a K^- to balance strangeness. The density too will be suppressed because one has two exponential

factors. Strangeness conservation requires that at least two kaons are produced, and we have learnt in Chapter 2 that for a small system this makes a substantial difference. The motivation for exact strangeness and baryon number conservation (canonical formalism) has been presented in Chapter 2. We therefore want to see it in action, and particularly its application to heavy ion collisions. Figure 4.13 shows the K/π ratios as a function of the interaction volume for different collisions ranging from $p-p$ to $Si-Au$ collisions. The curves are for exact baryon number and strangeness conservation at a fixed temperature T and baryon density n_B. For zero volume both ratios become zero, while for increasing V/V_0 both ratios increase. They finally reach an asymptotic value at volumes in which the grand canonical ensemble may be used. The calculation was done for a hadronic gas containing particles of up to strangeness $=\pm 3$ with all resonances below 2 Gev in mass.

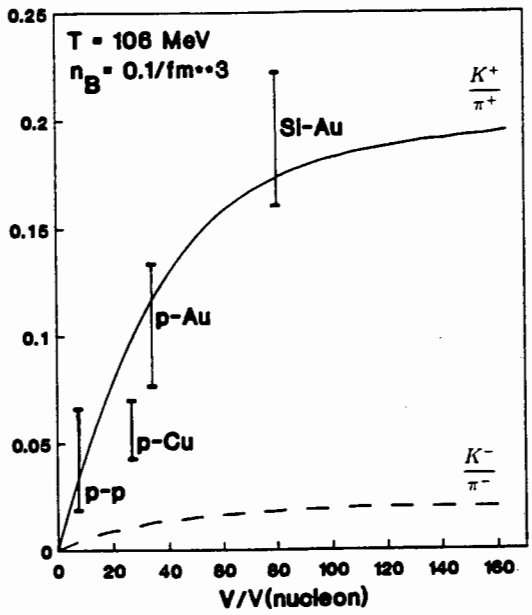

Figure 4.13: The K^+/π^+ and K^-/π^- ratios as a function of the interaction volume at a fixed temperature T and baryon density n_B [31].

4.4.2 Application of Hadron Gas Model to $Au + Au$ Collisions

The $Au + Au$ system is an example of $A - A$ collisions, where the two nuclei in collision are identical and where there will be geometrical symmetry in the collisions. This means that the participating number of nucleons from the projectile will be the same as target participating nucleons.

Preliminary results on the dependence of hadronic ratios on the number of projectile participants have recently been presented by the E866 collaboration [55] for relativistic $Au - Au$ collisions at the BNL-AGS. These results give insight into the behavior of the produced hadronic system as a function of the baryon number and the size of the interaction volume. In this work we try to analyze these results using a thermal resonance gas model at a fixed temperature and a fixed baryon density. This treatment differs from the ones considered in [46, 47] in that here we consider baryon and strangeness content exactly. This means that we do not introduce chemical potentials for baryon number nor for strangeness. Chemical potentials are usually introduced to enforce the right quantum number in an average sense. We will use the canonical formalism results from Chapter 2. We will use the fact that since the net baryon number, B corresponds to the total number of participants, then $B = 2N_{pp}$, where N_{pp} is the number of projectile participants with the factor 2 reflecting the symmetry of the $Au - Au$ collision system. Furthermore it is useful to group all particles in the Particle Data Booklet [36] depending on their quantum numbers (we leave out charm and bottom). We do not include cascade particles (the Ξ's and Ω's) as their contribution is unimportant for the energy range under consideration. However it can be done according to Chapter 2. Thus we will make use of Eq. 2.48 from Chapter 2 as our basis. In Chapter 2 we have outlined the way of determining all the particle densities. We consider now the behavior at the freeze-out. In this case all the resonances in the gas are allowed to decay into the lighter stable particles. This means that each particle density is multiplied by with its appropriate branching ratio (indicated by Br below). The abundances of particles in the final state are thus determined by

$$n_H = \sum n_i Br(i \longrightarrow H) \ , \tag{4.20}$$

where each sum runs over all particles contained in the hadronic gas and H refers to a hadron

$(\pi^+, K^+, p, ...)$

The hadronic ratios to be investigated have been studied as a function of the net baryon number B [118]. This will correspond to the investigation of the same ratios as a function of the total number of participants in the reaction. The studies were done so as to incorporate large values of B. The dependence on B/V and T was investigated. It was found that the results show the expectations of Chapter 3. The only difference is that at large values of B, we no longer have the quadratic behaviours seen in Chapter 3. The dependence of the ratios on B becomes negligible. The results are shown in Fig. 4.14(a)-(h).

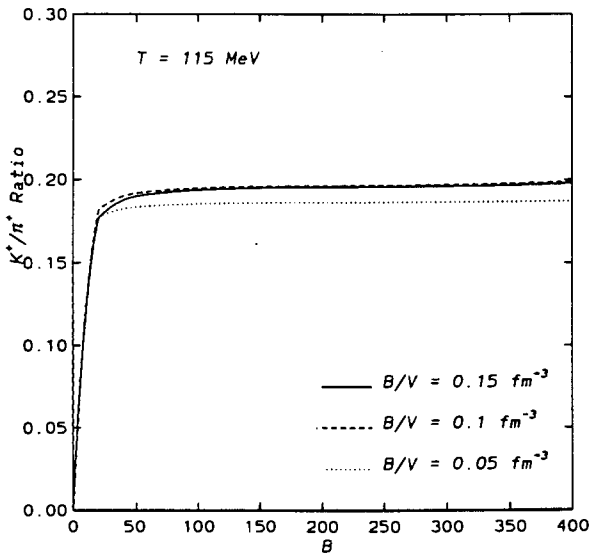

a

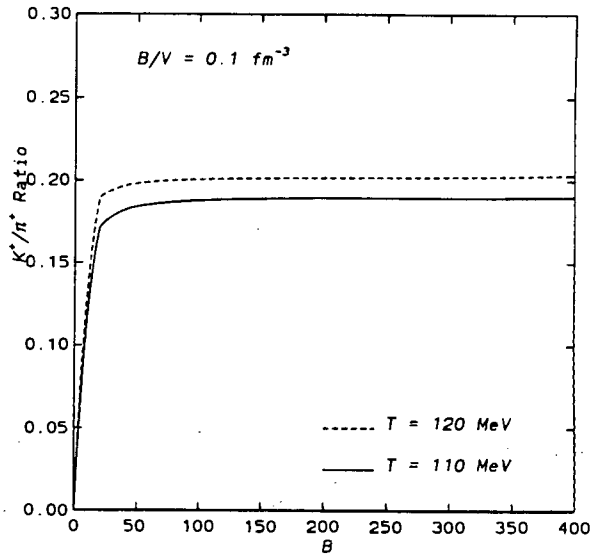

b

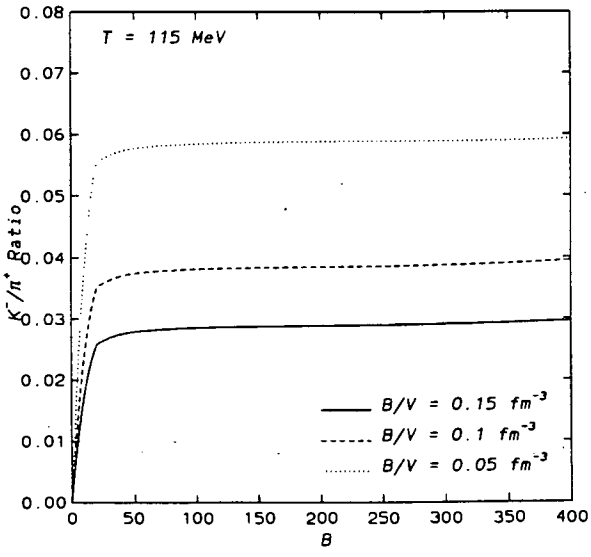

c

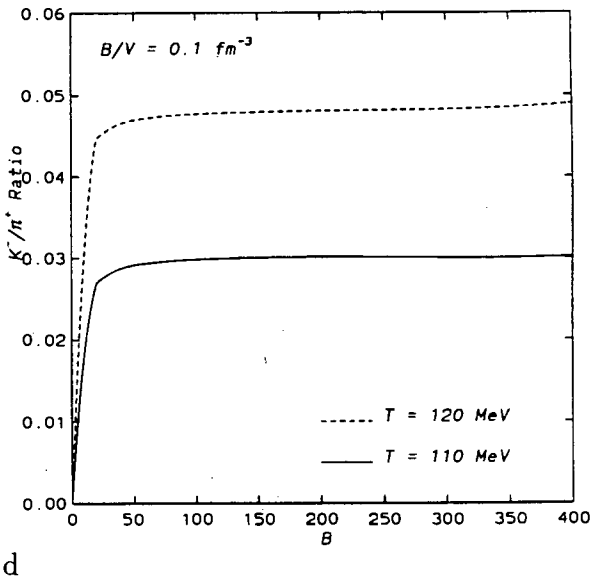

d

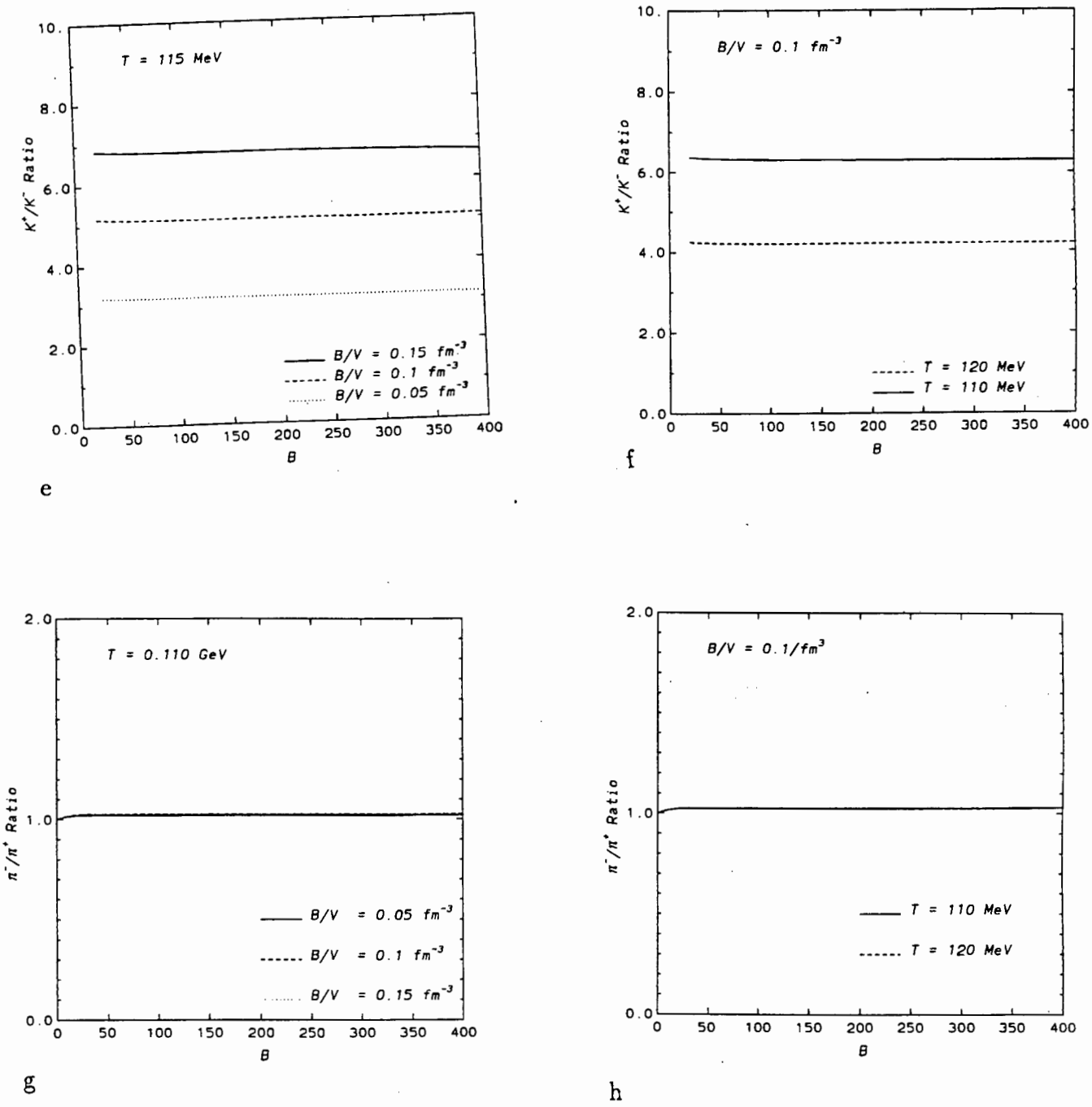

Figure 4.14: Hadronic ratios as a function of baryon number, B.

We now turn to the E866 experimental data. The comparison with the experimental results is shown in figures 4.15 to 4.17. To compare with earlier calculations [46, 47] we keep the temperature T and the baryon density B/V fixed. This corresponds to keeping the baryon chemical potential fixed in the standard hadronic gas calculations using the grand canonical ensemble. In figure 4.15 we compare our results (of K^+/π^+) with the recent data from AGS [55][112]. The set of data with long error bars is included to indicate that the data is still preliminary and therefore not yet converged. We thus prefer to fit the data with short error bars, the advantage being that the set with short error bars comes with other ratios. This makes the question of thermalisation more interesting since a good agreement will mean that one can indeed describe the particle species produced from the fireball by one temperature and also by one baryon density. As one can see, our results show a steep rise with the number of participants, N_{pp}, before levelling off while the experimental data indicates a slower rise than the model predicted. In figures 4.16 and 4.17 we show the K^-/π^+ and the K^+/K^- ratios. From the investigations of pion dependency on temperature and baryon density it is obvious that the result will perfectly agree with the experimental data , this is so if one looks at figures 4.14((g) and (h)). Like the experimental data, our model's result does not stay at unity but rises a little bit above unity. However a direct comparison of the model and the data indicates that the rise in experimental data is larger than that of our model. This is also attributed to Coulomb final state interaction which is responsible for the difference in the shape of π^- and π^+ spectra together with the electrical chemical potential which is responsible for the total π^-/π^+ ratio [62]. The importance of Coulomb effects for π^+ and π^- spectra in nuclear collisions was seen, in both experiment and theory, for a long time (see references in a recent paper [119]). Analytical formulas for Coulomb final state interactions were derived by Gyulassy and Kaufman in [120]. (We might have even a better agreement in the pion ratio if the model could be modified to include the coulomb effects).

Because the data is still preliminary (and also depending on the error bars) we use three different values of temperature T and B/V. For the final converging experimental data, one will have to use one value of temperature and baryon density. In each case the good agreement is obtained with the results of the E866 collaboration [55]. The relevant temperature is around $T \approx 100\ MeV$, the baryon density is in the range $B/V \approx 0.02 - 0.05/fm^3$, which is an indication of considerable expansion before freeze-out. In the grand canonical ensemble

this corresponds to a baryon chemical potential of $\mu_B \approx 540\ MeV$.

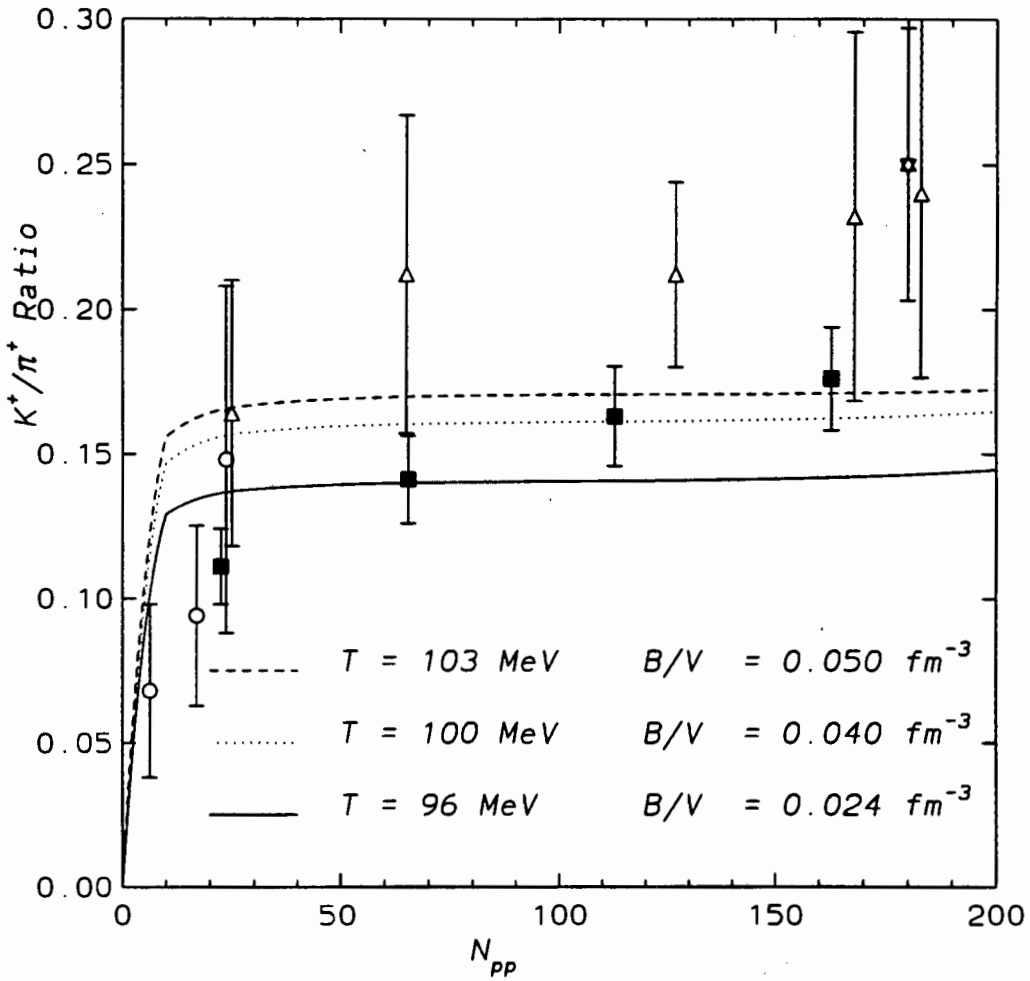

Figure 4.15: The K^+/π^+ ratio as a function of the number of projectile participants, N_{pp}. The open circles indicates $Si - Al$ collision [121].

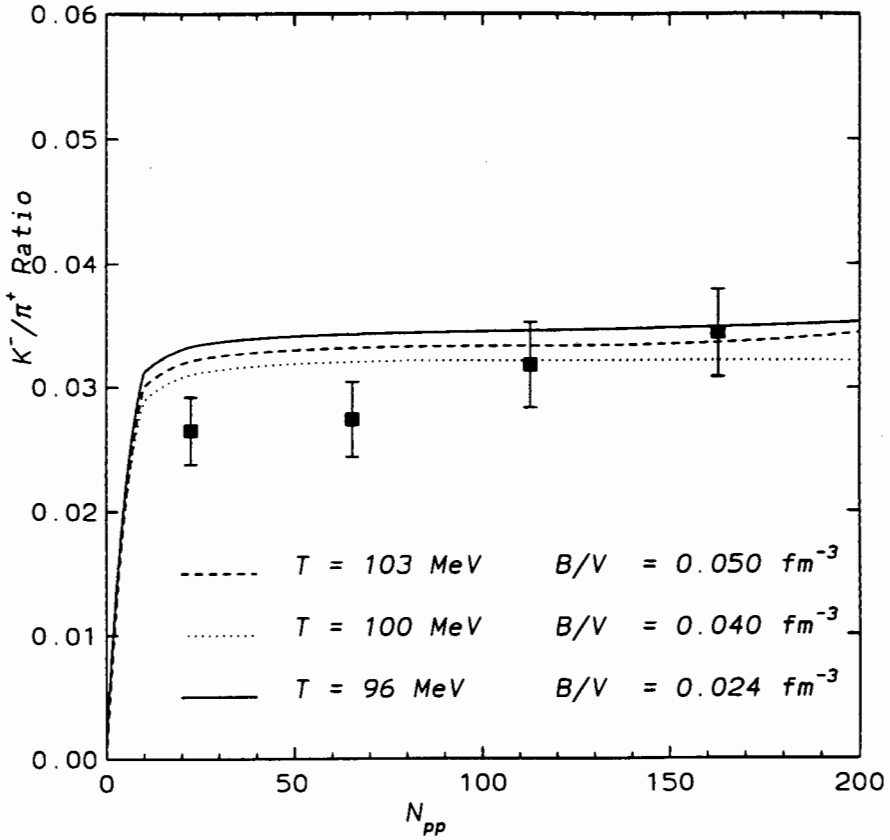

Figure 4.16: The K^-/π^+ ratio as a function of the number of projectile participants, N_{pp} [121].

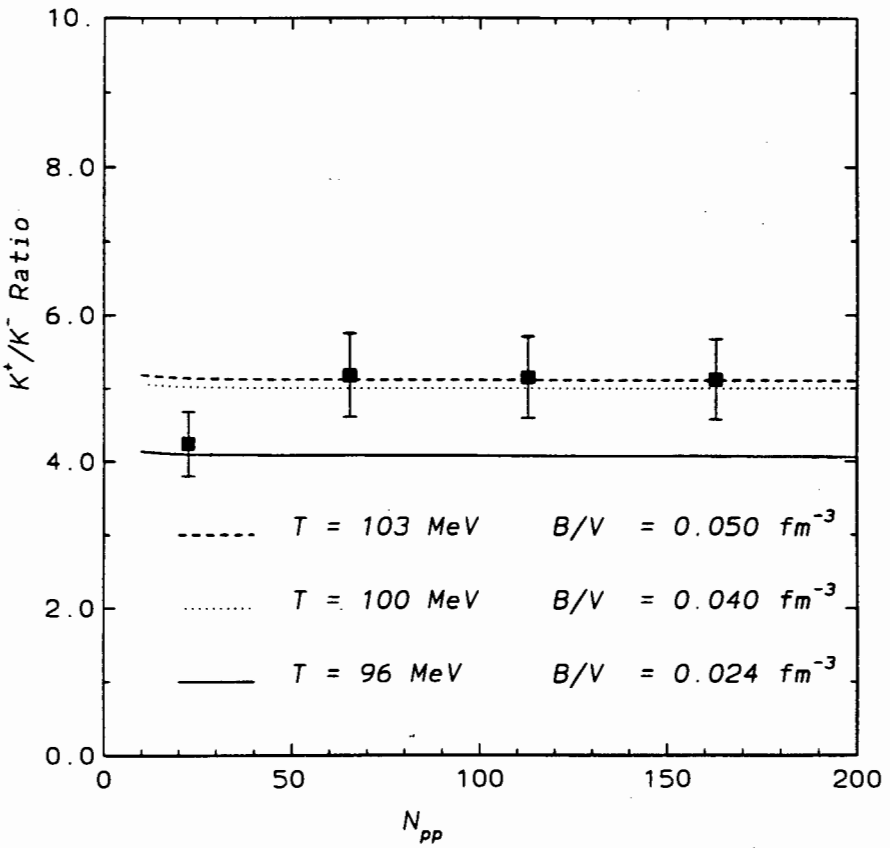

Figure 4.17: The K^+/K^- ratio as a function of the number of projectile participants, N_{pp} [121].

Using the same formalisms of the Hadron Gas Model presented in this work, one can also analyze the E859 data presented by [112], particularly the kaon production. In figure 4.18 we compare our results to the experimental data. Again one sees a good agreement with the experimental data. The same plot has been done by D.Morrison in his PhD thesis [111], see also [122] where the data is read from. As seen previously, he argues that the data can be

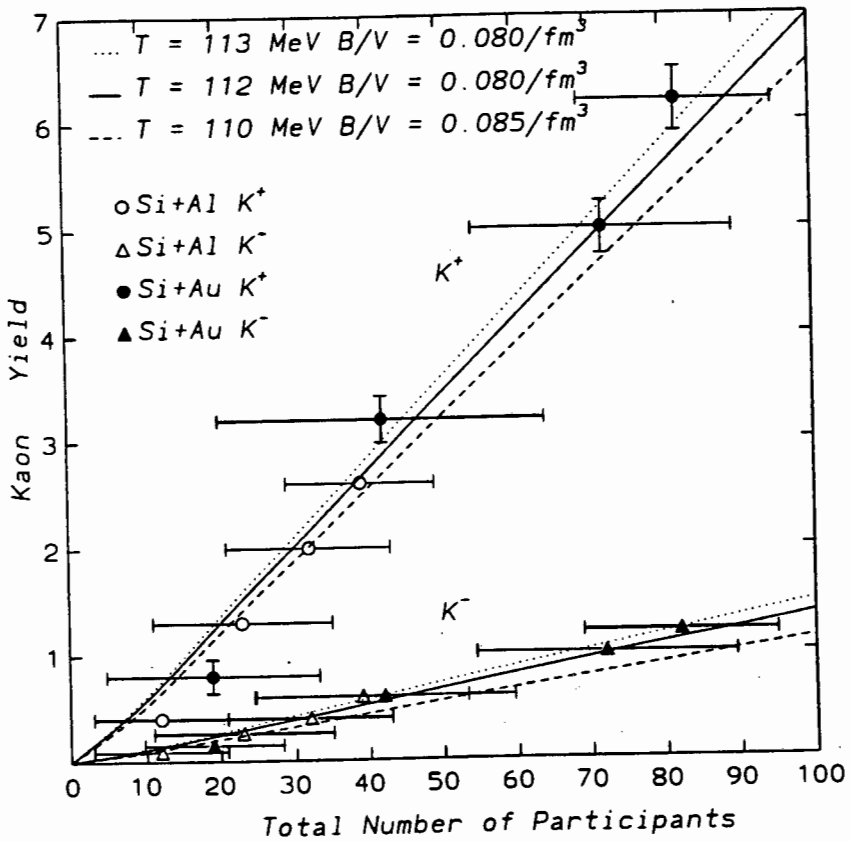

Figure 4.18: The total yield of both positive and negative kaons is plotted as a function of the number of total participants in Si induced reactions at 14.6 A.GeV/c.

fitted with a single straight line, with which the Hadron Gas Model considered here, almost agrees. However, it turns out that the model goes along with the quadratic dependence near zero total number of participants. The model also shows that the $Si + Al$ and the $Si + Au$ have slightly different freeze out conditions, T and B/V. Finally, we note that the model is in good agreement with the data.

4.4.3 Thermalisation

Within the framework of the hadron gas model, we seek to determine the temperature of the system at the point when the particles cease to interact strongly (freeze-out) as well as the net baryon density at freeze-out. Large freeze-out temperatures would imply that even higher temperatures are reached earlier in the collision. Low freeze-out temperatures can also imply that the produced matter in collision do expand considerably before freeze-out. The information on whether we have reached thermalisation in heavy ion collisions can be found from the produced hadrons and hadronic ratios. It is noted in the paper of Cleymans et. al. [46] that thermalisation at the AGS energy range can lead to an increase or decrease of hadron abundance in heavy ion collision relative to those measured in $p-p$ or $p-A$ collisions. One such example is the enhancement of K^+/π^+ ratio. Figure 4.19 shows a hand drawn K^+/π^+ ratio taken from [10] measured at the AGS [113]. The ratio grows from a $p-p$ value near 0.05 to a four times larger thermal value, above 0.2, in central $Si-Au$ and $Au-Au$ collisions [113, 123, 124]. On the other hand, the number of pions produced per participating nucleon decreases at the AGS energies towards its thermal value. Figure 4.20 shows the π/N_{part} ratio (taken from [48]) in $p-p$ collisions at 14.6 GeV beam momentum. Here N_{part} is the average number of participants in a $p-A$ collision. It is also noted that in a high baryon density environment, where one will have more annihilation processes, the ratio of anti-baryon to baryon production is also expected to decrease. This is confirmed by the ratio $\overline{p}/p$ which appears to decrease in going from $p-p$ to $A-B$ collisions [127].

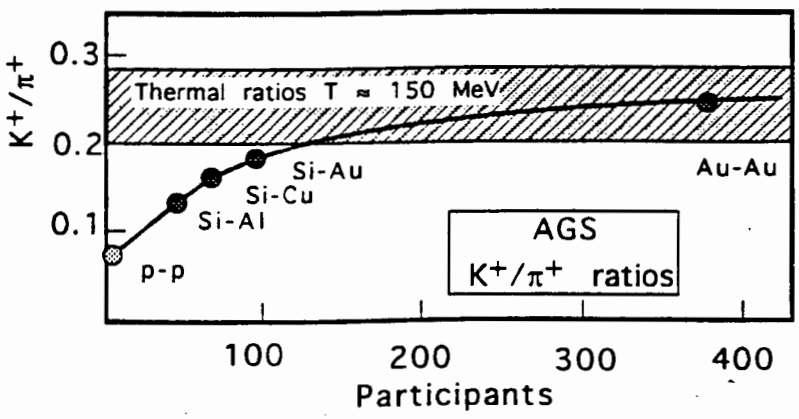

Figure 4.19: The K^+/π^+ ratio versus the total number of participants [10].

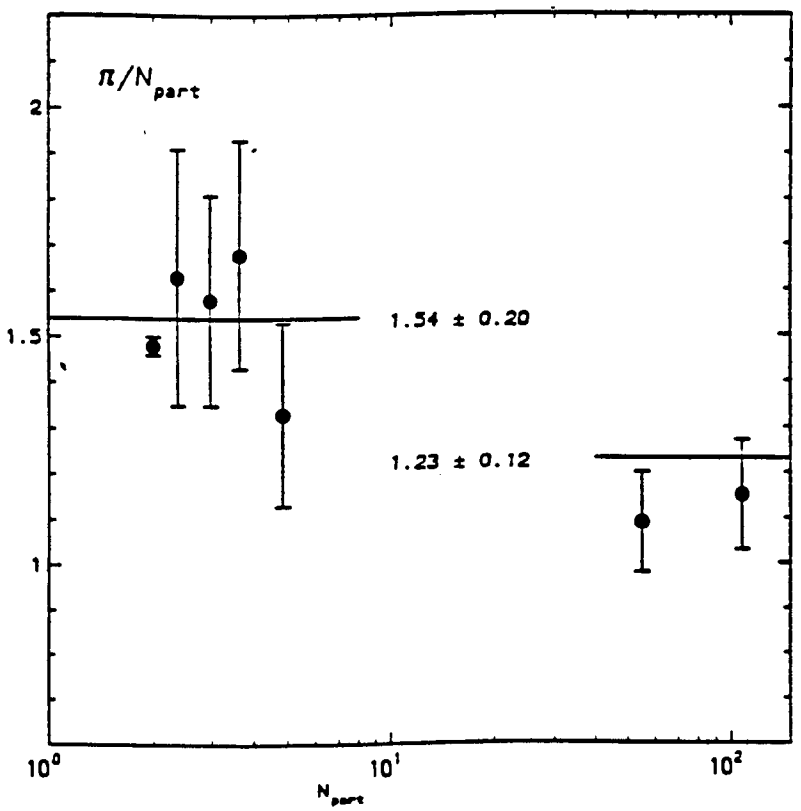

Figure 4.20: The π/N_{part} ratio as a function of participating nucleons N_{part} in $p-A$ and in $Si-Al$ and $Si-Au$ collisions at the AGS. Taken from [48].

4.4.4 Conclusion

The hadron gas model has been tested on the experimental results. The agreement is remarkable, keeping in mind one freeze-out temperature T and baryon density B/V for all particle species. Since particle emission is expected when the mean free path is comparable to the size of the system, different particles could decouple at different times which will imply different temperatures and baryon densities. In view of this one would not expect all the particle yields and the hadronic ratios to approach thermalisation at the same time and by the same rate. Also, the mechanisms which brought different particles towards freeze-out might be different. There are more processes in heavy ion collisions such as pion-nucleon and pion-pion interactions, which results in high kaon production, than in nucleon-nucleon interactions. Thus one will expect an enhancement of kaon/pion ratio. In view of this one should not take strangeness enhancement as the sole factor behind the kaon/pion ratio, but rather it should be taken as one of the ingredients in trying to understand the enhancement of the ratio. Also, because the pion production per nucleon decreases as one moves from $A-A$ via $p-A$ to $p-p$ collisions, one will expect the kaon/pion ratio to increase from $p-p$ to $p-A$ collisions until we have a constant kaon production. It should be noted that if it can somehow be shown that we do indeed reach thermalisation in heavy ion collisions, that alone will not rule out the possibility of the claimed QGP's existence. One has to keep in mind that the thermal model provides only the scenario at the freeze-out and it does not tell us about the evolution and the dynamics of how the system got there.

- QGP Formation

Based on the characteristics of the behavior of the Hadron Gas Model results and the reviewed experimental information in combination with the simple comparisons in this thesis, it seems though that the results of kaon production and the kaon/pion ratio can be understood without invoking formation of the QGP. If the QGP is formed we expect to see a dramatic change in the way the kaon/pion ratio increases as one goes from small systems to large ones or equivalently from peripheral to central collisions compared to the usual trend which we saw in this thesis. This is not even seen in $Au+Au$ collisions where the motivation is primarily the hope that QGP will be formed in larger systems. Also, one cannot draw a

conclusion that QGP is not formed either, considering that our hadron gas model does not know anything about the history of the hadronic matter produced, except at the freeze out. At RHIC (and/or LHC) for large collision systems and high energies it might be possible to create a new state of matter, the quark-gluon plasma. In order to clearly distinguish this from possible alternatives of a hadron gas, one would like to know the state of the plasma in its different stages throughout its lifetime.

The competition between the model and the experiment continues and along the way, even if they don't agree, new physics will be established.

4.4.5 Improvements

Excluded and Finite Volume corrections

Because the hadron gas system is strongly interacting, it is expected that the simple free gas approximation used should be modified. Two different approximation models which incorporate only the repulsive interactions are the excluded volume and mean field. In the excluded volume approach, the interactions are incorporated by allowing hadrons to have a finite hard core, effectively reducing the over-all volume in which the hadrons move to

$$V - \sum_i V_i N_i \ , \tag{4.21}$$

where i runs over all species and N_i is the number of particles of type i. As a consequence the baryon number density B/V (n_B) becomes

$$n_B = \frac{n_B^0}{[1 + V n_B^0]} \ , \tag{4.22}$$

where n_B^0 denotes the density calculated for an ideal gas of pointlike baryons. Note that for $n_B^0 \longrightarrow \infty, n_B \longrightarrow 1/V$, that is we have dense packing limit of hard-sphere baryons with an intrinsic volume V. In the case of several baryon species $\alpha = 1, 2, 3, \cdots, r$, this becomes

$$n_B = \frac{n_B^0}{[1 + \sum_{\alpha=1}^{r} V_\alpha n_\alpha^0]} \ , \tag{4.23}$$

and V_α proportional to the mass as suggested , e.g., by the bag model. For a review on the hard-core repulsive(geometrical) approach see for example [129, 130, 131, 132]

As a consequence of the finite volume corrections discussed in [133], the integrand

$$n_i = \frac{g_i}{2\pi^2} \int_0^\infty \frac{p^2 dp}{\exp(E_i/T) \pm 1} \ , \tag{4.24}$$

has to be multiplied by a correction factor [134], see also [135]. For an estimate of this correction we assume a spherical volume with radius R giving a correction factor

$$f_c = 1 \pm \frac{3\pi}{4pR} + \frac{3}{8(pR)^2} \ . \tag{4.25}$$

The positive and negative signs in Eq 4.25 refers to von Neumann and Diritchlet boundary conditions respectively. The implications of this correction factor can be found in Ritchie's PhD. thesis [136] and [137]. See also Appendix I.

Other considerations

Besides the finite volume effects discussed above, one can still modify the model. The alternative consideration would be to use experimental data points to find out the freeze-out temperature and baryon density in a $T - n_B$ plane as done in grand canonical on the $T - \mu_B$ plane [46]. The other proposal which deals very much with geometrical considerations and was considered by [31, 138]. In this picture the freeze-out volume is found in the following way: A given projectile of radius R_P and mass number A_P bore a volume V_{in} out of the target given by:

$$V_{in} = \pi R_P^2 2R_T = \frac{3}{2} V_0 A_P^{\frac{2}{3}} A_T^{\frac{1}{3}} \ . \tag{4.26}$$

The target is labelled with the subscripts $_T$ and V_0 is the volume of a nucleon. The baryon number, B, inside this volume is

$$B = A_P + \frac{V_{in}}{V_T} A_T \ . \tag{4.27}$$

After the collision the system expands up to the freeze-out time after which the hadrons cease to interact. This expansion is characterized by the expansion parameter α. The pointlike baryon density is then given by

$$n_B^0 = \frac{B}{\alpha V_{in}} , \tag{4.28}$$

and the extended baryon density n_B is given by

$$n_B = \frac{B}{\alpha V_{in} + B V_0} , \tag{4.29}$$

which follows from reducing the available pointlike volume by B times the volume of a baryon, $V_{point-like} = V - BV_0$.

A rather naive geometrical picture for calculating the number of participating nucleons in central collisions, for e.g $A - B$ collision where $A < B$, follows: the radii of the nuclei can be obtained from $4R^3\pi n_0/3 = A$, where A in this relation denotes the mass number of the nucleus in question and n_0 is the nuclear density taken to be $0.17/fm^3$. Now, the height of the cylinder cut out of the target by the path of the projectile is $H = 2\sqrt{R_T^2 - R_P^2}$. Thus the volume of this cylinder is $V_{cyl} = 2R_P^2\pi H$. The height of the spherical slices at the two

ends of the cylinder is $h = R_T - \sqrt{R_T^2 - R_P^2}$, so the volume of the two spherical slices is $V_{slc} = \frac{2}{3}\pi h^2(3R_T - h)$. Thus the total number of target participants is $N_{Part}^{Tar} = n_0(V_{cyl} + V_{slc})$ and for the total number one add the projectile nucleons of which in central collision they all participate.

One can also use an oversimplified approach using the participant-spectator model. Assuming a hard sphere nuclei of radius R and constant density inside, the number of projectile participants is given by

$$N_{pp} = \frac{A}{\frac{4}{3}\pi R^3}\int_{b-R}^{R}\pi(R^2 - x^2)dx = A\left(1 - \frac{3b^2}{4R^2} + \frac{b^3}{4R^3}\right) \quad , \tag{4.30}$$

with impact parameter b. The most general method is the one considered by Salmeron [139]. Here not only the number of projectile participants is calculated, but also the number of the target participants, and the model is b dependent. This model together with Glauber model is of interest to see its impact on the hadron gas model considered here.

Appendix A

Kinematic Variables

The kinematic variables commonly used in high-energy heavy ion collisions are transverse mass, m_T, and rapidity, y. In any collision there is a unique defined direction, the beam axis z. Consider a particle of mass m and momentum $\mathbf{p}$. The momentum component along the beam direction is called the longitudinal momentum, p_l (or p_z). The components perpendicular to the beam are combined and called the transverse momentum, p_T (or $p_\perp$). p_T is Lorenz invariant in any frame (including the lab system) moving parallel to the z direction. The longitudinal momentum, p_l and energy, $E = \sqrt{p^2 + m^2}$, are not Lorenz invariant. The transverse mass is defined as

$$m_T = \sqrt{p_T^2 + m^2} \ , \tag{A.1}$$

and the rapidity is defined as

$$y = \frac{1}{2} \ln \left(\frac{E + p_l}{E - p_l} \right) = \ln \left(\frac{E + p_l}{m_T} \right) \ . \tag{A.2}$$

Rapidity has a very nice property in that it is additive under Lorenz transformation just like a Galilean velocity under Galilean transformations. Therefore, the differential dy is Lorenz invariant. Using transverse mass and rapidity, we can easily derive the energy and longitudinal momentum: From Eq. A.2, we have

$$e^y = \sqrt{\frac{E + p_l}{E - p_l}} \ , \tag{A.3}$$

and

$$e^{-y} = \sqrt{\frac{E - p_l}{E + p_l}} \ . \tag{A.4}$$

Adding Eqs. A.3 and A.4, we get the relation between the energy and the rapidity of the particle:

$$E = m_T \cosh y \ , \tag{A.5}$$

and subtracting Eq. A.4 from Eq. A.3, we obtain the relation between the longitudinal momentum p_l and the rapidity y of the particle

$$p_l = m_T \sinh y \ . \tag{A.6}$$

This makes the energy and longitudinal momentum transformation easy. To characterize the rapidity of the particle it is necessary to measure two quantities of the particle, such as its energy and its longitudinal momentum. However, in many experiments, it is only possible to measure the angle of the detected particle relative to the beam axis. In that case, it is convenient to use the *pseudorapidity variable* η to characterize the detected particle This variable is closely related to rapidity and it depends only on the polar angle, θ, which is the angle between the particle momentum $\mathbf{p}$ and the beam axis.The pseudo-rapidity is defined as

$$\begin{aligned} \eta &= \frac{1}{2} \ln \left(\frac{|p| + p_l}{|p| - p_l} \right) = \ln \left(\frac{p + p_l}{p_T} \right) \\ &= -\ln[\tan(\theta/2)] \ . \end{aligned} \tag{A.7}$$

Looking at Eqs. A.2 and A.7, one quickly see that the pseudo-rapidity variable coincides with the rapidity variable when the momentum is large, i.e, when $|\mathbf{p}| \approx E$. Consider now the change of variables from $(y, \mathbf{p_T})$ to $(\eta, \mathbf{p_T})$. One can change from y to η and vice versa. From Eq. A.7, we have

$$e^{\eta} = \sqrt{\frac{|\mathbf{p}| + p_l}{|\mathbf{p}| - p_l}} \ , \tag{A.8}$$

and

$$e^{-\eta} = \sqrt{\frac{|\mathbf{p}| - p_l}{|\mathbf{p}| + p_l}} \ . \tag{A.9}$$

Adding Eqs. A.8 and A.9, we obtain the relation

$$|\mathbf{p}| = p_T \cosh \eta \ , \tag{A.10}$$

where p_T is the magnitude of the transverse momentum

$$p_T = \sqrt{\mathbf{p} - p_l} \ . \tag{A.11}$$

Subtracting Eq. A.9 from A.8, we obtain

$$p_l = p_T \sinh \eta \ . \tag{A.12}$$

Using these results we can express the rapidity variable y in terms of the pseudorapidity variable η as

$$y = \frac{1}{2} \ln \left[\frac{\sqrt{p_T^2 \cosh^2 \eta + m^2} + p_T \sinh \eta}{\sqrt{p_T^2 \cosh^2 \eta + m^2} - p_T \sinh \eta} \right] \ , \tag{A.13}$$

where m is the rest mass of the particle. Conversely, the pseudo-rapidity variable η can be expressed in terms of the rapidity variable y by

$$\eta = \frac{1}{2} \ln \left[\frac{\sqrt{m_T^2 \cosh^2 y - m^2} + m_T \sinh y}{\sqrt{m_T^2 \cosh^2 y - m^2} - m_T \sinh y} \right] \ . \tag{A.14}$$

If particles have a distribution $dN/dyd\mathbf{p}_T$ in terms of the rapidity variable y, then the distribution in the pseudo-rapidity variable η is

$$\frac{dN}{d\eta d\mathbf{p}_T} = \sqrt{1 - \frac{m^2}{m_T^2 \cosh^2 y}} \frac{dN}{dyd\mathbf{p}_T} \ . \tag{A.15}$$

In experiments, only the pseudo-rapidity variable of the detected particles is measured to give $dN/d\eta$, which is the integral of $dN/d\eta d\mathbf{p}_T$ with respect to transverse momentum. One can compare this quantity with dN/dy which is the integral of $dN/dyd\mathbf{p}_T$ with respect to transverse momentum. For massless particles η and y are identical.

Appendix B

The Thermodynamics of Quark-Gluon Plasma

B.1 Quarks and Gluons at high T and μ_{quark}=0

The phase space volume of quarks in a spatial volume V with momentum p in the momentum interval dp is $4\pi p^2 dp\, V$. Each state occupies a phase space volume of $(2\pi\hbar)^3$. Therefore the number of states characterized by a momentum p in the interval dp is $4\pi p^2 dp\ V/(2\pi)^3$. For a given temperature T, not all the states are occupied. The occupation probability for the state with a momentum p is given by the Fermi-Dirac distribution for that particular temperature T.

The number of quarks in a volume V with momentum p within the interval dp is

$$dN_q = \frac{g_q V 4\pi p^2 dp}{(2\pi)^3} \left\{ \frac{1}{1 + e^{(p-\mu_q)/T}} \right\} , \tag{B.1}$$

where the factor in the curly brackets is a Fermi-Dirac distribution, μ_q is the quark chemical potential and g_q is the degeneracy of quarks.

The number density of antiquarks is therefore

$$\begin{aligned} n_{\bar{q}} &= \frac{g_q}{(2\pi)^3} \int_{-\infty}^{0} 4\pi p^2 dp \left[1 - \frac{1}{1+e^{(p-\mu_q)/T}}\right] \\ &= \frac{g_q}{(2\pi)^3} \int_{0}^{\infty} 4\pi p^2 dp \, \frac{1}{1+e^{(p+\mu_q)/T}} \ , \end{aligned} \tag{B.2}$$

and

$$n_q = \frac{g_q}{(2\pi)^3} \int_{0}^{\infty} 4\pi p^2 dp \, \frac{1}{1+e^{(p-\mu_q)/T}} \ . \tag{B.3}$$

When the number density of quarks is the same as that for antiquarks, we have $\mu_q = 0$. For $\mu_q = 0$, the energy of the massless quarks in the system of volume V and temperature T is

$$\begin{aligned} E_q &= \frac{g_q}{2\pi^2} \int_0^\infty \frac{p^3 dp}{1+e^{p/T}} \\ &= \frac{g_q V}{2\pi^2} T^4 \int_0^\infty \frac{z^3 dz}{1+e^z} \\ &= \frac{g_q V}{2\pi^2} T^4 \int_0^\infty z^3 dz \, e^{-z} \sum_{n=0}^{\infty} (-1)^n \, e^{-nz} \\ &= \frac{g_q V}{2\pi^2} T^4 \, \Gamma(4) \sum_{n=0}^{\infty} (-1)^n \frac{1}{(n+1)^4} \ , \end{aligned} \tag{B.4}$$

where Γ is the gamma function. One can show that

$$\begin{aligned} \sum_{n=0}^{\infty} (-1)^n \frac{1}{(n+1)^4} &= \sum_{m=1,3,5\cdots} \frac{1}{m^4} - \sum_{m=2,4,6\cdots} \frac{1}{m^4} \\ &= \sum_{m=1,2,3\cdots} \frac{1}{m^4} - 2 \sum_{m=2,4,6\cdots} \frac{1}{m^4} \\ &= \sum_{m=1,2,3\cdots} \frac{1}{m^4} - 2 \sum_{m=1,2,3\cdots} \frac{1}{(2m)^4} \\ &= (1-2^{-3})\, \zeta\,(4) \, , \end{aligned} \tag{B.5}$$

where $\zeta(x)$ is the Riemann zeta function defined by [20]

$$\zeta(x) = \sum_{m=1,2,3\cdots} \frac{1}{m^x} \, . \tag{B.6}$$

The function $\zeta(4)$ has the value $\pi^4/90$ [20]. The energy of the system due to quarks is therefore

$$E_q = \frac{7}{8} \, g_q \, V \, \frac{\pi^2}{30} \, T^4 \, , \tag{B.7}$$

and the energy density is given by

$$\varepsilon_q = \frac{7}{8} \, g_q \, \frac{\pi^2}{30} \, T^4 \, . \tag{B.8}$$

From the pressure-energy density relation,

$$P = \frac{1}{3}\frac{E}{V} \tag{B.9}$$

the pressure due to quarks is

$$P_q = \frac{7}{8}\, g_q\, \frac{\pi^2}{90}\, T^4 \,, \tag{B.10}$$

and the pressure due to antiquarks is

$$P_{\bar{q}} = \frac{7}{8}\, g_{\bar{q}}\, \frac{\pi^2}{90}\, T^4 \,. \tag{B.11}$$

Thus the pressure of the quark-antiquark gas at temperature T will be

$$P_q + P_{\bar{q}} = \frac{7}{8}\,(g_q + g_{\bar{q}})\, \frac{\pi^2}{90}\, T^4 \tag{B.12}$$

and the number density of quarks and antiquarks are

$$\begin{aligned} n_q = n_{\bar{q}} &= \frac{g_q}{2\pi^2}\int_0^\infty \frac{p^2 dp}{1+e^{p/T}} \,, \\ &= \frac{g_q}{2\pi^2}\, T^3\, \frac{3}{2}\, \zeta(3) \,. \end{aligned} \tag{B.13}$$

where $\zeta(3)$ has the value of 1.20205 [20].

The energy of gluons in the system of volume V and temperature T is

$$E_g = \frac{g_g V}{2\pi^2}\int_0^\infty p^3 dp \left\{\frac{1}{e^{p/T}-1}\right\} , \tag{B.14}$$

where the factor in brackets is the Bose-Einstein distribution for bosons and g_g is the gluon degeneracy,

$$\begin{aligned} E_g &= \frac{g_g V}{2\pi^2}\, T^4 \int_0^\infty \frac{z^3 dz}{e^z - 1} \\ &= \frac{g_g V}{2\pi^2}\, T^4 \int_0^\infty z^3 dz\, e^{-z} \sum_{n=0}^{\infty} e^{-nz} \\ &= \frac{g_g V}{2\pi^2}\, T^4\, \Gamma(4) \sum_{n=0}^{\infty} \frac{1}{(n+1)^4} \\ &= \frac{g_g V}{2\pi^2}\, T^4\, \Gamma(4)\, \zeta(4) \\ &= g_g\, V\, \frac{\pi^2}{30}\, T^4 \,, \end{aligned} \tag{B.15}$$

$$\text{Therefore, } E_g = g_g\, \frac{\pi^2}{30}\, T^4 \,.$$

Again using $P = \frac{1}{3}$ E/V, we have

$$P_g = g_g \frac{\pi^2}{90} T^4 . \tag{B.16}$$

The number density of gluons are

$$\begin{aligned} n_g &= \frac{g_g}{2\pi} \int_0^\infty p^2 \, dp \left\{ \frac{1}{e^{p/T} - 1} \right\} \\ &= \frac{g_g}{2\pi^2} T^3 \, \Gamma(3) \, \zeta(3) \\ &= \frac{g_g}{\pi^2} 1.202 \, T^3 . \end{aligned} \tag{B.17}$$

B.2 Quarks and gluons at High Baryon Density

We consider a relativistic degenerate quark gas. For simplicity, we shall neglect the contributions from antiquarks and gluons. The number of state in a volume V with momentum p within the momentum interval dp is

$$\frac{g_q V}{(2\pi)^3} 4\pi p^2 dp . \tag{B.18}$$

The total number of quarks up to the Fermi momentum μ_q is

$$\begin{aligned} N_q &= \frac{g_q V}{(2\pi)^3} \int_0^{\mu_q} 4\pi p^2 dp \\ &= \frac{g_q V}{6\pi^2} \mu_q^3 . \end{aligned} \tag{B.19}$$

The number density of quarks is given by

$$n_q = \frac{N_q}{V} = \frac{g_q}{6\pi^2} \mu_q^3 . \tag{B.20}$$

The energy of the quark gas in a volume V is

$$\begin{aligned} E_q &= \frac{g_q V}{(2\pi)^3} \int_0^{\mu_q} 4\pi p^3 dp \\ &= \frac{g_q V}{8\pi^2} \mu_q^4 . \end{aligned} \tag{B.21}$$

The energy density of the quark is therefore

$$\varepsilon = \frac{g_q}{8\pi^2} \mu_q^4 . \tag{B.22}$$

And from the relation between the pressure and the energy density, we have

$$P_q = \frac{g_q}{24\pi^2}\mu_q^4 \ .$$

When this pressure, $P_q = B$, the bag pressure, the critical change of state takes place. This leads to

$$\mu_q = \left(\frac{24\pi^2}{g_q}B\right)^{1/4} \ , \tag{B.23}$$

which corresponds to a critical quark number density given by

$$n_q(\text{quark-gluon plasma}) = 4\left(\frac{g_q}{24\pi^2}\right)^{1/4} B^{3/4} \ , \tag{B.24}$$

and the corresponding critical baryon number density is

$$n_B(\text{quark-gluon plasma}) = \frac{4}{3}\left(\frac{g_q}{24\pi^2}\right)^{1/4} B^{3/4} \ . \tag{B.25}$$

Appendix C

The Density of Particles at Temperature T

The density n_i of particle i with rest mass m_i at temperature T is given by

$$n_i = \frac{1}{(2\pi)^3} \int_0^\infty \frac{4\pi \mathbf{p}^2 d\,|\mathbf{p}|}{e^{\sqrt{\mathbf{p}^2+m_i^2}/T} - 1} \ . \tag{C.1}$$

This can be written as

$$\begin{aligned} n_i &= \frac{T^3}{2\pi^2} \int_0^\infty \frac{z^2 dz}{e^{\sqrt{z^2+(m_i/T)^2}} - 1} \\ &= \frac{T^3}{2\pi^2} \int_0^\infty z^2\, dz\, e^{-\sqrt{z^2+(m_i/T)^2}} \sum_{k=0}^{\infty} e^{-(k)\sqrt{z^2+(m_i/T)^2}} \\ &= \frac{T^3}{2\pi^2} \sum_{k=0}^{\infty} \int_0^\infty z^2\, dz\, e^{-(k+1)\sqrt{z^2+(m_i/T)^2}} \ . \end{aligned}$$

By using Eq.(9.6.23) of [20], we have

$$\begin{aligned} &\int_0^\infty z^2\, dz\, e^{-(k+1)\sqrt{z^2+(m_i/T)^2}} \\ &= \frac{1}{k+1} \left(\frac{m_i^2}{T}\right)^2 K_2\left(\frac{(k+1)m_i}{T}\right) \ . \end{aligned} \tag{C.2}$$

The density is therefore

$$n_i = \frac{T m_i^2}{2\pi^2} \sum_{k=1}^{\infty} \frac{1}{k} K_2\left(\frac{m_i}{T}\right) \ . \tag{C.3}$$

(C.4)

As a special case: For large m_i such that $m_i/T >> 1$, Eq.(9.7.2) of [20] gives

$$K_2\left(\frac{km_i}{T}\right) \cong \sqrt{\frac{\pi T}{2km_i}}\, e^{-km_i/T} .$$

and in this limit the density n_i is

$$n_i = \left(\frac{m_i T}{2\pi}\right)^{3/2} \sum_{k=1}^{\infty} \frac{1}{k^{3/2}} e^{-km_i/T} . \tag{C.5}$$

The ratio of two different densities of two types of particles at the same temperature is

$$\frac{n_i}{n_j} \sim \left(\frac{m_i}{m_j}\right)^{3/2} e^{-(m_i - m_j)/T} . \tag{C.6}$$

Appendix D

Particle Yields in dn/dy and Thermal Model

The Boltzmann approximation Eq. 1.6 gives the particle density in an infinite volume. Ignoring the finite volume corrections, it gives particle yields of

$$\frac{d^3n}{dp^3} \propto e^{-E/T} \quad . \tag{D.1}$$

To transfer from (p_x, p_y, p_z) to (p_T, y, ϕ) in the nucleon-nucleon center of momentum frame, we made use of the Jacobian

$$\frac{\partial(p_x, p_y, p_z)}{\partial(y, p_T, \phi)} = \begin{vmatrix} \frac{\partial p_x}{\partial y} & \frac{\partial p_x}{\partial p_T} & \frac{\partial p_x}{\partial \phi} \\ \frac{\partial p_y}{\partial y} & \frac{\partial p_y}{\partial p_T} & \frac{\partial p_y}{\partial \phi} \\ \frac{\partial p_z}{\partial y} & \frac{\partial p_z}{\partial p_T} & \frac{\partial p_z}{\partial \phi} \end{vmatrix} = E p_T \quad , \tag{D.2}$$

and we get

$$\begin{aligned} d^3n &\propto E\, p_T\, e^{-\frac{m_T \cosh y}{T}} dp_T dy d\phi \\ &\propto m_T^2 \cosh(y) e^{-\frac{m_T \cosh y}{T}} dm_T dy d\phi \; . \end{aligned} \tag{D.3}$$

Integrating Eq. D.3 over m_T, given azimuthal symetry, we obtain

$$\frac{dn}{dy} \propto \int_m^\infty m_T^2 \cosh y\, e^{-\frac{m_T \cosh y}{T}} dm_T \tag{D.4}$$

$$\propto \left[\frac{m^2}{T^2} + \frac{2m}{T\cosh y} + \frac{2}{\cosh^2 y}\right] T^3 e^{-\frac{m\cosh y}{T}} \ . \tag{D.5}$$

For massless particles, this reduces to the familiar T^3 relation. For small y, dn/dy can be approximated as a Gaussian distribution with its width given by

$$\Gamma_{thermal} = \sqrt{\frac{T}{m}} \ . \tag{D.6}$$

Appendix E

Particle density ratios and transverse flow

The Boltzmann equation for the density of particle species i

$$n_i = g_i \lambda_i \int \frac{d^3p}{(2\pi)^3} e^{-\frac{E_i}{T}} , \tag{E.1}$$

can be written in the form

$$\frac{dn}{m_T dm_T} = \frac{g}{(2\pi)^2} \lambda 2mT \; K_1\left(\frac{m_T}{T}\cosh y_T\right) \; I_0\left(\frac{p_T}{T}\sinh y_T\right) . \tag{E.2}$$

We rearrange the above equation by using $m_T dm_T = p_T dp_T$ to get

$$n \propto \int_0^\infty dp_T \; p_T m_T \; K_1\left(\frac{m_T}{T}\cosh y_T\right) \; I_0\left(\frac{p_T}{T}\sinh y_T\right) . \tag{E.3}$$

Let us rescale Eq. (E.3) by dividing p_T and m_T by m to obtain

$$n \propto m^3 \int_0^\infty \frac{dp_T}{m}\frac{p_T}{m}\frac{m_T}{m} \; K_1\left(\frac{m_T}{mT} m \; \cosh y_T\right) \; I_0\left(\frac{p_T}{mT} m \; \sinh y_T\right) , \tag{E.4}$$

which leaves the integral dimensionless. Using [140], one can show that

$$\begin{aligned} &\int_0^\infty dx \; x\sqrt{x^2+y^2} \; K_1\left(c\sqrt{x^2+y^2}\right) \; I_0(bx) \\ &= \frac{c}{(c^2-b^2)} y^2 K_2\left(y\sqrt{c^2-b^2}\right) . \end{aligned} \tag{E.5}$$

Comparing Eq. E.4 and Eq. E.5 we have

$$n \propto m^2 T \; \cosh y_T \; K_2\left(\frac{m}{T}\right) . \tag{E.6}$$

And finally we have

$$n_i = \lambda_i \frac{g_i m_i^2 T}{2\pi^2} \cosh y_T \; K_2\left(\frac{m}{T}\right) \; . \tag{E.7}$$

This shows that the ratios of particle densities are independent of transverse flow. One notices that the only difference from a stationary fireball is that now we have a factor $\cosh y_T$ which is attributed to the Lorenz contraction in the transverse direction of the fireball, since $\cosh y_T = \gamma$, which then reduces the volume to $\gamma V_{stationary}$.

Appendix F

Thermal Boltzmann spectra and Rapidity windows

Beginning from relation

$$E\,\frac{d^3n}{d^3p} = \frac{g\lambda}{(2\pi)^3}\,m_T\,\cosh(y-y_{FB})\,e^{-\frac{m_T}{T}\cosh(y-y_{FB})}\,. \tag{F.1}$$

We integrate the above equation by parts over m_T and make use of $y' = y - y_{FB}$ to arrive at

$$\frac{dn}{dy} = \frac{g\lambda}{(2\pi)^3}m^2Te^{-\frac{m}{T}\cosh y'}\left(1+2\left(\frac{T}{m\cosh y'}\right)+2\left(\frac{T}{m\cosh y'}\right)^2\right)\,. \tag{F.2}$$

The behaviour of the above equation for $m \geq T$ is

$$\frac{dn}{dy} \sim e^{-\frac{m}{2T}(y-y_{FB})^2}\,. \tag{F.3}$$

For massless particles, the rapidity and pseudorapidity spectra becomes equal: $dn/dy \sim 1/\cosh^2 y'$ Looking at the above equation, Eq. F.3, data which have been collected in a small rapidity window (compared with the total rapidity distribution width, say $\delta y \leq 0.5$ or so) should be compared with a thermal model by using a fit of the form

$$\frac{dn}{dydm_T} \propto m_T\,e^{-\frac{m_T}{T_{eff}}}\,, \tag{F.4}$$

with $T_{eff} = T/\cosh(y-y_{FB})$. In a large rapidity window around y_{FB}, the y integrated form of the above equation, in the limit where $m_T \gg T$ produces the relation

$$\frac{dn}{dm_T} \propto m_T^{\frac{3}{2}}\,e^{-\frac{m_T}{T}}\,. \tag{F.5}$$

In this case one should plot

$$\frac{dn}{m_T^{3/2} dm_T} \; vs \; m_T \quad . \tag{F.6}$$

Appendix G

Transformation of d^3p into cylindrical coordinates

Due to the cylindrical symmetry of the collision we are modelling, it is convenient to introduce two variables: y, longitudinal rapidity (which is Lorentz-additive), and m_T, transverse mass. We define y, the longitudinal rapidity, as

$$y = \tanh^{-1}\left(\frac{p_z}{E}\right) . \tag{G.1}$$

We have chosen the boost to be only along the z-axis, so $p_z/E = (\beta\gamma)/\gamma = \beta$, which is just v_L as we use units where $c = 1$. Defining m_T as

$$m_T = \sqrt{m^2 + p_x^2 + p_y^2} , \tag{G.2}$$

and writing the momentum 4-vector of the beam as

$$p^\mu = (E, p_x, p_y, p_z) = (m_T \cosh y, p_x, p_y, m_T \sinh y) , \tag{G.3}$$

and using

$$p^\mu\, p_\mu = m_T^2\, \cosh^2\, y - p_x^2 - p_y^2 - m_T^2\, \sinh^2\, y = E^2 - p_x^2 - p_y^2 - p_z^2 = m^2 , \tag{G.4}$$

the familiar relation

$$E^2 - p_x^2 - p_y^2 - p_z^2 = m^2 , \tag{G.5}$$

is regained.

Now we transform d^3p into cylindrical coordinates:

$$d^3p = 2\pi\ p_T\ dp_T\ dp_z\ d\phi\ , \tag{G.6}$$

with p_T = transverse and p_z = longitudinal momenta respectively. If one recalls that $m_T^2 = m^2 + p_T^2$, it follows that $m_T\ dm_T = p_T\ dp_T$, which transforms the above equation into

$$d^3p = 2\pi\ m_T\ dm_T\ dp_z\ d\phi\ . \tag{G.7}$$

Using the definition of rapidity we have $dy = dp_z/E$, we finally have the transformation of d^3p into the cylindrical coordinates y and m_T ,

$$d^3p = 2\pi\ m_T\ dm_T\ E dy\ d\phi\ . \tag{G.8}$$

Appendix H

Excluded volumes

The density of a system of N "real" particles in a volume V is

$$n^{real} = \frac{N}{V} \ . \tag{H.1}$$

If we shrink the "real" particles to point-like particles the volume of the point-like particle becomes $V - V_0$, where V_0 denotes the original "real" particle volume and density of point-like particles becomes

$$\begin{aligned} n^{point-like} &= \frac{N}{V - NV_0} = \frac{N/V}{1 - \frac{N}{V}V_0} \\ &= \frac{n^{real}}{1 - n^{real}V_0} \ . \end{aligned} \tag{H.2}$$

From this it follows that

$$n^{real} = \frac{n^{point-like}}{1 + n^{pointlike}V_0} \ . \tag{H.3}$$

In the thermodynamic limit where the temperature and chemical potential goes to infinity

$$\begin{aligned} \lim_{T \longrightarrow \infty} n^{pointlike} &= \infty \\ \lim_{T \longrightarrow \infty} n^{real} &= \frac{1}{V_0} \qquad \equiv \text{dense packing limit} \ . \end{aligned} \tag{H.4}$$

If each particle species has the same excluded volume then the particle ratios calculated using the 'excluded volume' ensemble are the same as those calculated in the ideal free gas of pointlike, non- interacting particles. However, if the excluded volume varies from species to species, the particle ratios are affected.

Appendix I

Finite volume correction for a spherical fireball

The quantum mechanical wave functions that describe the spherical fireball are subject to a surface boundary condition that requires these wavefunctions to vanish at that surface. Quantitatively, we look for solutions of

$$\nabla^2\Psi + k^2\Psi = 0\,, \quad \Psi_{\text{surface}} = 0\,. \tag{I.1}$$

Each proper solution $\Psi(x,y,z) = \sin(k_x x)\ \sin(k_y y)\ \sin(k_z z)$ corresponds to a lattice point in k space, with $k_x = l\pi/a,\ k_y = m\pi/a,\ k_z = n\pi/a$ is the radius of the sphere. Each state fills out a characteristic volume π^3/a^3, and the states are filled to a k_{max}. This can be visualized as the states occupying an octant of a sphere, except for slablike regions at coordinate planes (x or y or $z = 0$), and on the shell, where the boundary condition applies. Volume = shell − correction for ring-like strips + recorrection for corners subtracted twice in counting volume of rings, or more elegantly, if we look at the number of states dN with wave number k found in the interval k + dk

$$dN = \frac{Vk^2}{2\pi^2}\,d\mathrm{k} - \frac{Sk}{8\pi}\,d\mathrm{k} + \int \chi\, dS\, d\mathrm{k}/8\pi^2\,, \tag{I.2}$$

with V the volume, S the surface area and χ the local total curvature of the sphere, which

is just L, the characteristic length of the fireball. So N, the number of allowed states with wave number less than k

$$N = \frac{Vk^3}{6\pi^2} \pm \frac{Sk^2}{16\pi} + \frac{Lk}{8\pi^2} \,. \tag{I.3}$$

In other words, the entire geometric volume is not free to be populated by quantum states. The forbidden regions, when the volume is small, have to be taken into account, hence the term 'finite volume correction'. The plus and minus signs refers to von Neumann and Diritchlet conditions respectively.

Bibliography

[1] J.D. Bjorken, *Phys. Rev.* **D27** (1983) 140.

[2] B.D. Keister and L.S. Kisslinger, *Phys. Lett.* **B64** (1976) 117.

[3] T.D. Lee, *Rev. Mod. Phys.* **47** (1975) 267.

[4] Gell-Mann, *Phys. Lett.* **8** (1964) 214.

[5] G. Zweig, CERN-TH/412, 1964.

[6] H. Satz, *Nucl. Phys.* **A544** (1992) 371c.

[7] L. McLerran, *Rev. Mod. Phys.* **58** (1986) 1021.

[8] N.H. Christ, "Finite temperature in QCD", Proceedings of Quark Matter '91, *Nucl. Phys.* **A544** (1992) 81c.

[9] H.H. Gutbrod, In International Conference on the Physics and Astrophysics of Quark Gluon Plasma, Bombay (1988)

[10] I. Tserruya, CERN-PPE/95-185.

[11] T. Alber *et al.*, *Phys. Rev. Lett.* **75** (1995) 3814.

[12] A. Chodos *et al.*, *Phys. Rev.* **D9** (1974) 3471.

[13] C.D. DeTar and J.F.Donoghue, *Ann. Rev. Nucl. Part. Sci.* **33**, (1983) 235.

[14] L. Wilets, "Bag Models of Nucleus", World Scientific, 1989.

[15] T. Åkesson *et al.*, *Nucl. Phys.* **B353** (1991) 1.

[16] C. Wong, "Introduction to High-Energy Heavy-Ion Collisions", World Scientific, 1994.

[17] F. Wilczek, *Ann. Rev. Nucl. Part. Sci.* **32** (1982) 177.

[18] K. Werner, *Phys. Rep.* **232** (1993) 87.

[19] H.C. Eggers and J. Rafelski, *Int. J. Mod. Phys.* **A6** (1991) 1067.

[20] M. Abramowitz and I.A. Stegun, "Handbook of Mathematical Tables", Dover Publications, New York. 1965.

[21] E.V. Shuryak, *Phys. Lett.*, **B78** (1978) 150.

[22] T. Matsui and H. Satz, *Phys. Lett.* **B178** (1986) 416.

[23] R. Hagedorn, *Suppl. Nuovo Cimento* **6** (1968) 311.

[24] R. Hagedorn and J. Ranft, *Suppl. Nuovo Cimento* **6** (1968)169.

[25] R. Hagedorn, CERN yellow report 71-12 (1971).

[26] "Statistical Mechanics of Quarks and Hadrons", (Ed) H. Satz, North Holland, Amsterdam, 1981.

[27] R. Hagedorn and K. Redlich, *Z. Phys.* **C27** (1985) 541.

[28] C. Dereth, W. Greiner, H.-Th. Elze and J. Rafelski, *Phys. Rev.* **C31** (1985) 1360.

[29] M. Gorenstein, V.K. Petrov and G.M. Zinovjev, *Phys. Lett.* **B106** (1981) 327.

[30] R. Hagedorn and J. Rafelski, *Phys. Lett.* **B97** (1980) 136.

[31] J. Cleymans, E. Suhonen, G.M. Weber, *Z. Phys.* **C53** (1992) 485.

[32] J. Cleymans and H. Satz, *Z. Phys.* **C57** (1993) 135.

[33] B. Müller, Lecture Notes in Physics 225, "The Physics of Quark-Gluon Plasma", Springer-Verlag , 1985.

[34] B. Müller and J. Rafelski, *Phys. Lett.* **B116** (1982) 274.

[35] B. H.-Th. Elze, W. Greiner and J. Rafelski, *Phys. Lett.* **B124** (1983) 515.

[36] Review of Particle Properties, *Phys. Rev.* **D50** (1994) 1177.

[37] K. Redlich and L. Turko, *Z. Phys.* **C5** (1980) 201.

[38] J. Kapusta, "Finite Temperature Field Theory", Cambridge University Press (1989).

[39] J. Cleymans, K. Redlich and E. Suhonen, *Z. Phys.* **C51** (1991) 137.

[40] J. Rafelski and M. Danos, *Phys. Lett.* **B97** (1980) 279.

[41] J. Schukraft, CERN Preprint, PPE-91-04.

[42] G. Odyniec, In Hot Hadronic Matter: Theory and Experiment, J.Letessier, H. Gutbrod and J. Rafelski(Eds.), Plenum Press, New York (1995) 405.

[43] J. Cleymans, H. Satz, E. Suhonen and D.W. von Oertzen, *Phys. Lett.* **242B** (1990) 111.

[44] N.J. Davidson, H.G. Miller, R.M. Quick and J. Cleymans, *Phys. Lett.* **B255** (1991) 105.

[45] N.J. Davidson, H.G. Miller and D.W. von Oertzen, *Phys. Lett.* **B256** (1991) 554.

[46] J. Cleymans, D. Elliott, H. Satz and R.L. Thews, CERN TH/95-298.

[47] P. Braun-Munziger, J. Stachel, J.P. Wessels and N. Xu, *Phys. Lett.* **B344** (1995) 43.

[48] Duncan Elliott, M.Sc. Thesis, University of Cape Town (1996) (unpublished).

[49] U. Heinz and K.S. Lee, *Phys. Lett.* **B259** (1991) 162.

[50] J. Cugnon and R.M. Lombard, *Nucl. Phys.* **A422** (1984) 635.

[51] S. Nagamiya, *Phys. Rev. Lett.* **49** (1982) 1383.

[52] Y. Akiba, Phys. Rev. Lett. **70** (1993) 70.

[53] G.S.F. Stephans, *Nucl. Phys.* **A566** (1994) 269c.

[54] H Baker *et al.*, *Z. Phys.* **C64** (1994) 209

[55] Y. Akiba for E802 Collaboration, Particle Production in Au+Au Collisions from BNL E866, Talk presented at Quark Matter '96, Heidelberg, Germany, may 1996.

[56] Low p_t pion enhancement in $^{28}Si + Pb$ at 14.6 GeV/c, T.K. Hemmick, Proceedings of Quark Matter '93, *Nucl. Phys.* **A566** (1994) 435c.

[57] Low p_t phenomena observed in high energy nuclear collisions, J Simon-Gillo, In Proceedings of Quark Matter '93, *Nucl. Phys.* **A566** (1994) 175c.

[58] Transverse momentum distributions of hadrons, B. Jacak, Proceedings of Quark Matter '90, *Nucl. Phys.* **A525** (1991) 77c.

[59] K.S. Lee and U. Heinz, *Z. Phys.* **C43** (1989) 425.

[60] Collective effects and nuclear stopping, M. Hoffmann *et al*, Proceedings of Quark Matter '93, *Nucl. Phys.* **A566** (1994) 15c.

[61] Particle spectra and correlations from experiment 814, J. Stachel, Proceedings of Quark Matter '93, *Nucl. Phys.* **A566** (1994) 183c.

[62] M.I Gorenstein and H.G Miller, The coulomb interaction and the electrical chemical potential in heavy ion collisions, preprint (unpublished).

[63] S. Nagamiya, *Nnucl. Phys.* **A461** (1987) 239c.

[64] K. Guettler *et al.*, *Nucl. Phys.* **B116** (1976) 77.

[65] T. Abbott, *Phys. Rev.* **D45** (1992) 3906.

[66] T. Abbott, *Phys. Rev. Lett.* **66** (1991) 1567.

[67] R. Mattiello *et al.*, *Phys. Rev. Lett.* **63** (1989) 1459.

[68] H. Sorge *et al,Phys. Lett.* **B271** (1991) 37.

[69] B.H. Sa *et al,Phys. Rev.* **C48** (1993) 2995.

[70] C.M. Mader *et al,*, *Phys. Rev.* **C45** (1992) 2438.

[71] "Strangeness production in relativistic ion collisions - theoretical overview", J. Cleymans, Proceedings of Quark Matter '90, *Nucl. Phys.* **A525** (1991) 205c.

[72] "Strangeness production in relativistic heavy ion collisions - an experimental survey", O. Villalobos Baillie, Proceedings of Quark Matter '90, *Nucl. Phys.* **A525** (1991) 189c.

[73] G. Giacomelli and M. Jacob, *Phys. Rep.* **55** (1979) 1.

[74] B. Müller, P. Koch and J. Rafelski, *Phys. Rep.* **142** (1986) 167.

[75] Proceedings of AIP Conference 340 on Strangeness in Hadronic Matter,J. Rafelski(Ed.),Tucson, AZ, 1995.

[76] Proceedings of the Quark Matter '95, *Nucl. Phy.* **A590** (1995).

[77] J. Cleymans, K. Redlich, H. Satz and E. Suhonen, *Z. Phys.* **C58** (1993) 347.

[78] K. Redlich, J. Cleymans, H. Satz and E. Suhonen, *Nucl. Phys.* **A566** (1994) 391c.

[79] J. Letessier, A. Tomsi, U. Heinz, J. Sofrank and J. Rafelski, *Phys. Rev.* **D51** (1995) 3408.

[80] J. Letessier, A. Tomsi, U. Heinz, J. Sofrank and J. Rafelski, *Phys. Rev. Lett.* **70** (1993) 3530.

[81] J.P. Davies (WA85), In Proceedings of AIP Conference 340 "Strangeness in Hadronic Matter", J. Rafelski (Ed.), Tucson, Az, 1995, page 223.

[82] S. Abatzis *et al*, *Nucl. Phys.* **A566** (1994) 225c.

[83] AFS Collaboration: T. Åkesson *et al.*, *Nucl. Phys.* **B246** (1984) 1.

[84] O. Villalobos Baillie (WA94 Collaboration), In Proceedings of AIP Conference 340, "Strangeness in Hadronic Matter", J. Rafelski (Ed.), Tucson, Az ,(1995) page 259.

[85] J. Rafelski, *Phys. Rep.* **88** (1982) 331.

[86] U. Heinz *et al. Phys. Rev. Lett.* **58** (1987) 2292.

[87] A. Shor, *Phys. Rev. Lett.* **54** (1985) 1122.

[88] L. McLerran, Proceedings of Quark Matter '86, *Nucl. Phys.* **A461** (1987) 245c.

[89] B. Müller, Proceedings of Quark Matter '91, *Nucl. Phys.* **A544** (1992) 95c.

[90] S. Nagamiya, Proceedings of Quark Matter '91, *Nucl. Phys.* **A544** (1992) 5c.

[91] J. Rafelski, *Nucl. Phys.* **A418** (1984) 215.

[92] J. Rafelski and B. Müller, *Phys. Rev. Lett.* **48** (1982) 1066.

[93] C.M. Ko *et al.*, *Nucl. Phys.* **498** (1989) 561c.

[94] C.M. Ko *et al. Phys. Rev.* **C38** (1988) 179.

[95] C.M. Ko, Z.G. Wu and L.H. Xia, *Phys. Rev.* **C43** (1991) 1881.

[96] Y. Pang, T.J. Schlagel and S.H. Kahana, *Phys. Rev. Lett.* **18** (1992) 2743.

[97] H. Sorge *et al.*, *Phys. Lett.* **B243** (1990) 7.

[98] H. Bøggild *et al.*, *Nucl. Phys.* **B57** (1973) 77.

[99] H. Bøggild *et al.*, *Nucl. Phys.* **B27** (1971) 285.

[100] J.V. Allaby *et al.*, CERN Report No.70-12, 1970.

[101] H. Fesefeldt *et al.*, *Nucl. Phys.* **B147** (1979) 317.

[102] Review of Particle Physics, *Phys. Rev.* **D54** (Part One) (1996) 196-197.

[103] V. Blobel *et al.*, *Nucl. Phys.* **B69** (1974) 454.

[104] D. Deckers *et al.*, *Phys. Rev.* **B137** (1965) 962.

[105] U. Becker *et al.*, *Phys. Rev. Lett.* **37** (1976) 1731.

[106] T. Abbott *et al.*, (E802 Collaboration), *Phys. Rev. Lett.* **64** (1990) 847.

[107] W.M. Geist, Proceedings of Quark Matter '90, *Nucl. Phys.* **A525** (1991) 149c.

[108] S. Fredrikson *et al.*, *Phys. Rep.* **144** (1987) 187.

[109] T. Abbott *et al.*, (E802 Collaboration), *Phys. Rev. Lett.* **70** (1993) 1393.

[110] Private discussions with Shoji Nagamiya and Fuqiang Wang.

[111] D. Morrison, PhD. Thesis, Massachusetts Institute of Tecnology (1994) (unpublished).

[112] G.S.F.Stephas, In Proceedings of AIP Conference, "Strangeness in Hadronic Matter", J. Rafelski (Ed.), Tucson, AZ (1995) page 124.

[113] W.A. Zajc, (E802 Collab), *Nucl. Phys.* **A544** (1992) 237.

[114] T. Abbott *Phys. Lett.* **B291** (1992) 341.

[115] R.M. Quick, N.J. Davidson and H.G. Miller *Z. Phys.* **C50** (1991) 37.

[116] R. Hagedorn and J. Rafelski, Proceedings of Statistical Mechanics of Quarks and Hadrons, H. Satz (Ed.), North-Holland, Amsterdam, 1981.

[117] J. Cleymans, H. Satz, E. Suhonen and D.W. von Oertzen, Talk presented by J. Cleymans at the Summer School in Theoretical Physics "Phase Structure of Strongly Matter", Cape Town, 1990.

[118] J. Cleymans and A. Muronga, Hadronic Ratios as a function of Baryon Number, UCT-TP 234/96 to be published in *Phys. Lett.* **B**.

[119] B.A. Li, *Phys.Lett.* **B346** (1995) 5.

[120] M.Gyulassy and S. Kauffmann, *Nucl. Phys.* **A362** (1980) 503.

[121] J. Cleymans and A. Muronga, Hadronic Ratios and the Number of Projectile Participants, UCT-TP 230/96, Talk presented by A. Muronga at the First RHIC Theory Workshop, BNL, NY, 1996, to be published in Proceedings of RHIC Theory Workshop 1996.

[122] B. Cole (E802) Collaboration, In Proceedings of Quark Matter '95, *Nucl.Phys.* **A590** (1995) 179c.

[123] M. Gonin, Preprint, (E802/E866 Collaboration) BNL - 47925

[124] M. Gonin, in *Heavy Ion Physics at the AGS*, G.S.F. Stephans *et al.*(Eds.), MITLNS-2158 (1993) p184.

[125] Y. Wang (E859), In Proceedings of AIP Conference 340, "Strangeness in Hadronic Matter", AZ, J. Rafelski (Ed.) (1995) page 138.

[126] M. Gazdzicki and D. Rőhrich, *Z. Phys.* **C65** (1995) 215.

[127] B. Shiva Kumar, in *Heavy Ion Physics at the AGS*, G.S.F. Stephans, it et al.(Eds.), MITLNS-2158 (1993) 144.

[128] U. Heinz, *Nucl. Phys.* **A566** (1994) 205c.

[129] J.Cleymans, K.Redlich, H.Satz and E.Suhonen, *Z. Phys.* **C33** (1986) 151.

[130] J. Cleymans and E. Suhonen, *Z. Phys.* **C37** (1987) 51.

[131] A.G Schnabel, Preprint UCT-TP 97/88, Cape Town, 1988 (unpublished).

[132] D.W von Oertzen, N.J Davidson, R.A Ritchie, and H.G Miller, University of Pretoria preprint, UPTG 7/91.

[133] D. Hill and J. Wheeler, *Phys. Rev.* **89** (1953) 1177.

[134] H.R Jaqaman, A.Z Mekjian, and L. Zamick, *Phys. Rev.* **C29** (1984) 2067.

[135] R.Balian and C.Block, *Ann. Phys.* **60** (1970) 401.

[136] R. A. Ritchie, PhD. thesis, University of Pretoria, (1996) (unpublished).

[137] P. Braun-Munziger *et al.*, State University of New York at Stony Brook preprint, SUNY-RHIC-95-8.

[138] M.G. Weber, MSc. Thesis, UCT (1992) (unpublished).

[139] R.A. Salmeron, *Nucl. Phys.* **B389** (1993) 301.

[140] A. Prudnikov, U. Brischkov and O. Maritsev, "Integrals and Series : Special Functions", Moscow (1983) 378

[141] Private discussions with J. Cleymans, K. Redlich and D. Srivastava.